UNIVERSITY OF TRENTO - Italy

International Doctoral School in Biomolecular Sciences XXV Cycle

"Surface functionalizations towards Nucleic Acid Purification: a nanoscale study"

Tutor:
Cecilia Pederzolli
Bruno Kessler Foundation

Advisor:
Lorenzo Lunelli
Bruno Kessler Foundation,
CNR-Institute of Biophysics

Ph.D. thesis of:
Lorenza Marocchi
University of Trento
Bruno Kessler Foundation

Academic Year 2012-2013

Declaration

I hereby confirm that this is my own work and the use of all material from external sources has been properly and fully acknowledged.

Abstract

Protein byosynthesis is performed by ribosomes, that translate the genetic information contained in a strand of mRNA and assemble the peptide chain. During translation, several ribosomes associate to a single strand of mRNA, forming supramolecular complexes known as polyribosomes (polysomes).

This project is aimed at developing and studying a miniaturized purification system able to isolate and extract polysome-associated mRNA, namely mRNA under active translation.

The resulting microdevice will constitute a faster, simpler and low-cost alternative to the time-consuming traditional laboratory procedures for polysome purification and mRNA extraction (sucrose gradient centrifugation and phenol/ethanol RNA extraction).

Polysome purification on microdevice will be based on the immobilization of polysomes to the device surfaces, opportunely treated to enhance polysome adhesion. Surface funtionalization will be achieved by formation of Self-Assembled Monolayers (SAM) of organic molecules. In particular, since both ribosomes and nucleic acids expose an high quantity of electrical charged moieties towards the environment [Anger et al., 2013], organic molecules containing charged functional groups will be used as SAM constituents.

In this thesis a characterization of gold and silicon oxide plane samples functionalized with different alkanethiols and alkylsilanes SAMs will be presented as well as a quantitative and qualitative evaluation of polysome adhesion performed mainly by Atomic Force Microscopy (AFM). A proof of principle of the purification and extraction of RNA from polysomes using a silicon/Pyrex microdevice will be also reported.

Contents

Chapter 1

Introduction

This work is aimed at developing and studying a purification system for mRNA undergoing translation, namely the mRNA associated with polysomes. The long term outcome of this work is the design and realization of a microsystem based on the results of this thesis, that will constitute a faster, simpler and low-cost alternative to the traditional procedures for polysome isolation and mRNA extraction.

Polysome purification on microdevice will be based on the interaction between the polysomes and the device surfaces that will be opportunely treated to enhance polysome adhesion.

The surfaces of the microdevice will be chemically functionalized using Self-Assembled Monolayers of organic molecules, a well known and reliable method to tailor the chemical properties of several solid substrates, among which are some of the materials most commonly used in microsystem manifacturing: silicon, glass and polymers (i.e. PDMS). In particular, since both ribosomes and nucleic acids expose an high quantity of electrical charged moieties towards the environment [Anger et al., 2013], the microdevice surfaces will be treated with SAM capable to endow them with a positive or negative charge distribution. In this way it will be possible to exploit electrostatic interaction of attraction and repulsion to direct the binding of polysomes and nucleic acid on the walls of the microdevice, without resorting to specific, often expensive, binding molecules (for example, antibodies).

1.1 Actively translated mRNAs

Of the total mRNA present in a cell at any given time, only a fraction mRNA is effectively translated into protein. After transcription, in fact, there are many regulatory mechanisms that determine if the mRNA will be immediately translated, or stored or degraded. Actively translated mRNA is associated with ribosomes, the cellular machinery that reads the genetic information contained in the mRNAs and assembles the proteins. During translation multiple ribosomes are loaded on a same strand of mRNA, forming large complexes known as polyribosomes (polysomes) (in
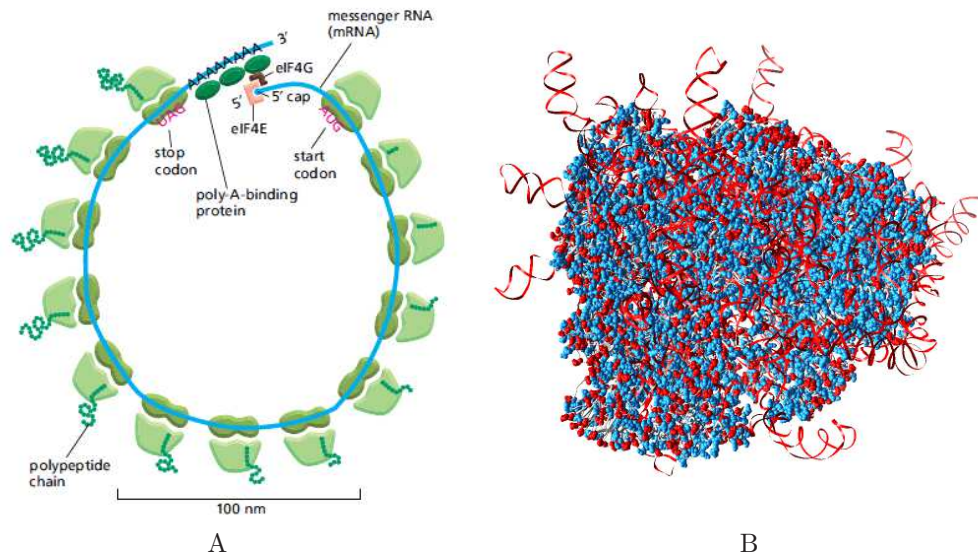
Figure 1.1: Panel A: a model of polysome. Multiple ribosomes are translating the same strand of mRNA into proteins. The polysome has a circular structure, in which the mRNA ends are linked by several proteins involved in the translation process (eucaryotic initiation factor eIF4 complex and poly-A binding proteins) (adapted from Alberts et al. 5th Edition [Alberts et al., 2008]). Panel B: Human ribosome. Blue: the positively charged amino acids. Red: negatively charged amino acids. Red ribbons: rRNA phosphate groups (adapted from [Anger et al., 2013]).

Figure 1.1 a cartoon showing a model of polysome is shown).

Polysome-bound mRNA has undergone most of the post-transcriptional and translational regulatory processes (the latters, take place at the initiation/ribosome loading step of the translation [Mathews et al., 2000]), therefore polysome-bound mRNA constitutes a good indicator of the translational control of a cell, and its analysis is considered a good approximation of the protein production state of a cell [Del Prete et al., 2007, Pradet-Balade et al., 2001].

1.2 Polysome purification

The extraction of the polysome-bound mRNA fraction has been routinely achieved by fractionation of polysomes of different size by differential centrifugation through density sucrose gradients. This technique is able to separate polysomal fraction of different weight: after lysis of the cellular membrane (that can be achieved through different methods: detergents, osmotic shock, ultrasonic vibration) the cell extract is loaded on a gradient of sucrose (usually linear) and then centrifuged with an ultracentrifuge able to reach at least 150,000 g. The polysomes migrate through the mixture and separate in bands depending on their buoyant density that can be collected separately, usually by means of a dedicated fraction collector. The RNA is then extracted from the collected fraction. A common extraction procedure is the precipitation in a phenol-chlorophorm/aqueous solution in high salt condition, 1.5 -2 M NaCl.

The sucrose gradient fractionation, although widely used, presents some distinct disadvantages: it requires special equipment (i.e. an ultra-centrifuge, a sucrose gradient fractionator/collector system) that may not be available in every laboratory, it is a time-consuming procedure, lasting at least several hours, and not allowing multiple sample in parallel, it requires a skillful operator to be successfully completed and high amounts of starting samples (up to 10^9 cells [Kudo et al., 2010]) that may not be conveniently available in some critical application, such as, for example, when working with clinical samples obtained from tissue biopsies. Althoug, this thechnique achieve a very precise separation, the resulting polysomes-they are diluted in a high concentration of sucrose and heparin, often used as a non-specific RNase inhibitor, that can hinder subsequent steps of polysome and extracted mRNA analysis, or complicate the RNA extraction procedure.

In the last decade alternative polysome purifications strategies have been explored.

In the years between 1970 and 1980 some chromatographic technique has been employed on bacterial ribosomes: adsorption chromatography on hydroxyapatite [Hoffman and Ilan, 1974], size exclusion chromatography (SEC) [Jelenc, 1980], and hydrophobic interaction chromatography (HIC) [Kirillov et al., 1978]. Chromatographic purifications of ribosomes have been occasionally readopted by some laboratories [Maguire et al., 2008] but never achieved widespread use, and furthermore they do not offer particular advantages in terms of rapidity or simplicity in sample-handling.

More recently, ribosome affinity purification strategies have been researched. This technique involve the modification of ribosomal proteins (RP) that have been tagged with suitable ligands (IgG-binding protein [Halbeisen and Gerber, 2009, Halbeisen et al., 2009], FLAG-epitope tagging [Inada et al., 2002, Zanetti et al., 2005, Sanz et al., 2009]) and then immobilized by immuno precipitation or receptor-coupled beads. Alternatively rRNAs belonging either to the small or large subunit of the ribosomes have been modified [Dorywalska et al., 2005, Uemura et al., 2008], and purified by hybridization with biotinylated oligomers specific for the engineered modification. These approach however involves the incorporation of a modified ribosomal protein or strand of rRNA in the ribosomes at the moment of its bio-

genesis, a difficult operation due to the ribosome complexity and high degree of structural conservation. This, not only requires a careful choice of the ribosomal component to be tagged, for it to be functionally incorporated, but introduces a transgenic modification in the cell aimed to express the mutant protein or rRNA, hence preventing an analysis of cells in natural/unadulterated conditions. Furthermore, tagging each of the (usually) multiple copies of rRNA or RP genes is often not practicable: therefore the tagged ribosomes constitute a sub-population of the total pool of ribosomes produced by the cell.

Immuno-precipitation has even been applied to proteins closely associated with the polysome complex, for example chaperon proteins involved in the folding of the nascent peptide [Kudo et al., 2010], an approach that, although avoids modification on the ribosomes, target only the fraction of polysomes associated with a determined chaperon protein.

1.3   Lab-on-a-chip approach

The purification of polysome bound mRNA is achieved at the moment only utilizing traditional, but cumbersome method based on sucrose gradient centrifugation, despite its aforementioned disadvantages: it is time-consuming, laborious, requires special equipment and large quantities of starting sample, finally the resulting polysomes are diluted in a solution with considerable amounts of sucrose.

However, a new approach, based on the use of miniaturized devices, or Lab-On-a-Chip (LOC) platforms, has become recently feasible thanks to the development of functionalized microfluidic systems. This kind of strategy has gained popularity in the early 1990s, when technologies for silicon microfabrication, have started to be employed in the realization of several miniaturized actuators and analysis microsystems: micropumps and microvalves for liquid samples hydrodynamics, micro-heater units, micro-electrodes, micro-detectors and micro-sensors for analyses [Chen et al., 2007].

These elements have been then integrated on miniaturized devices or chips, capable to perform a wide range of analyses, replacing many, if not all steps of a chemical or biological analysis, going from the sample preparation to detection, with semi-automaded procedures on a single platform [Crevillén et al., 2007].

This approach offer many advantages that could play a critical role for polysome purification purposes.

First of all LOCs are particularly suited to replace a time-consuming, or highly dependent on operator skills, traditional laboratory procedure with semi-automated and faster procedures. This would bring a significant saving of operator time and labor; moreover, the mycrosystem utilization is often of much more simple handling than traditional techniques steps.

Sample contamination is a particular critic problem when handling RNA, due to the ubiquitous presence of RNase. Sample confinement within a microdevice for the most part, if not the whole duration of a procedure can greatly reduce this risk.

microdevices generally require amounts of sample ranging from a few picoliters few to microliters, in any case several order of magnitude smaller than the traditional approach, thus saving reagents in the analytical chemistry field, but also offering the possibility of working on low quantities of samples, with great efficiency of purification and sensitivity, in cases were this was not possible or convenient (as, for example, the traditional polysome purification). Moreover, the high efficiency of these microsystem offer the possibility of high-throughput analyses from small quantities of sample. These qualities, coupled with the simplicity of a semi-automated process may open the way for several applications for which obtaining large amounts of starting sample it is not possible or convenient, as, for example, in the clinical field or the pharmaceutical industry, where the necessity of microscale sample analysis, on multiple sample in parallel, for substance (drugs, pathogens or toxins) detection and analysis is a critical advantage.

In the last two decades LOCs have been employed in numerous application in the analytical chemistry, life science and biomedical fields. A great number of works have been published in particular, regarding LOCs dedicated to genetic analyses of DNA extracted from blood, either for analysis or diagnostic purposes [Kricka, 1998, Cho et al., 2007, Price et al., 2009].

RNA extraction and analyses on microdevices has also been reported in literature: virus detection based on RNA extracted from blood [Hui et al., 2007] or mammalian cells [Hong et al., 2004, Bhattacharyya and Klapperich, 2008] for diagnostic purposes or genetic analyses purposes [Lien et al., 2007]. These microdevices, however, are all based on the same principles of DNA extraction (and so have been used [Hong et al., 2004, Hui et al., 2007]) and their target is constituted by total RNA. Works on microdevice for polysome-bound mRNA are not yet reported in the literature.

1.4 Surface functionalization: the Self-Assembled Monolayers

When working with miniaturized technologies, often interfaces and surface properties are more important than the bulk properties of the materials: the fact that volume decreases more rapidly than surface area becomes critical at micro and nanoscale level. Controlling surface properties as wettability, conductance, affinity for other organic molecules is therefore one of the fundamental steps to work in the nanotechnology field.

One of the simplest and historically more studied methods to tailor such surface properties are the Self-Assembled monolayers.

A solid substrate in a liquid or gas-phase environment tends naturally to adsorb organic molecules on its exposed surfaces. The adsorbed molecules may have considerable effects on the solid surface properties: they can act as electrostatic or physical barriers between the solid surface and the environment, or viceversa promote its affinity for other molecules present in the environment, promote or decrease aggregation for example in the case of nano-particle. However the transformation incurred by the substrate surface because of adventitious material are

hardly reproducible or controllable.

This is not true for a particular case: the Self-Assembled Monolayers (SAMs). These are assemblies of organic molecules that adsorb on a solid metal or metal oxide surface and spontaneously arrange themselves in ordered (crystalline or semicrystalline) structures. The assembly of SAMs is guided by a functional group (*head-group*) of the organic molecules that has a particular affinity for a specific type of substrate. There are, thus, molecules that form SAM on specific materials. The most known and studied are SAMs formed by molecules containing a thiolic group (-SH) or a disulfide (-S-S-), on transitional metals such as gold, silver, palladium, copper, platinum and mercury [Love et al., 2005]. Silanes, molecule containing a silanol (-S-O-) are preferred to form SAM on hydroxylated surfaces such as silicon oxide, aluminum oxide, titanium oxide, glass and mica[Vericat et al., 2010].

SAMs have several properties that make them interesting for nantechnology purposes. They constitute a smart method to modify surface properties such as wettability, conductance and charge distribution, chemistry and affinity for organic molecules without altering significantly the morphology of the surfaces. SAM are usually easy to prepare: they do not require specialized equipment nor high amount of reagents. In principle they assemble on objects of any size and a variety of shapes in a few hours.

The applications are countless and involve different fields of technology. In the nanotechnology field alone they are widely employed in the stabilization and functionalization of nanoparticles, nano-rods and nano-wires. They are used as inks or resist in lithography, photolitography and microfabrication. Their ability to connect inorganic and organic environments make them fundamental for the functioning of sensors and biosensors but also as surface agents for control cell adhesion and growth, bio-molecular carriers, coatings for implants. In the field of material protection and device fabrications they are often used as ultra-thin layers for corrosion prevention and friction reduction. They are often employed as components in electronic devices as transistor [Vericat et al., 2010]

SAM structure

Each molecule that constitute the building block of a SAM can be divided in three parts: head-group, carbon chain and terminal group as shown in Figure 1.2. The head-group is a functional group that has a specific affinity for a material. It guides the formation of the SAM forming a strong bond, often a covalent bond, with an atom of the substrate surface.

More often than not, the molecules forming SAMs are constituted by long alkanes. The long hydrocarbon chains are able to arrange themselves in a ordered and strictly packed structure, sustained by Van Der Waals and hydrophobic interactions. Although Van Der Waals interactions are often orders of magnitude weaker than the bond between headgroup and substrate, their strength increases with the length of the carbon chain, stabilizing structures formed by long chain molecules ($\gtrsim$18 carbons). When these ordered structures are complete the molecules assume a tilted conformation: the chains are tilted by an angle α defined from the axis orthogonal to the surface plane, depending on the nature of the molecule and the
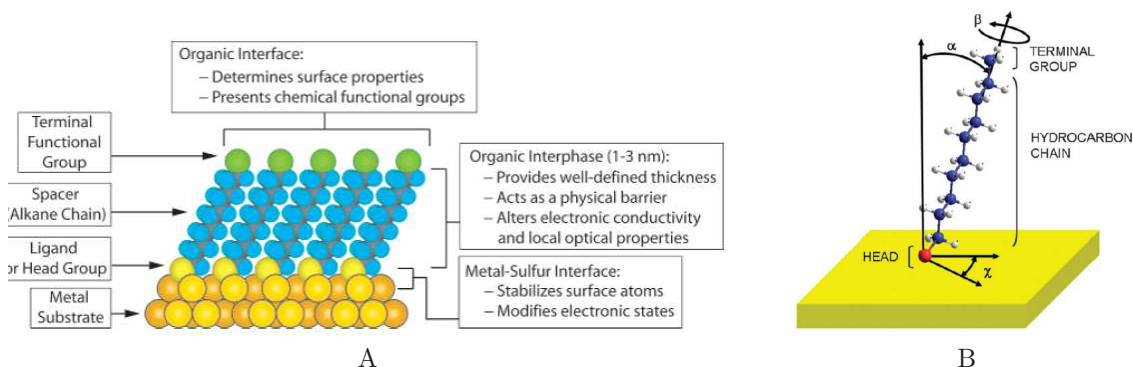
Figure 1.2: Panel A. The structure of a SAM formed by alkanethiols on a metal surface [Love et al., 2005]. Panel B. Scheme of a thiol (dodecanethiol) in standing-up configuration [Vericat et al., 2010]. α indicates the tilt between the molecule and the direction orthogonal to the surface. Angle β conventionally indicates the rotation of the molecule with respect to the first neighbors, and angle χ the orientation respect an arbitrary direction parallel to the gold surface.

material on which the SAM is formed. The angle β defines the molecule proper rotation (the rotation around the natural axis of the molecule) that minimizes the energy between adjacent carbon chains. In Figure 1.2 a schematics of a complete SAM and the angle convention are shown.

Finally the terminal group, often is a functional group and is the main contributor to the new chemical properties the surface acquires thanks to the formation of the SAM: among the most used $-CH_3$ and $-CF_3$ groups turn the SAM surface hydrophobic and highly anti-adherent, $-COOH$, $-NH_2$ or $-OH$ groups produce hydrophilic surfaces with good protein binding properties, -SH (dithiols) are often used to bind metallic ions and nanoparticles to the SAMs.

The self-assembly process

The assembling process may occur both in liquid and gas-phase and can be divided in consecutive steps (Figure 1.3). The kinetics and energies involved in each step can be very different between diverse systems, depending, of course, on the nature of both substrate and molecule.

In the first phase, the molecules from the liquid or gas-phase environment initially adsorb on the surface thanks partially to the affinity of the headgroup for the substrate, but also by interaction of the carbon chains (physisorption) with the substrate. This step brings the head-group and the substrate material in close contact, thus leading to the chemisorption of the molecules, namely the formation of the proper (often covalent) bond between the head-groups and the atoms of the surface.

The most common model used to describe this phase kinetics is the first order Langmuir adsorption model.

The reaction that take place can be thought as a reversible adsorption reaction:

$$S + A_{ad} \rightleftharpoons S \cdot A_{ad} \tag{1.1}$$

This model assumes that the adsorption process occur on a perfectly plane surface endowed with a number of equivalent adsorption sites S, capable to hold a single adsorbate molecule.

The rate of adsorption R_{ad} depends on the concentration (or partial pressure in case of a gas-phase deposition) of the molecules in proximity to the surface, the presence of avaible sites, and the probability of bond formation between the molecule and the adsorption site. that may depend upon various factors: amongst these the presence of any activation barrier to the adsorption.

While the inverse process, the desorption depends on the number of sites already occupied on the surface and the probability of desorption, which depends mainly on the temperature of the systems and the energy necessary to break the adsorbate-surface bond.

The adsorption and desorption rates may be written as:

$$R_{ad} = c \cdot (1 - \theta) \cdot k_{ad} \tag{1.2}$$

$$R_{des} = \theta \cdot k_{des} \tag{1.3}$$

Where θ represents the fraction of adsorption sites occupied by an adsorbate molecule, thus the coverage of the surface. In this model it is implied that adsorption and desorption are simple process with a first order dependency on θ.

At equilibrium, the adsorption and desorption rates equal each other.

$$\frac{R_{ad}}{R_{des}} = \frac{c(1 - \theta)}{\theta} \frac{k_{ad}}{k_{des}} \tag{1.4}$$

Rearranging this equation we obtain the Langmuir isotherm, that represent the relation between coverage and concentration of molecules in solution.

$$\theta = \frac{k_A c}{1 - k_A c} \tag{1.5}$$

where k_A is the equilibrium constant of the adsorption reactio, or k_{ad}/k_{des}.

However the Langmuir adsorption model ignores two characteristics of the adsorption process: the surface roughness and interactions between adjacent adsorbate. Rough surfaces have multiple site-types available for adsorption, and some
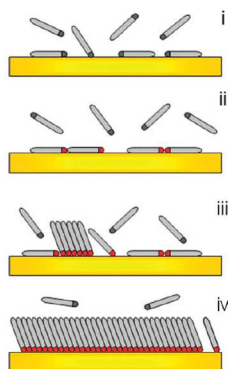
Figure 1.3: Steps of the self-assembling process: i. physisorption of molecules on the substrate, ii. binding of the head-groups with the substrate in the striped phase, iii. and iv. nucleation, growth and completion of the standing-up phase [Vericat et al., 2010].

parameters vary from site to site, such as the activation energy of adsorption. Adsorbate/adsorbate interactions may affect the adsorption process by favouring or hindering the adsorpion near an already immobilized molecule. Several modification of the Langmuir equation have been proposed to take into account these phenomenons (for example the Freundlich equation for inhomogeneous surfaces, or the Temkin isotherm for adsorbate/adsorbate interaction.

This first steps is are usually very fast, taking up to some minutes. This situation, a surface covered in lying-down molecules, is known as *striped phase*, due to the presence of different domains deriving from distinct growing islands.

The following, much slower, steps consist in the rising of molecules from a lying-down configuration to a standing-up one, once again starting from nucleation sites and growing to the final coverage of the surface with a densely packed crystalline layer, in which the carbon chains optimize their interaction with the next neighbors. This process is much slower and can take from hours to a few days.

SAM formed by organosulfur on gold

Gold surfaces, especially in the crystallographic orientation (111), coupled with thiolated molecules, in particular alkanethiols, are the most historically studied system of SAM, for a number of reasons. Gold is a relatively inert material, it does not react with atmospheric oxygen nor with most chemicals, making it possible to handle samples in air, or wet environments, therefore it can be conveniently used in biology.

Sulfur has an high affinity for gold. Therefore thiols bind rapidly to gold substrates, forming well organized SAMs that are stable for days to weeks even in physiological conditions or cell culture environment; and furthermore, they are able to displace eventual adventitious material from the surface. One of the most

important reasons, however is that gold surfaces are easy to manifacture. It can be obtained as thin films, as colloid phase or as nanoparticles, by vapor deposition, sputtering or electrodeposition [Love et al., 2005]. In the course of this work, gold samples obtained through vapor deposition on mica substrates will be used. Both X-ray diffraction [Hooper et al., 1999] and STM [Hegner et al., 1993a] has been used to show that evaporated gold deposited on this kind of substrate assumes Au(111) as its predominant crystallographic orientation characterized by a hexagonal geometrical disposition of the exposed gold atoms with a lattice constant 0.288 Å (see Figure 1.4).

SAMs of thiols on gold can be reliably prepared both in liquid and by vapor deposition, the former method being very convenient in terms of simplicity and quantity of reagents. Liquid phase self-assembly can be carried out in numerous solvent, depending on the nature of the thiol. By far the most commonly used one is ethanol: it can solvate a range of different thiols in terms of polarity and chain lenght, can be conveniently purchased at high purity, and has low toxicity. Other solvent may reveal themselves as more efficient for the formation of SAM of n-alkanethiols on gold: for example non polar solvents may speed up the chemisorption of the sulfur atom but impede the following phase of carbon chain rearrangements, thus yielding to less organized monolayers; on the other hand, polar solvents, less capable of solvating long alkanethiols, may segregate them for hydrophobic interaction and enable them to form highly organized SAM, containing far less defects.

The most common procedure is to immerse a freshly prepared or clean gold substrate in a solution of the desired thiol in ethanol ($\sim$1-10 mM) for 12-18 hours [Love et al., 2005, Ulman, 1996].

In these conditions, chemisorption of the sulfur atoms on the gold surfaces happen within minutes from the starting of the incubation. The reaction of formation of a covalent bond between the thiolate group and a gold atom can be formally described as an oxidative addition of the S-H bond to the gold surface immediately followed by reduction and elimination of the hydrogen [Ulman, 1996].

$$R\text{—}S\text{—}H + Au_n^0 \rightarrow R\text{—}S^- Au^+ \cdot Au_n^0 + \frac{1}{2}H_2 \qquad (1.6)$$
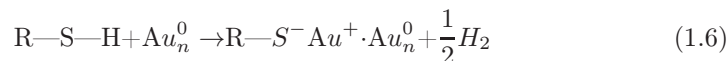
The kinetic of this reaction has been found to be strongly dependent on the concentration of thiol: at 1 mM it can be completed within 1 minute, while at 1 μM it can last up to 100 minutes [Ulman, 1996].

Density of chemisorbed molecules increases rapidly in this phase, rapidly skipping the striped down phase and reaching the standing up conformation with tilt angle $\alpha \sim 30°$ and coverage close to the final one ($\sim 4.5 \cdot 10^{14}$molec/cm^2) [Love et al., 2005].

At final (maximum) coverage the structure of the sulfur binding to the gold (111), is generally assumed to adopt a rotated hexagonal overlayer from the gold (111) lattice, generally indicated as ($\sqrt{3} \times \sqrt{3}$) R30°, with a nearest sulfur–sulfur spacing of 4.97 Å [Stroeve, 2004]. In Figure 1.4 the relative orientations of a thiols adsorbed on a gold (111) plane are shown.
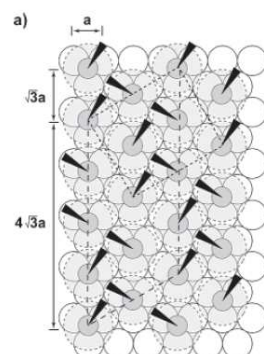
Figure 1.4: Schematic illustrations of the structure of SAMs formed from alkanethiols on single crystals of gold. Open circles represent gold atoms: (a), the lattice constant of Au(111) is equal to 2.88 Å Dark gray circles represent sulfur atoms, that assume an orientation rotated by 30° with respect to the underlying gold plane, with a lattice constant equal to $\sqrt{3}a$=4.98 Å(indicated as $(\sqrt{3}\times\sqrt{3})$R30° in the text). Light gray circles with dashed lines represent the projected area of the carbon chain, ~ 21.4 Å^2 [Ulman, 1996]. Black wedges represents the projections of the CCC plane of the carbon chains. The larger rhombus shows a c(4×2) superlattice with respect to the$(\sqrt{3}\times\sqrt{3})$R30° structure defined by the relative orientation of the carbon chains[Love et al., 2005].

To minimize the free energy of the layer the hydrocarbon chains adopt a conformation that favors Van Der Waals interactions between the carbon chains: they arrange themselves in a strictly packed and tilted configuration with tilt angle $\alpha \sim 30°$ and proper rotation angle $\beta \sim 55°$ [Vericat et al., 2010].The disposition of the carbon chains define a further superlattice structure (showed in Figure 1.4) indicated as c(4×2) unit cell.

The energy of the S-Au bond has been estimated from desorption experiment performed in solvent and in void, and reported in numerous works as ~ 50 kcal/mol, comparable with the bonding energy of a disulphide bond (62 kcal/mol) [Love et al., 2005] while Van Der Waals interactions energy has been estimated to 1-2 kcal/mol per methylene [Vericat et al., 2010, Love et al., 2005], yielding to particularly stable to mechanical and chemical stimulation SAM formed by alkane longer than 10 carbon atoms [Love et al., 2005].

Even when the most carefulness is taken into choosing the condition of temperature, solvent and incubation times during the SAM formation, the monolayers are seldom perfect as schematized so far. In fact, there are several types of defects that can occur in a SAM structure, and some of them can have an important influence for some the applications. These defects can be either a small number of missing molecules (also called pinholes), or regions where the molecules have a certain degree of disorder. In Figure 1.5 some of he typical defects that can verify on polycrystalline gold surfaces are portraied.
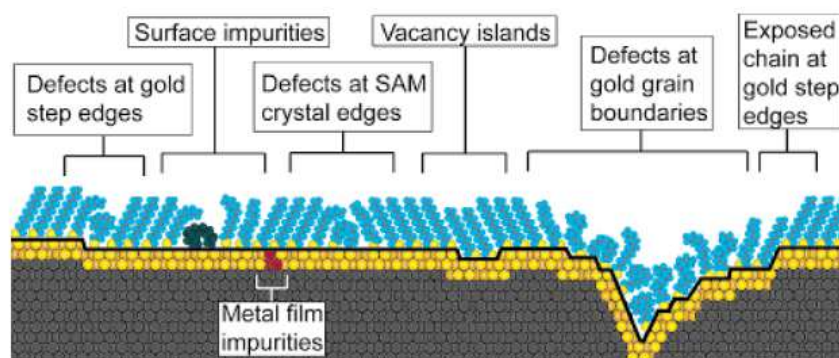
Figure 1.5: Schematic illustration of some of the intrinsic and extrinsic defects found in SAMs formed on polycrystalline substrates. The dark line is a visual guide that indicating the gold-sulfur interface [Love et al., 2005].

Some defects are caused by irregularities of the gold substrates, caused either by edges at the crystalline plane in a polycrystalline substrare or caused by the presence of monoatomic holes and vacancies islands, impurities on the gold surface, defects or boundaries between different grains of the gold substrate.

Other defects are generated during the SAM formation: as already mentioned the standing up phase is formed starting from nucleation sites, that grow into domains of tightly packed and ordered chains, that can however be characterize by different orientation (different angles χ). Defects at the domain edges has been observed at the STM.

A third kind of defect originates from the dynamic behavior of the SAM, and may be caused by adjacent areas with different phase (from striped down to standing up). So disordered, liquid-like domains can be found beside regions with well-packed molecules, or regions in which the molecules sport not fully extended hydrocarbon chains, or a differnet angle α .

Several strategies can be employed to improve the quality of thiol and dithiol monolayers on Au(111). A careful choice of the solvent and of the self-assembly conditions can yield SAMs with lower defect density and better chain ordering.

An alternative is to apply thermal annealing processes. During the annealing process defects in the hydrocarbonchain orientations caused by phase transition, domains or even vacancy islands, or missing molecules can be recovered, but if the annealing is prolonged or carried out at too high temperatures the molecules start to desorb from the surfaces. The desorption process, in turn depends on several factors such as hydrocarbon length, defects on the substrate, temperature of the substrate at the moment of adsorption, surface roughness. Typical temperature of annealing do not surpass 100 °C [Love et al., 2005].
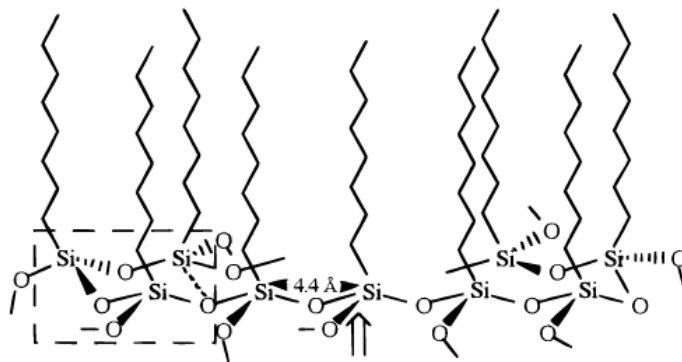
Figure 1.6: A schematic description of a polysiloxane at the monolayer-substrate interface. The arrow points to an equatorial Si-O bond that can be connected either to another polysiloxane chain or to the surface [Ulman, 1996]. The dotted line on the left is a bond in a possible precursor trimer.

SAM formed by organosilanes on hydroxylated surfaces

The main alternative to SAMs formed by thiol on gold (and more generically transition metals) are SAMs formed by alkylsilanes on hydroxylated surfaces, such as silicon oxide, glass, aluminum oxide, titanium oxide, quartz and mica. The driving force for this self-assembly is the formation of a polysiloxane connected to surface silanol groups (-SiOH) via Si-O-Si bonds, after a first, rapid step of hydrolysis of eventual residues of the Si-O- moieties belonging to the molecule.

The same bond forms between molecules once the molecule are adsorbed and/or chemisorbed on the surface, in proximity with each other, as illustrated in the model in Figure 1.6; this cross-linking greatly contributes to the the stability of the SAM on the substrate.

This reaction is in competition with the same reaction between the hydrolyzed silyl groups of the molecules occurring in solution, that generates a polymer. Among the factors that shifts the balance between the two reactions are water content and temperature: as temperature decreases the surface reaction is favored [Ulman, 1996]. This tendency depends strictly on hydrocarbon chain length: the longer the chain, the higher the temperature below which an ordered SAM can be achieved [Ulman, 1996].

A small quantity of water is necessary to start the hydrolysis and the following O-Si-O bond formation to obtain complete SAMs, but excess water facilitate the polymerization reaction in solution, hence resulting in deposition of aggregates, yielding non-uniform, "grainy" layers of polysiloxanes. This characteristic has been observed in particular for aminosilanes, where the polymerization is further eased by the possibility of hydrogen bonding between and with the amino groups. Therefore silanizations reactions performed in liquid are usually carried out in anhydrous solvent, ethanol, hexane and toluene being the most commonly used.

Chapter 2

Purpose of the thesis

The aim of this thesis is the study and the development of functional surfaces for the isolation and separation of a selected class of nucleic acids, namely the messenger RNA under translation. Such molecules are associated with polysomes, supramolecular complexes where ribosomes scan the mRNA strand while synthesizing the encoded protein.

The final purpose of the project in which this thesis work is included, is the design and realization of a microdevice able to offer a fast, efficient and semi-automated alternative to the traditional method of purification of polyribosomes via centrifugation in sucrose gradient and extraction of the associated mRNA. Both purification and extraction traditional techniques have some operative drawback, the major being the long duration and necessity of large amounts of initial sample. The final microdevice will reunite the two processes of the purification of polysomes and the mRNA extraction from the purified polysomes on a single platform, thus reducing eventual sample loss and contamination. The scale of the sample involved will vary from a few tens of microliters to hundreds of microliters, depending on the final application. In principle, this device will be also useable in application fields, such as diagnostics, where only small amount of sample is available.

The working strategy will exploit the results obtained in this work on the immobilization of polyribosomes to the functionalized surfaces of the microdevice itself.

The functionalization has been carried out taking advantage of the formation of Self-Assembled Monolayers of organic molecules exposing an opportune functional group to tailor wettability and surface charge distribution of the materials composing the microdevice and generate an attractive interaction able to immobilize polysomes, without resorting to prior ribosome modifications.

Here, a characterization of the adhesion of polysomes on gold and silicon oxide plane samples functionalized with different alkanethiols and alkylsilanes is presented, mainly by Atomic Force Microscopy. A proof of principle of the purification and extraction of RNA from polysomes using a silicon/Pyrex microdevice is also shown.

Chapter 3

Materials and Methods

3.1 Materials

Solid substrates: Gold substrates were produced in house at the FBK-microfabrication facility using gold with a purity of 99.99% (Leybold Optics Italia S.r.l) and Highest Grade V1 mica disk, with a diameter of 0.9 cm (TedPella Inc., Redding, CA). Thermally grown silicon oxide (TG-SO) surfaces (thickness 205.3 $\pm$ 2.8 nm, area 1 cm^2) were also produced in house at the FBK-microfabrication facility. Silicon oxide/Pyrex microdevices (substrate area 3×3 cm^2) were produced by Olivetti I-Jet (Italy).

Reagents for surface functionalization: Alkanethiols (see Table 3.1): 11-Mercaptoundecanoic acid (MCOOH), 11-Mercapto-1-undecanol (MOH), 11-Amino-1-undecanethiol hydrochloride (MNH$_2$), 1-Undecanethiol (M-11CH$_3$), ethanol, toluene and anhydrous toluene (99.8%), tetrahydrofuran (99%) powders for buffer solutions, were purchased from Sigma-Aldrich (USA).
Silanes: (3-aminopropyl)triethoxysilane (APTES) and (3-aminopropyl)trimethoxy-silane
(APTMS) were purchased from Sigma-Aldrich (USA), N-(trimethoxysilylpropyl)-ethylene-diamine triacetic acid, trisodium salt (triCAS) 45% in water and carboxyethyl-silanetriol, disodium salt (CST) 25% in water were purchased from Gelest (USA).

Adhesion and quantification of biological materials: Pyrogen-free DEPC water and RNase-free water were purchased from Life technologies Corporations (USA).
Quant-iT™ PicoGreen® dsDNA Assay kit (PG) and Quant-iT™ RiboGreen® RNA Assay kit (RG) Invitrogen Ltd. (UK) were used for DNA and RNA quantification. λDNA standard standard kit component was used for deposition on functionalized gold samples. Synthetic RNA miR21-TIO (5'-DTPA-UAGCUUAUCAGACUG-AUGUUGA-3'), DNA-TIO (5'-DTPA-TAAGTTTGAATGTCATTTCTT-3'), modified at the 5' end with dithiol phosphoramidite and their unmodified DNA complementary strands for AFM tips functionalizationwere purchased from Integrated

DNA Technologies inc. (USA).

Ribosome and polyribosomes were obtained from MCF-7 cell cultures and purified by sucrose gradient centrifugation at FBK-LaBSSAH laboratory. See Section 3.2.3.1 for details.

Buffers: Buffer A, 30 mM Tris-HCl pH 7.5, 0.1 M NaCl, 10 mM MgCl. Buffer B, 10 mM Hepes adjusted to pH 7.4, 10 mM NaCl, 10 mM $MgCl_2$, 20 μm/ml cycloheximide and 3% (w/v) sucrose.

3.2   Methods

3.2.1   Analytical methods

3.2.1.1   Spectrophotometry

A V-550 UV/VIS spectrophotometer (Jasco Corporation, Japan) was employed to quantify nucleic acids concentration. For ribosomes in undiluted ribosomal and polysomal fractions absorption spectra have been recorded from 200 nm to 600 nm, with a band width of 1 nm. Quantification of ribosomes has been performed using a molar extinction coefficient of $5 \cdot 10^7$ $M^{-1}cm^{-1}$ at 260 nm, after background subtraction [Algire et al., 2002].

For DNA quantification absorption spectra have been recorded from 200 nm to 350 nm, with a band width of 1 nm, using an extinction coefficient of 0.020 $(\mu g/ml)^{-1}$ cm^{-1}.

3.2.1.2   Spectrofluorimetry

Fluorescence of DNA samples stained with PG was measured with a SPEX Fluor-Max spectrofluorimeter (Horiba Jobin Yvon, USA), using an excitation wavelength of 480 nm and recording the emission spectrum from 496 to 700 nm. The area between 520 and 540 nm was integrated and the value obtained compared with a calibration curves previously worked out

RNA extracted from chips was stained with RG and measured with a SPEX FluorMax spectrofluorimeter (Horiba Jobin Yvon, USA), using an excitation wavelength of 480 nm and recording the emission spectrum from 515 to 700 nm. The area between 520 and 540 nm was integrated and the value obtained compared with a calibration curves previously worked out.

3.2.1.3   Bioanalyzer analysis

The RNA extracted from silicon/Pyrex microdevices was analyzed after purification to asses its integrity and its type. The analysis was performed with an Agilent 2100 Bioanalyzer. Agilent RNA 6000 Pico chips were employed and manufacturer instructions were followed

3.2.1.4 Fluorescence microscopy

Fluorescence images of DNA and RNA adsorbed on various surfaces and stained with PG and RG respectively were taken with a Leica DMLA microscope (Leica Microsystems, Germany) with a mercury lamp and a fluorescence filter cube L5 (Leica Microsystems, Germany). Samples were observed with 20x and 40x magnifications objectives and measured with a cooled CCD camera (DFC 420C, Leica Microsystems, Germany).

3.2.2 Surface preparation and functionalization

3.2.2.1 Gold samples preparation

Ultraflat gold surfaces were obtained by the method developed in 1993 by Hegner and coworkers [Hegner et al., 1993b]. A gold layer was evaporated onto freshly cleaved mica muscovite disks, of the diameter of 0.9 cm, until a thickness of 150 nm is reached. The evaporation is performed by an electron beam evaporator (Ulvac EBX-16C with Ferrotec EV S-6 e-gun) with an evaporation rate of 0.2-0.3 Å/s at room temperature in ultra-high vacuum (base pressure of 2×10^{-7} Torr). The gold surface thus obtained was then glued to a glass support using epoxy glue (Bostik, Perfecta Chemie B.V., Goues, Nederland) and stored at room temperature.

Immediately before use, the mica was stripped off the gold surface with a pair of tweezers, after soaking in tetrahydrofuran (THF) at room temperature for a few minutes to facilitate the mica detachment from gold.

3.2.2.2 Gold functionalization with thiols

In table 3.1 the four thiols used in this work are listed, along with their condensed formulas and molecular weight. The four terminal groups: carboxyl, amine, hydroxyl and methyl groups have been chosen to tailor mainly the charge distribution of the surface, as well as its hydrophobic/hydrophilic behavior.

Thiol		Molecular weight	Linear Formula
11-Mercaptoundecanoic acid	(MCOOH)	218.36	$HS(CH_2)_{10}COOH$
11-Mercapto-1-undecanol	(MOH)	204.37	$HS(CH_2)_{11}OH$
11-Amino-1-undecanethiol hydrochloride	(MNH$_2$)	239.85	$HS(CH_2)_{11}NH_2 \cdot HCl$
1-Undecanethiol	(M-11CH$_3$)	188.37	$HS(CH_2)_{10}CH_3$

Table 3.1: List of four undecanethiols used to functionalize gold substrates.

Functionalization of gold surfaces with thiols was performed as follows.

The gold sample, freshly stripped off mica, was immersed in a 1 mM solution of alkanethiol in ethanol for 24 hours at room temperature, then rinsed in pure ethanol for 2 minutes and finally dried under a stream of nitrogen. Functionalization with MCOOH has been performed using different incubation times, from 6 to 72 hours.
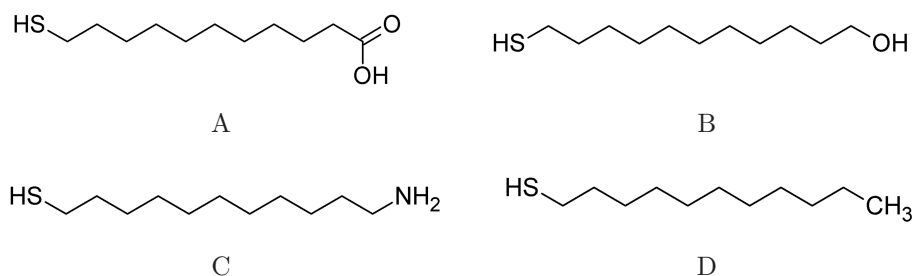
Figure 3.1: MCOOH (A), MOH (B), MNH$_2$ (C) and M-11CH$_3$ (D) thiols used to functionalize gold substrates.

3.2.2.3 Silicon oxide silanization

A) Plasma treatment. Silicon oxide films, thermally grown on 1 cm^2 silicon substrates (TG-SO) were treated in a PDC-32Gplasma cleaner (Harrick Scientific Corporation, New York USA) with 6.8 Watt of power applied to the RF coil at a pressure of 2 mbar of argon for 2 minutes, to eliminate contaminants and activate surface silanol groups [Suni et al., 2002].

   B) Wet treatment. An alternative procedure has been used to enrich the silicon oxide surface with silanol groups, developed by Hau et al. [Hau et al., 2003]: the TG-SO samples were first cleaned in "piranha solution" (H$_2$SO$_4$:H$_2$O$_2$ = 10:1) at 120 °C for 10 minutes to remove organic impurities, then, after rinsing extensively in deionized water, immersed in an aqueous solution of 1% w/v NaOH at 90°C for 30 minutes, washed in deionized water, immersed in a 3% v/v HCl aqueous solution for 10 minutes at room temperature, and finally rinsed with copious amounts of deionized water. During the first immersion in NaOH solution, the silicon oxide bonding are hydrolyzed to form a silanol group and silanol sodium salt; the latter is then converted in a silanol group during the immersion in HCl solution [Hau et al., 2003]:

$$\equiv\text{Si-O-Si}\equiv + \text{N}a^+ + \text{O}H^- \rightleftharpoons \equiv\text{Si-OH} + \equiv\text{Si-ONa} \tag{3.1}$$

$$\equiv\text{Si-ONa} + H^+ + Cl^- \rightleftharpoons \equiv\text{So-OH} + \text{N}a^+ + Cl^- \tag{3.2}$$

Silanization was performed using two different silane molecules containing carboxy groups (triCAS and CST), shown in Figure 3.2 employing the following four different protocols:

Silanization 1P: the plasma treated samples were immersed in a 4.5 % v/v triCAS solution in water (corresponding to 973 mM) for 2 hours, at room temperature, rinsed in ultrapure water and finally cured at 80°C for 30 minutes;

Silanization 2P: the plasma treated samples were immersed in a 9.73 μM triCAS ethanol:toluene (1:100) solution at 60°C for 10 minutes, rinsed in toluene and dried under a nitrogen stream;

Silanization 3P: CST was dissolved at 12.7 mM in a ethanol:water (5:100) solution, adjusting the pH to 5 with acetic acid, and incubated 5 minutes at room temperature; the plasma treated samples were then immersed in this solution and gently stirred with an orbital shaker at 100 rpm for 30 minutes at room temperature, then rinsed with the ethanol/water solution and finally cured at 110°C for 30 minutes;

Silanization 4W: CST was dissolved at 12.7 mM in a ethanol/water (5:100) solution, adjusting the pH to 5 with acetic acid, and incubated 5 minutes at room temperature; wet treated samples were immersed in this solution and gently stirred with an orbital shaker at 100 rpm for 30 minutes at room temperature, then rinsed with the ethanol/water solution and finally cured at 110°C for 30 minutes.
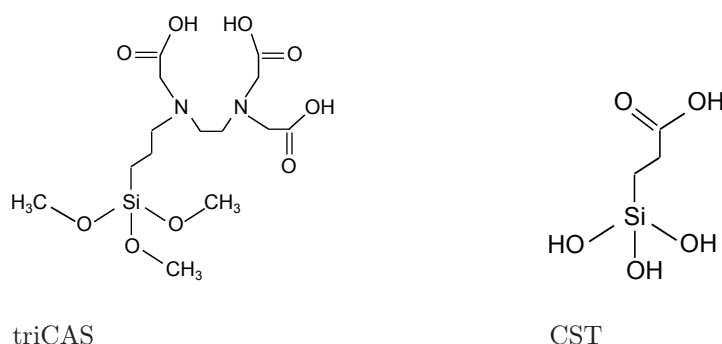
triCAS   CST

Figure 3.2: Carboxysilanes used to functionalize silicon oxide surfaces*: N-(trimethoxysilylpropyl)ethylenediamine triacetic acid* (triCAS) containing three carboxy groups, *Carboxyethylsilanetriol* (CST) terminating with one carboxy group.

3.2.2.4 Mica silanization

Freshly cleaved mica sheets were incubated in a aqueous solution of the silane of interest (APTMS or APTES) 0.1% v/v at room temperature for 10 minutes, then rinsed extensively in ultrapure water and dried in nitrogen stream.

3.2.3 Ribosome/polyribosomes deposition on plane samples

Already purified ribosomes and polysomes were deposited on plane surfaces using the following protocol.

3.2.3.1 Ribosome and Polysome purification

Polysomes were purified at BioSint laboratories (FBK). Briefly, MCF-7 breast carcinoma cells were seeded at a density of 2.5×10^4 cells/cm^2 and maintained for 3
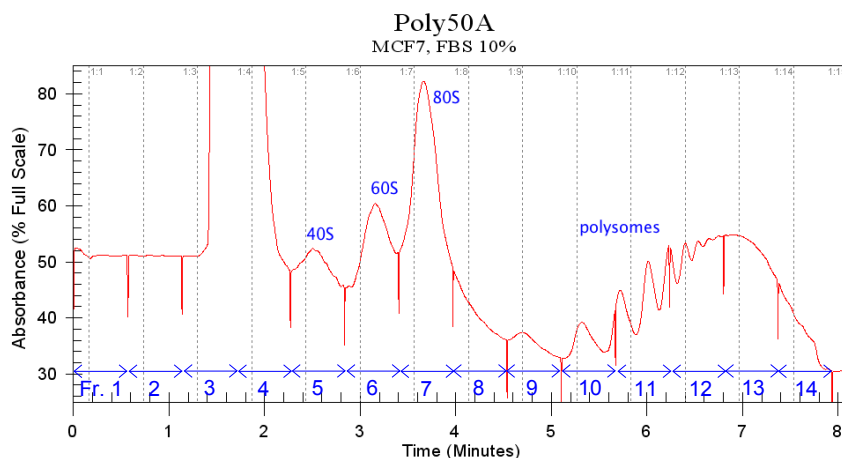
Figure 3.3: Typical polysome sedimentation profile of a MCF-7 cell lysate after sucrose gradient centrifugation and fractionation. The sample has been divided in fractions of 1 ml, marked in this profile by the spikes in the sedimentation profile. The subpolysomal fractions 5, 6, and 7 correspond to 40S, 60S and 80S particles. Several polysomal peaks, corresponding to fractions with increasing weight (fractions 10, 11, 12 and 13) are clearly visible.

days in DMEM growth medium (supplemented with 10% FBS, 2 mM glutamine, 100 units/ml penicillin, and 100 mg/ml streptomycin) at 37 °C, 5% CO_2. Once the 80% confluence was reached cells were incubated for 3-4 minutes with cycloheximide 10 µg/ml at 37°C to interfere with the translocation step during protein synthesis and block translational elongation trapping the ribosomes on the mRNA. Cells were washed with phosphate buffered saline (PBS + cycloheximide 10 µg/ml) and scraped directly on the plate with 300 µl lysis buffer (10 mM NaCl, 10 mM $MgCl_2$, 10 mM Tris–HCl, pH 7.5, 1% Triton X-100, 1% sodium deoxycholate, 0.2 U/µl RNase inhibitor (Fermentas), cycloheximide 10 µg/ml, dithiothreitol 1 mM) and transferred to an Eppendorf tube. After a few minutes of incubation on ice with occasional vortexing, nuclei and cellular debris were removed by centrifugation for 5 min at 12000 g at 4°C. The supernatant was directly transferred onto a 15–50% linear sucrose gradient containing 30 mM Tris–HCl, pH 7.5, 100 mM NaCl, 10 mM $MgCl_2$, and centrifuged in a Sorvall ultra-centrifuge on a swinging rotor for 100 minutes at 180000 g at 4°C.

In Figure 3.3 the absorbance spectrum at 254 nm of one of the utilized lysate after the centrifugation and fractionation procedure is shown. The peaks relative to the ribosome and four polysomal fractions used in the course of this work are highlighted.

The fractions have been extracted, aliquoted and flash frozen in liquid N_2 without any further dilution and stored at -80°C till the moment of use.

3.2.3.2 Ribosome deposition

Ribosomes and polysomes from MCF7 cells, pre-purified by sucrose gradient centrifugation were deposited on functionalized gold surfaces as follows:

Immediately after functionalization (or stripping off the mica, in case of the bare gold) the substrates were rinsed in DEPC water[1].

An aliquot of 20μl of ribosomal fraction, diluted typically ten times in *buffer A* , plus sucrose in the same concentration as the ribosomal fraction's was deposited on the substrates (micagold and functionalized gold samples) for 3 minutes. Then 150 μl of *deposition buffer* (Hepes 10 mM pH 7.4, 10 mM NaCl, 10 mM MgCl$_2$, 20 μm/ml cycloheximide and 3% (w/v) sucrose) was added and left $\sim$1 hour at 4°C. Eventually, the sample was rinsed gently but extensively in DEPC water (treated with 10 μg/ml cycloheximide, an antibiotic that inhibits ribosome detachment from the mRNA).

3.2.3.3 Polysome deposition

An aliquot of 40 μl of the medium-heavy polysomal fraction (e.g. fraction 12 in the Figure 3.3), diluted four times in *buffer A* plus sucrose at the same concentration that is present in the polisomal fraction was deposited on the gold samples, immediately after functionalization and let to incubate for 3 minutes. Then the samples were covered with buffer B and left $\sim$1 hour at 4°C. The sample then was rinsed very gently with the same hepes buffer, followed by DEPC water with 10 μg/ml cycloheximide, and let dry to be observed at the AFM.

3.2.4 Nucleic Acids deposition on plane samples

A) Bacteriophage λ DNA. After functionalization (described in section 3.2.2.2) the substrate have been rinsed in DEPC water, then 100 μl of λDNA 1 ng/μl in Hepes buffer (10 mM pH 7.4, 10 mM NaCl, 10 mM MgCl$_2$) were deposited on the functionalized surfaces and left 1 hour at 4°C. The sample then was rinsed gently in the same Hepes buffer and DEPC water. Samples have been then imaged by AFM after drying.

B) Human genomic DNA. DNA was purified from whole blood of healthy donors using the Puregene Gentra System purification kit (Minnesota, USA). The quantity of recovered DNA was assessed by spectrophotometry. Genomic DNA was deposited on functionalized gold samples and observed by fluorescence microscope. After functionalization (described in section 3.2.2.2) 100 μl of genomic DNA 1 ng/μl in TE buffer (Tris 10 mM, EDTA 1 mM, pH 7.5) were deposited on the functionalized surfaces and left 20 minutes at room temperature, gently

---

[1]Water intended to be used with RNA, ribosomes and polysomes was treated to inhibit RNase activity: diethylpyrocarbonate (DEPC) was diluted 1 mM in sterile water and gently stirred overnight. The water was then autoclaved at 120 °C for 20 minutes to break down the DEPC.

All solution and buffers involved in ribosome and polysome deposition experiments have been prepared with DEPC water.

orbitating at 40 rpm. The sample then was rinsed with 300 μl in ultra-pure water. Samples have been then covered for at least 5 minutes with the fluorescent dye Quant-iT ™ PicoGreen® (PG), which has a fluorescence quantum yield in its DNA bound form more than a thousandfold greater than the quantum yield in its free form [Singer et al., 1997], and observed with a fluorescence Leica DMLA microscope (Leica Microsystems, Germany) with a mercury lamp and a fluorescence filter cube L5 (Leica Microsystems, Germany). Samples were observed with a 40x magnifications objectives and measured with a cooled CCD camera (DFC 420C, Leica Microsystems, Germany).

3.2.5 Surface characterization

3.2.5.1 Morphological characterization by AFM

Surface topography was characterized by Atomic Force Microscopy. Measurements were performed with two instruments: a Cypher AFM (AsylumResearch, Santa Barbara, CA) with a flexure scanner system in closed-loop configuration, with a full range of $40{\times}40{\times}5$ μm^3 and a NT-MDT Solver-Pro (Russia) with a scanner system ranged $50{\times}50{\times}3$ μm^3.

Samples were imaged either in air or liquid environment.

Samples in air environment were analyzed in AC mode with silicon MikroMasch NSC35 cantilevers or silicon Olympus Corporation OMCL-AC 240 TS and OMCL-AC 200 TS. Samples in liquid environment, (buffer or water) were imaged with Olympus Corporation cantilevers: triangular shaped silicon nitride (TR 400 PSA and TR 800 PSA) and gold coated silicon nitride (TR 400 PB). The cantilever characteristics and nominal resonance frequencies are showed in Figure 3.4 and Table 3.2.

In all cases the tips mounted on the cantilevers are pyramidal tips with an estimated radius on the apex of 8 nm (Mikromasch NSC 35), 7 nm (Olympus AC series), 15 nm (Olympus TR PSA series) and 30 nm (Olympus TR PB series).

The lateral size of objects imaged with a non-zero tip radius are subjected to the phenomenon known as *tip-broadening*: they are the result of the convolution of the actual lateral dimension of the objects and the tip shape. This phenomenon is often modeled as in Figure 3.5 where the imaged object is a sphere with radius r, while the tip is a cone with an apex curvature of radius R.

When imaging objects whose size is of the same order of magnitude of the tip radius, as in the case of ribosomes, the measured radius r' of an object can be related to the actual radius r using the following equation:

$$r' = \sqrt{4rR} \tag{3.3}$$

where R is the tip radius.

Images of functionalized surfaces and of polysomes deposited on various substrates (mica, gold) were acquired in areas from 200 nm to 5 μm wide, and processed (line by line levelling, and rendering) with SPIP™ V3.3.4.0 (Image Metrology, Denmark, www.imagemet.com) and Gwyddion (gwyddion.net) software packages.

As a numerical parameter to assess morphological differences among samples superficial average roughness (S_a) of the surface has been adopted. It represents
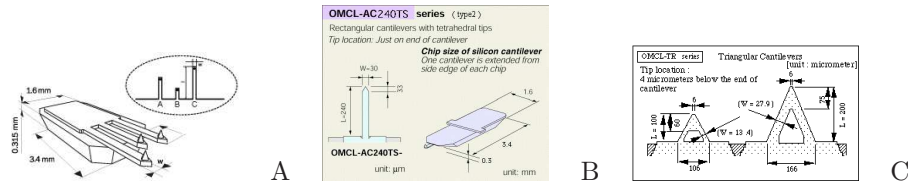
Figure 3.4: Cantilever schemes. Panel A: Mikromasch NSC 35 used for air environment AC mode analyses. The three 12-18 μm high pyramidal tips are mounted on silicon nitride cantilevers (35$\pm$3) μm wide, (2.0$\pm$0.5) μm thick and (110$\pm$5) μm (A), (90$\pm$5) μm (B) and (130$\pm$5)μm (C) long. Panel B: Olympus Corporation OMCL-AC series used for air environment AC mode. A 15 μm pyramidal tip is mounted on a 240 μm long, 30 μm wide and 2.7 μm thick silicon cantilever for the AC 240 TS series and on a 200 μm long, 40 μm wide and 3.5 μm thick silicon cantilever for the AC 200 TS series. Panel C: Olympus Corporation OMCL-TR series used for liquid environment analyses in contact and taping mode. The cantilevers thickness is 400 nm for the TR 400 series and 800 nm for the TR 800 series. The 2.9 μm pyramidal tips are mounted in proximity of the apex of the triangle. (Schematics as provided in the Mikromasch and Olympus catalogues.)

	NSC 35	
	cantilever length (μm)	resonance frequency (kHz)
A	110$\pm$5	210
B	90$\pm$5	315
C	130$\pm$5	150

	OMCL-AC	
	cantilever length (μm)	resonance frequency (kHz)
AC 240 TS	240	70
AC 200 TS	200	150

	TR 400 PSA	TR 800 PSA	TR 400 PB
	resonance frequency (kHz)	resonance frequency (kHz)	resonance frequency (kHz)
short	34	73	32
long	11	24	10

Table 3.2: Summary of lengths and typical resonance frequencies of the cantilevers used in this work. NSC 35 and OMCL-AC cantilevers were used in air environment, while TR cantilevers where used for measurements in liquid environment.
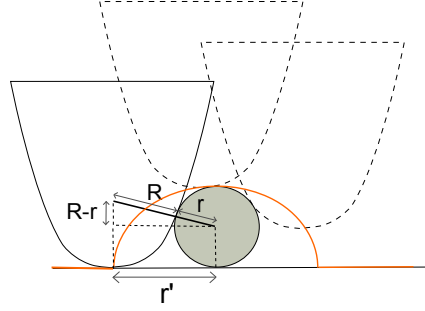
Figure 3.5: Tip-broadening effect: an object represented by a sphere with radius r measured with a tip with radius R is imaged as a emispherical shape whose radius r'. When the tip and the object radii are comparable the relation between r and r' can be obtained by simple geometrical considerations as $r' = \sqrt{(R+r)^2 - (R-r)^2} = \sqrt{4rR}$.

the mean deviation of the height of each point belonging on the surface from the height mean μ and is calculated as follows:

$$S_a = \frac{1}{MN} \sum_{i=1}^{M} \sum_{j=1}^{N} |z(x_i, y_j) - \mu| \tag{3.4}$$

with μ as:

$$\mu = \frac{1}{MN} \sum_{i=1}^{M} \sum_{j=1}^{N} z(x_i, y_j) \tag{3.5}$$

Grain analyses on ribosomes and polysomes deposited on surfaces were performed with Gwyddion and used to extract distributions of ribosome and polysome size values: height (the maximum value occurring inside the grain), projected area (the projected flat area of the grain), minimum and maximum diameter (the width and length of a rectangle circumscribing the grain), projected boundary length (the length of the grain boundary projected to the horizontal plane).

3.2.5.2 Chemical characterization by XPS

X-Ray Photoemission spectroscopy analyses were performed on gold samples with a SCIENTA ESCA 200 instrument while silicon oxide samples were analyzed with a KRATOS AXIS Ultra$^{\text{DLD}}$, both equipped with a hemispherical analyzer and a monochromatic Al Kα X-ray source (1486.6 eV) in transmission mode. Samples were inserted in the analysis chamber (at pressure of $\sim$5$\times$10^{-9} mbar) and analyzed with take-off angles relative to the sample surface of 90°, 30° and 15° corresponding to decreasing depths of analysis, with the maximum depth of about 10-12 nm at a take-off angle of 90° for both gold and silicon substrates.

Binding Energy scales were referenced to the CC/CH bond centered at 285.0 eV [Dadafarin et al., 2013]. XPS data were fitted with Gaussian peaks after Shirley

background subtraction. Gaussian peaks were integrated to obtain the relative elemental composition of the sample surface.

3.2.5.3   Chemical characterization by Tof-SIMS

ToF-SIMS spectra were acquired using a CAMECA TOF IV reflectron instrument using Ga+15KeV in the bunched mode (800 ps pulse width) of operation. All the spectra were acquired for 200 s and a 0.04 mm^2 analysis area was sampled. Operating conditions were maintained within the static regime. Charge neutralization was achieved with a pulsed low-energy (0–20 eV) electron flooding.

3.2.5.4   AFM: Force-distance measurements

Force-distance measurements have been performed with the Cypher AFM system. Force measurements have been taken between aminosilane (APTMS) treated mica substrates (obtained as explained in section 3.2.2.4) and silicon nitride gold coated cantilevers from Olympus Corporation (TR 400 PB) with a nominal spring constant of 90 pN/nm. Forces have been recorded either using cantilevers functionalized with a 21 base long double strand DNA ("DNA-tip") to measure DNA-APTMS interactions, with a 24 base long single strand RNA ("RNA tip") to measure the RNA-APTMS interactions or just after a plasma cleaning step, as a control ("Gold-tip"). The double strand DNA is formed allowing the hybridization of a 21 base long sequence (5'-TAAGTTTGAATGTCATTTCTT-3') modified at the 5' end with a cyclic dithiol group (DTPA) attached via a hydrocarbon chain linker and its complementary unmodified strand. The ssRNA is modified with the same molecule at the 5' end.

Before use, cantilevers were cleaned from contaminants by Argon plasma treatment, using a PDC-32G plasma cleaner (Harrick Scientific Corporation, New York USA) with applied power of 6.8 Watt at a pressure of 2 mbar, for 1 minute, then immersed in a 1 µM dsDNAs or ssRNAs solution in potassium phosphate buffer (1 M, pH = 6.9) for 10 minutes and then extensively rinsed with potassium phosphate buffer. In the case of the DNA, the double strand was formed in solution before the tip functionalization.

Force curves were acquired in liquid environment using a droplet cantilever holder; the pH of the solution in which the measurements were performed was varied from 4.5 to 10.5 using 20 mM ionic strength buffers, reported in Table 3.3.

Data acquisition and analysis have been performed with Igor 6.2 (Wavemetrics, Oregon, USA) Asylum Research routines.

Deflection curves were registered letting the cantilever approach the sample with a speed of 80 nm/sec, starting at 150 nm (for DNA experiments) and 100 nm (for RNA experiments) from the contact point with the sample surface, and then retreating it. Force measurement data are plotted as deflection versus position of the scanner/sample holder Z_p and then converted into force versus distance curves. The deflection Z_c is multiplied by the spring constant of the cantilever k_c to obtain forces: $F = k_c Z_c$ while the separation between cantilever and sample surface (or distance D) is the sum of the deflection and the vertical position of the scanner:

DNA tip	
pH	buffer
4.5	acetate
5.6	acetate
6.5	phosphate
7	phosphate
9.2	Tris-HCl
10.5	carbonate/bicarbonate

RNA tip	
pH	buffer
5	acetate
5.5	acetate
6	phosphate
7	phosphate
8	tris-HCl
9	carbonate/bicarbonate
10.5	carbonate/bicarbonate

Table 3.3: Buffers used in force distance AFM experiments with DNA and RNA functionalized tips.

$D = Z_c + Z_p$. In Figure 3.6 a schematics of the deflection and force versus distance curve is illustrated in panel B.

The spring constant of the cantilever can be obtained with the thermal noise fluctuation method originally proposed by Hutter and Bechhofer [Hutter and Bechhoefer, 1993]. The AFM cantilever is considered as an harmonic oscillator in equilibrium with its surroundings, which fluctuates in response to the thermal noise.

The term of this system Hamiltonian, relative to the oscillation is given by:

$$\frac{1}{2} m \omega_r \langle q^2 \rangle = \frac{1}{2} k_c \langle Z_c^2 \rangle \tag{3.6}$$

where m is the oscillator mass, q its position and ω_r its resonance frequency, and $\langle Z_c^2 \rangle$ the mean squared deflection.

According to the equipartition theorem, each term of the Hamiltonian is equal to $1/2 K_B T$, where K_B is the Boltzmann constant and T the temperature in Kelvin. In this way the spring constant k_c can be obtained by measuring solely the mean squared deflection.

$$\frac{1}{2} k_c \langle Z_c^2 \rangle = \frac{1}{2} K_B T \implies k_c = \frac{K_B T}{\langle Z_c^2 \rangle} \tag{3.7}$$

In reality however the cantilever is not an ideal oscillator, but has a solid shape: as a consequence several vibration modes are possible, and the term $\frac{1}{2} k_c \langle Z_c^2 \rangle$ is the sum of the energy of all vibration modes. The spring constant can be obtained from the first vibration mode alone applying a correction factor equal to 0.965 in case of a triangular cantilever [Butt et al., 2005], so:

$$k_c = \frac{K_B T}{\langle Z_1^2(L) \rangle} \tag{3.8}$$

where $\langle Z_1^2(L) \rangle$ is the mean squared deflection relative to the first vibrational mode, dependent on the length of the cantilever L.

In practice, a force-distance measurement has been taken to calibrate first the sensitivity of the detector, evaluating the proportionality coefficient in the linear zone of a deflection-versus-Z scanner position curve (zone c in Figure 3.6, Panel B). Then the power spectra in the frequency domain has been recorded. The first

vibration mode relative to thermal noise oscillations can be fitted with a Lorentzian curve centered around the resonance frequency ω_r [Hutter and Bechhoefer, 1993], whose integral has been used to estimate the spring constant.

Force-distance curves were recorded both during the approach and the retraction of the cantilever from the sample surface (see Figure 3.6, panel C for an example) over hundreds of points, and collected as "Force maps". At every pH at least two maps in different sample place, each containing 400 force curves, were acquired, each typically over areas of $500{\times}500$ nm^2 for DNA experiments and 50×50 nm^2 for RNA experiments. An example of one of such maps is shown in Figure 3.6: the false-color scale indicates the intensity of the adhesion between tip and surface, calculated as the difference between the minumum value recorded in the retraction curve and the mean value of the non-contact region (zone a in the schematics in Figure 3.6, panel B).

Finally force histograms have been computed from every map, using a bin width of 3 pN and fitted with Gaussian curves.

3.2.6 Microdevice

3.2.6.1 Silicon/Pyrex microdevices fabrication and functionalization

Microdevices were produced by Olivetti I-Jet, starting from a 6" silicon wafer. In Figure 3.7 schematics and a 3D rendering of the microdevice are shown. Microchannels were patterned in the silicon oxide via Reactive Ion Etching (RIE) technology; the microchannels walls were then passivated by a 100-160 nm thick silicon oxide coating, grown by Low Pressure Chemical Vapour Deposition (LPCVD). The channels are coiled shaped, 100 μm deep, 500 μm wide and 50 cm long, containing a volume of 25 μl, with a total channel surface of 11 cm^2. The microdevices were sealed by anodic bonding between the silicon substrate and a Pyrex cover, carryng two holes produced by sand blasting for fluids inlet and outlet. Finally each wafer was diced in 12 microdevices of $3{\times}3$ cm^2 area.

The microdevices were then extensively washed with RNase-free water and autoclaved for 20 minutes at 120°C before functionalization with carboxyl containing silanes (triCAS and CST). The silanization was performed following protocols similar to those used for silanization of plane silicon oxide samples (explained in section 3.2.2.3):

Silanization M1: a solution of triCAS 973 mM in RNase-free water was injected in the microdevice for 2 hours, at room temperature. The solution was then removed and replaced with RNase-free water for three times, the microchannels were dried with a nitrogen stream and the microdevice incubated at 80°C for 30 minutes.

Silanization M2: a solution of triCAS 9.73 μM in ethanol/toluene (1:100) was heated at 60°C, injected in the microdevice and left for 10 minutes; then three washing steps with toluene were performed and the microchannels were dried with a nitrogen stream;
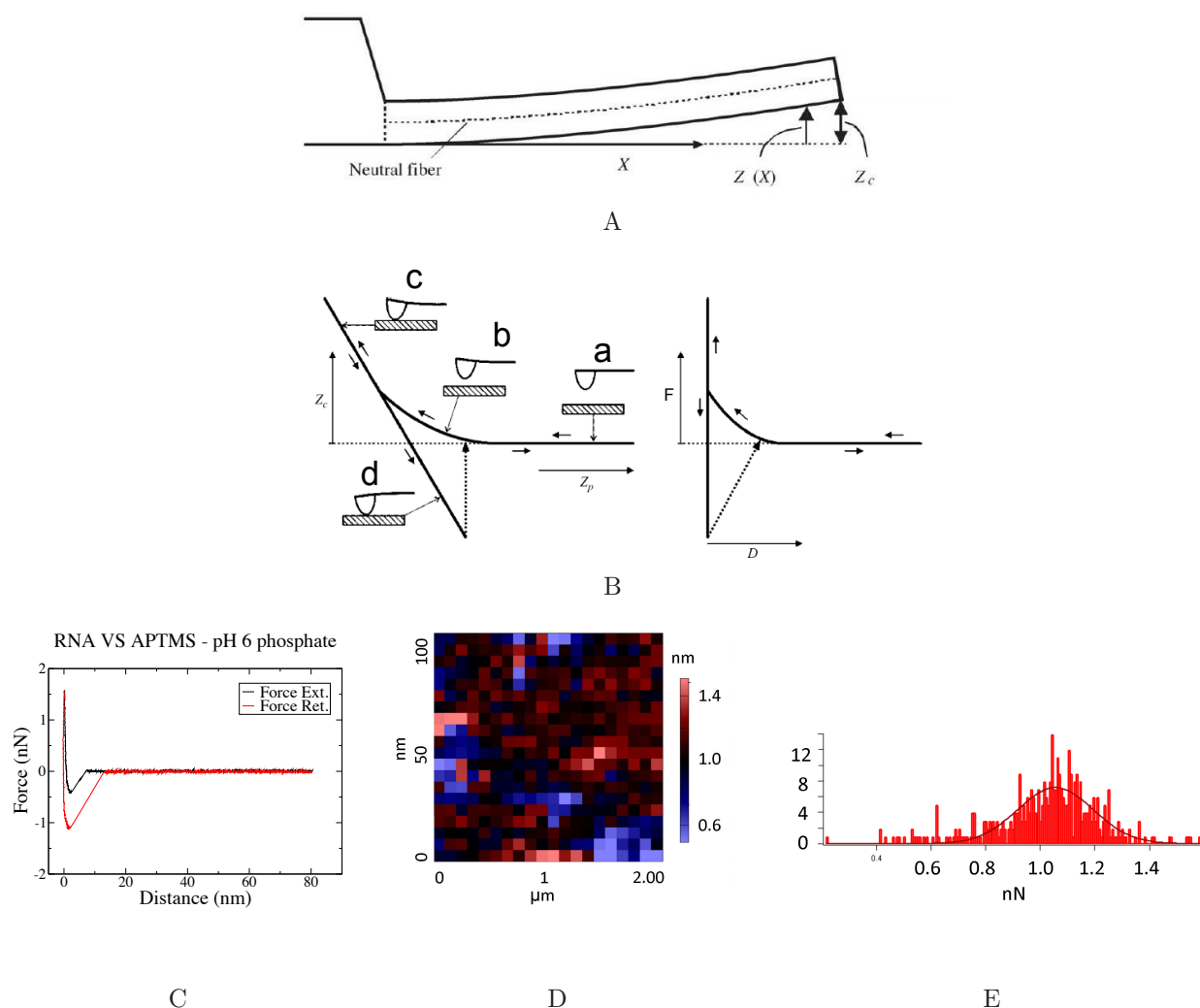
Figure 3.6: Panel A: schematic side view of a cantilever with a force applied at its end (from [Butt et al., 2005]). X is the horizontal coordinate originating at the basis of the cantilever, Z(X) is the cantilever deflection at a the position X, Zc is the cantilever deflection at its end. Panel B: on the left, schematics of a typical deflection versus Z piezo position curve (Zc versus Zp). Four schemes are shown depicting the cantilever behavior in four regimes: a. the cantilever is in non-contact regime, where the deflection Zc is zero, b. the cantilever is in a repulsive regime but not yet in contact with the sample, c. the cantilever is in contact but repulsive regime with the sample and d. the cantilever is in contact and attractive regime with the sample. On the right the corresponding Force versus Distance plot (F versus D), where the deflection Zc has been converted into Force after determining the spring constant of the cantilever and D = Zc+Zp (Adapted from [Butt et al., 2005]). Panel C: a typical Force versus Distance curve obtained in this work. In black the curve recorded during the approach of the cantilever and in red the retraction curve. Panel D: a typical force map , taken on an area of 100×100 nm^2, samplingt 400 points, with a RNA tip in phosphate buffer at pH 6. The false color scale indicates the intensity of adhesion calculated as the difference between the minimum and the mean value of the non contact region of the retraction curve. (region a in the schematics of panel B). The curve in Panel C corresponds to the third line from the bottom, fifth point from the left side. Panel E: The Force histogram extracted from the map in panel D.
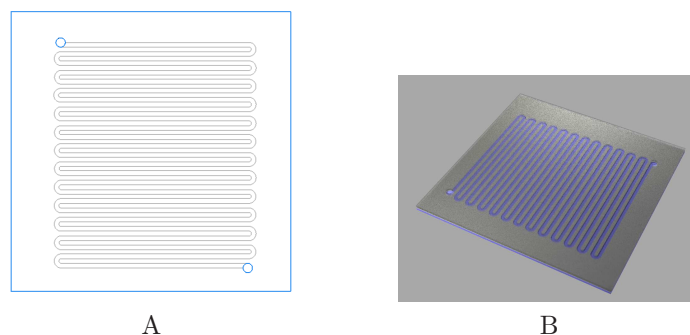
Figure 3.7: The silicon/Pyrex microdevice used in the course of this work: schematics (Panel A) and 3D rendering (Panel B). The microdevice surface is 3×3 cm. Dimensions of the microchannel are: 100 μm depth, 500 μm width and 50 cm long. Volume contained: 25 μl.

Silanization M3: CST was dissolved at 12.7 mM in ethanol/RNase-free water (5:100) pH 5 with acetic acid, and incubated 5 minutes at room temperature; the solution was injected in the microdevice for 30 minutes at room temperature, then the microdevice was washed with the ethanol/RNase-free water solution three times, the microchannels were dried with a nitrogen stream and the microdevice incubated at 110°C for 30 minutes.

Silanization M4: "piranha solution" (H_2SO_4:H_2O_2 = 10:1) was injected in the microdevice at 120 °C for 10 minutes to remove organic impurities, then, after washing 3 times with deionized water, immersed in a solution of 1% w/v NaOH in RNase-free at 90°C for 30 minutes, washed in RNase-free water, immersed in a 3% v/v HCl in RNase-free water for 10 minutes at room temperature, and finally rinsed with copious amounts of RNase-free water. CST was dissolved at 12.7 mM in ethanol/RNase-free water (5:100) pH 5 with acetic acid, and incubated 5 minutes at room temperature, then injected in the microdevice stirred with an orbital shaker at 100 rpm for 30 minutes at room temperature; three washing steps with ethanol/RNase-free water solution were performed, the microchannels were dried with a nitrogen stream and the microdevice incubated at 110°C for 30 minutes.

3.2.6.2 Extraction of RNA from polysome by Silicon/Pyrex microdevice

The Silicon/Pyrex microdevice has been used to extract RNA from MCF-7 polysomal fractions previously purified with sucrose gradient centrifugation (see section 3.2.3.2 for details). The freshly silanized microdevices were washed with RNase free water before incubation of polysomes.

The polysomal fractions 10, 11, 12, 13 and 14 (see polysomal sedimentation profile in Figure 3.3) were pulled together and injected in the silanizated microdevices, to be incubated for 1 hour at 4°C. After incubation the unbound sample was

collected and replaced with TE buffer (10 mM Tris-HCl, 1 mM EDTA, pH 7.5 made with RNase-free water). The chip was heated at 50°C for 10 minutes to release the mRNA from the ribosomes adherent to the microchannels walls. The TE containing the extracted RNA was then collected and analyzed to evaluate quantity, class (whether mRNA, miRNA or rRNA) and quality of the RNA extracted.

Chapter 4

Results and Discussion

4.1 Introduction

This work is aimed at developing and studying a microsystem for the purification of polysomes and extraction of the associated mRNA. Polysome isolation from cell lysate will be obtained within a microdevice, whose surfaces will be opportunely treated to enhance polysome adhesion.

The strategy chosen to allow and enhance selective polysome adhesion to the microdevice surfaces takes advantages on the fact that ribosomes, as well as nucleic acids expose many electrical charges towards the environment, due mainly to the negatively charged phosphate groups in the DNA and RNA backbone carbon chain and to many charged proteins forming the ribosome.Therefore, in the course of this work, surface modifications aimed mainly to endow the microdevice surfaces with a suitable charge distribution are investigated. The goals are: a) to investigate functional surfaces respect to their ability toward polysome adhesion and b) to characterize surfaces able to adhere or repel nucleic acids (namely mRNA) to be able to direct their adhesion to a specific region of the microdevice.

4.2 Ribosomes and Polysomes adhesion on Self Assembled Monolayers.
Gold substrates

Self-Assembled Monolayers (SAMs) of organic molecules constitute a convenient method to modify solid substrates superficial properties, in particular the surface chemistry, without drastically alter the substrate surface morphology. Choosing opportunely the nature of the molecule forming the SAM, and most of all its terminal group, it is possible to obtain surfaces exposing a wide range of functional groups. One of the most widely studied and well-known SAM systems is the one formed by thiols on gold (111). This system has been chosen as a model to study the adhesion of ribosomes and polysomes on gold surfaces with different kinds of

chemical functionalizations.

Four alkanethiols have been chosen to tailor mainly the charge distribution of the gold substrate in a range going from negative to neutral to positive charges, and the hydrophobicity property of the surfaces: 11-Mercaptoundecanoic acid (MCOOH), 11-Mercapto-1-undecanol (MOH), 11-Amino-1-undecanethiol (MNH_2) and 1-Undecanethiol ($M-11CH_3$). All these thiols have the same length (11 carbon atoms) and differ only for the terminal group, that will be exposed on the newly formed SAM surfaces: respectively a carboxyl acid, an hydroxyl, an amino and a methyl group. In environment with a pH higher than $\sim$5 the gold surfaces modified with a SAM formed by MCOOH expose the carboxyl groups mostly in their deprotonated form $-COO^-$ conversely gold modified with a MNH_2 SAM expose protonated amino groups $-NH_3^+$ at pH lower than $\sim$ 9, thus endowing this two surfaces with a neat negative and positive charge distribution at physiological pH. MOH and $M-11CH_3$ have been adopted as neutral surfaces at physiological pH, but with a marked hydrophilic and hydrophobic behavior.

In this chapter a morphological and chemical characterization of SAMs of alkanethiols on ultra-flat gold samples will be first presented. The capability of this surfaces to attract and retain polysomes from a solution will be evaluated with AFM analyses, starting from polysome samples previously purified with traditional methods (sucrose gradient centrifugation) as well as the eventual degree of morphological degradation of the polysomes, in order to determine the most promising kind of functionalization to be employed in a purification system.

These result will be then transferred on materials more commonly used for microsystems manufacturing, such as silicon oxides, glass and polymers (PDMS) that, as any hydroxylated substrate, can be functionalized using SAMs formed by silanes. A characterization of the adhesion of polysome on silanized silicon oxide plane samples will be carried out and finally a proof of principle of a silicon/Pyrex microdevice will be reported.

4.2.1   Characterization of gold substrates

One of the most widespread techniques of obtaining flat gold surfaces is by vapor deposition of gold onto a flat substrate, such as mica muscovite, or silicon slides. Although suitable for the deposition of biomolecules the mean roughness of this kind of surfaces (typically some nm) may be too high to be efficiently employed to image with AFM and characterize the morphological properties of proteins, nucleic acids or even larger complexes such as ribosomes. In 1993 Hegner and coworkers [Hegner et al., 1993b] developed an alternative method for preparing ultra-flat gold surfaces: gold is evaporated on mica templates and stripped off it immediately before use, uncovering the gold surface that was in contact with mica. The resulting surfaces consist of atomically flat terraces, with size varying from hundreds of nanometers to micrometers, whose shape follows its mica (former) counterpart, thus presenting a quite low roughness (1.8-2 Å). Observed by Scanning Tunneling Microscope gold samples prepared by this procedure are known to show typical features of a (111) gold plane with lattice constant 0.288 Å [Hegner et al., 1993a].
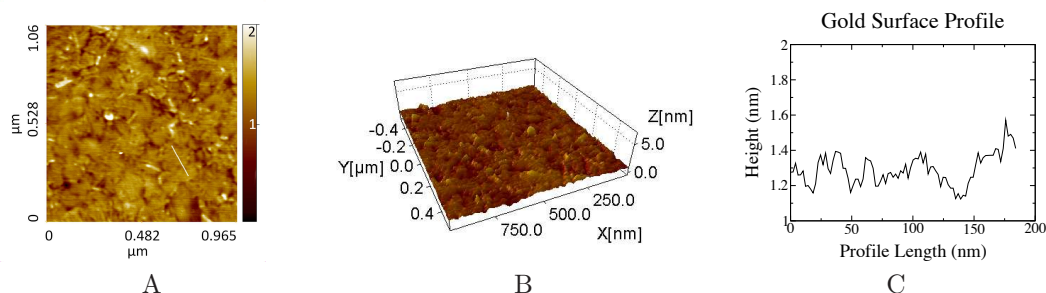
Figure 4.1: 1×1 μm^2 area observed with AFM of a gold surface stripped from mica (panel A) and its 3D reconstruction (panel B). The average roughness is S_a = (0.15±0.01) nm. Panel C shows the profile of the surface along the white line in panel A.

Furthermore, the mica template protects the gold surfaces before their use, which can then be produced in batches and stored for months.

Flat surfaces of gold stripped from a mica muscovite template prepared with this procedure (reported in section 3.2.2.1) were employed in the course of this work after an assessment of their morphological and chemical characteristics.

Morphology of the samples has been evaluated with atomic force microscopy: samples obtained with this procedure present a surface with large areas (from hundreds of nanometers to a few μm in size) of flat surface: one typical example is shown in Figure 4.1. The surface average roughness S_a calculated on several samples is equal to (0.15±0.01) nm, five times greater than the average roughness obtained on mica sheets in the same measuring conditions (0.04±0.02 nm), but still considerably lower than a gold surface prepared by evaporation in the same conditions ($\sim$ 1.71 nm) and suitable for observation of ribosomes, and nucleic acids.

The chemical quality of the exposed gold can be assessed through several methods.

X-ray photoemission Spectroscopy (XPS) can be employed to estimate the elemental composition of the outer layers of a sample surface. The thickness of the analyzed layer depends on the nature of the analyzed substrate and can be varied modifying the electron take-off angle θ relative to the surface. The maximum depth of analysis is reached at take-off angles of 90°, and for gold it corresponds to a depth of $\sim$10-12 nm. Table 4.1 shows the chemical composition of a sample of gold stripped from mica expressed as percentage of the three most abundant elements. Carbon (C 1s) and oxygen (O 1s) come from contaminants adsorbed on the surface, as can be inferred from the fact that their amount is greater for a lower take-off angle, i.e. reducing the depth of the analysis.

A small degree of carbon contamination is still acceptable for the SAM formation of thiols, because these are able to displace most adventitious material, thanks to their high affinity for gold. A more practical point is to determine whether there are still regions covered with mica.

Take-off θ	Au 4f %	C 1s %	O 1s %
90°	81.8	16.9	1.3
15°	42.5	53	4.5

Table 4.1: Elemental composition of gold stripped from mica determined by XPS analysis performed at take-off angles 90° and 15°.

Analyses performed with a Time of Flight - Secondary Ions Mass Spectrometer (Tof-SIMS) on gold stripped from mica confirm the presence of a small amount of hydrocarbon contaminants well as the complete absence of ionic components typical of mica muscovite, such as aluminum, potassium and silicon, from the gold sample stripped from mica (in Figure 4.2 and Figure 4.3 the intensity counts for positively charged ions for mica and gold stripped from micarespectively).

Finally, an analysis performed with a SEM-EDX system (Energy-Dispersive X-ray spectroscopy conjugated with a Scanning Electron Microscope) allows a morphological visualization of the sample surface conjugated with an elemental composition analysis. The surface of gold stripped from mica appears to be clean and pure gold, presenting, in fact, only a few mica fragments, several micron wide, scattered near the border of the sample. In Figure 4.4 an example of such a fragment is shown.

4.2.2 Functionalized gold surface characterization

4.2.2.1 Morphology of functionalized gold: AFM characterization

The gold samples were treated as illustrated in section 3.2.2.2 to allow the formation of self-assembled monolayers constituted by four different alkanethiols: MOH, MCOOH, MNH_2, M-11CH$_3$. The functionalized samples have been characterized then, both from the morphological and chemical point of view with the AFM and XPS techniques respectively. In Figure 4.5 3D-renderings of 2×2 μm areas of the gold surfaces functionalized with the four alkanethiols are shown.
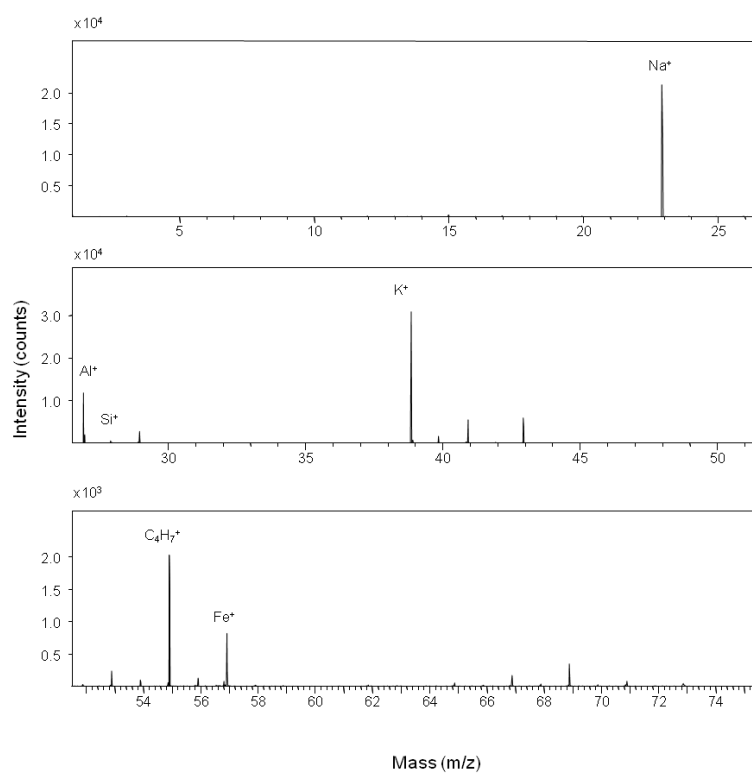
Figure 4.2: Tof-SIMS analysis of mica positive ions. The typical elements present in mica, Al^+, K^+, and Na^+ are concentrated in the range between 20 and 40 m/z.
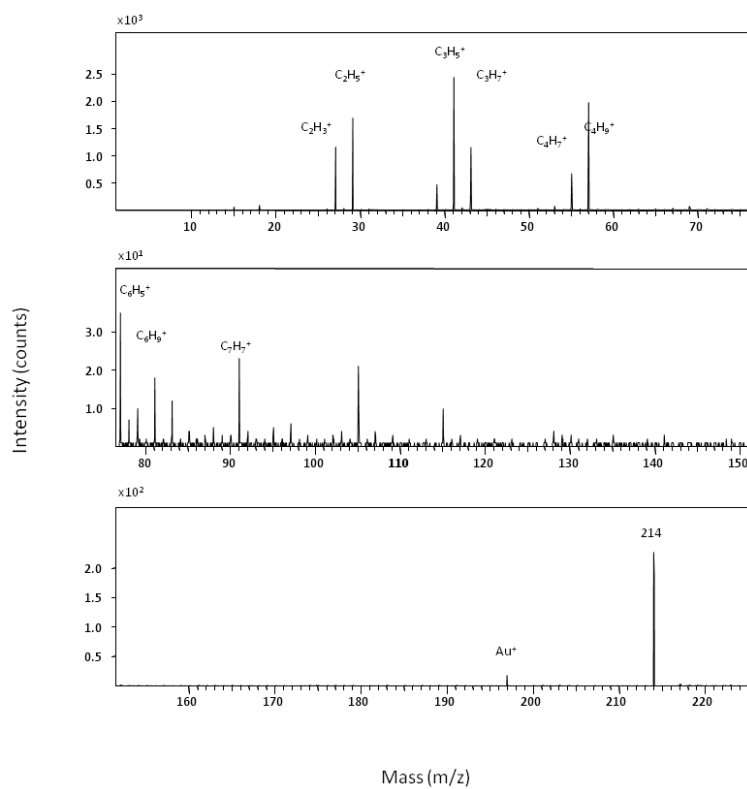
Figure 4.3: Tof-SIMS analysis of gold stripped from mica. The typical elements present in mica, Al^+, K^+, and Na^{++} (in the range between 20 and 40 m/z) are absent.
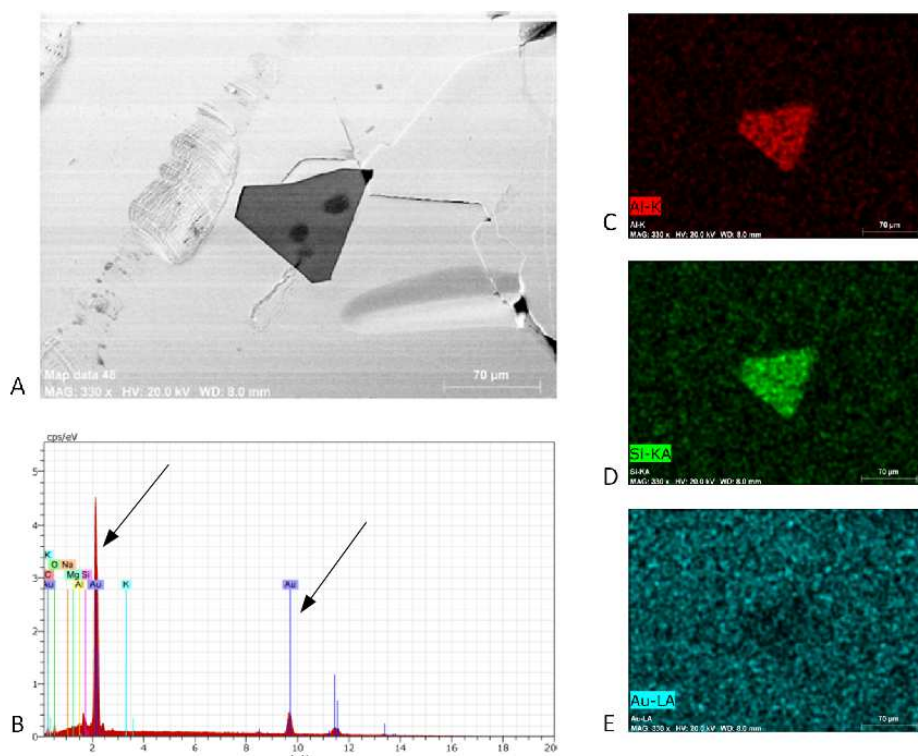
Figure 4.4: Gold stripped from mica at the SEM-EDX. Panel A: SEM image of a sliver of mica on the gold surface. Panel B shows the chemical composition of the surface, where gold (arrow) is clearly the prevalent component. Panel C, D and E show the signal associated with aluminum and silicon, the main elements composing mica, and gold, respectively for the mica fragment showed in panel A.
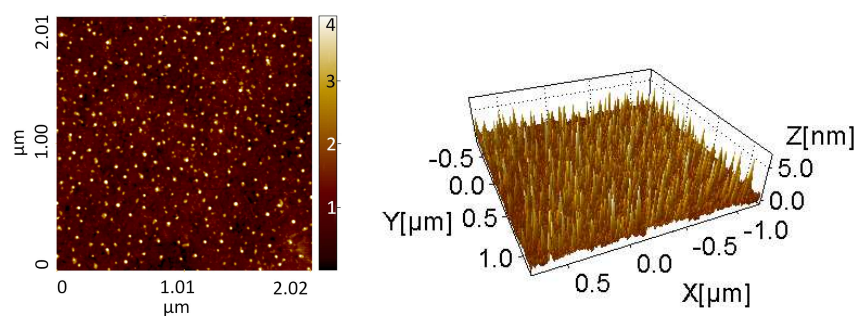
A. MOH
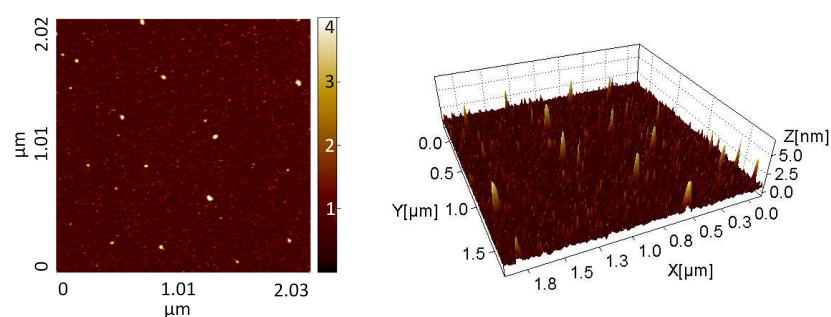
B. MCOOH
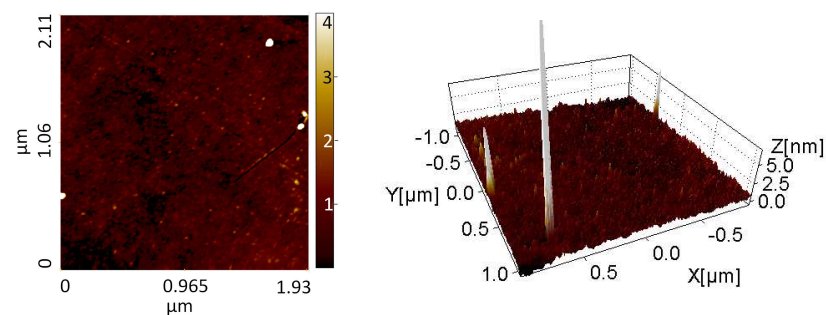
C. MNH$_2$
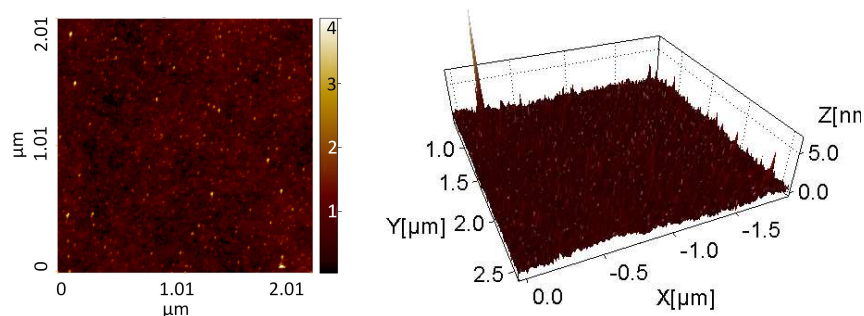
D. M-11CH$_3$

Figure 4.5: AFM images and the corresponding 3D reconstructions of gold surfaces functionalized with MOH (A), MCOOH (B), MNH$_2$ (C), M-11CH$_3$ (D). All samples have been incubated 24 hours in a 1 mM solution in ethanol of the corresponding thiol except from the MCOOH, that has been incubated for a longer time (65h). Images represent areas 2 μm wide acquired with Cypher instrument (AsylumResearch, Santa Barbara, CA) (A and B) and NT-MDT Solver-Pro (Russia) (C D) in air environment.

Surface Average Roughness
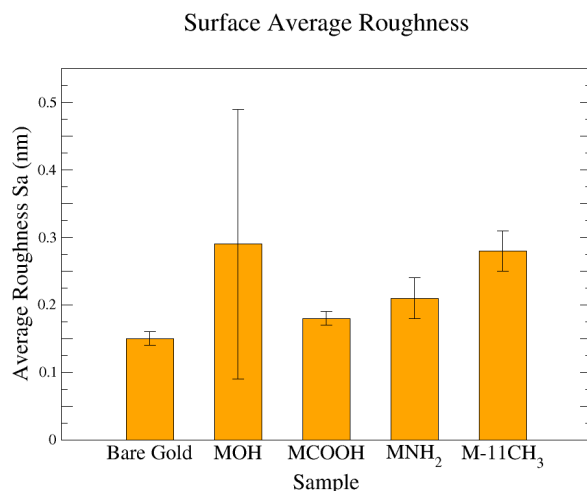
Figure 4.6: Average roughness for bare gold and functionalized gold samples.

The functionalizations indeed modify the original gold substrate morphology. The four functionalized surfaces (panel A, B,C and D) present structures with an height of 1-2 nm, with some occasional higher peaks, completely absent in the gold samples stripped from mica (panel E, F). However the average roughness of the surfaces (shown in Figure 4.6) is not drastically modified.

All the functionalized samples show a similar value of roughness, with average values under 0.3 nm, only slightly increased compared to the bare gold. This confirms that the functionalization did not change significantly the gold surface morphology suggesting the creation of a uniform, if not complete, thin layer.

The S_a value of MCOOH samples in Figure 4.6 refers to SAM obtained with an incubation time to 65 hours, while the other SAMs have been obtained with 24 hours of incubation time. MCOOH functionalized samples held in incubation for 24 hours showed a higher roughness ($S_a = 0.8$ nm). Judging from detailed AFM images of this kind of surface (Figure 4.7, Panel A) this feature seemed to arise from an incomplete SAM formation. In an attempt to allow MCOOH carbon chains enough time to arrange themselves the incubation time has been increased, until values of roughness similar to the other thiol SAMs were reached, resulting in an incubation times of ∼65 hours (Figure 4.7, Panel B). The difference in height between the lower and higher areas in the two images are 1.35 and 1.29 nm respectively, both are compatible with the theoretical length of a MCOOH molecule (1.58 nm [Albayrak and Danışman, 2013]), and consequently with the presence of a submonolayer of MCOOH molecules.
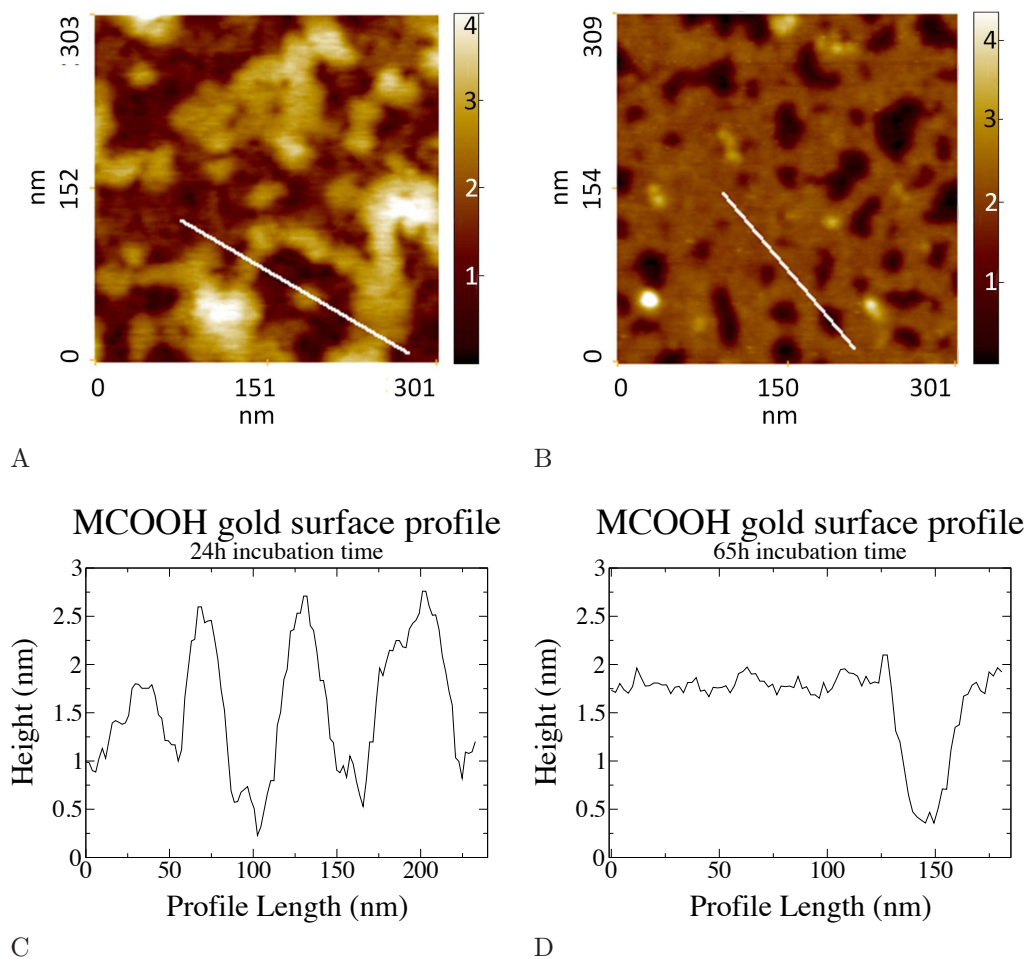
Figure 4.7: Detailed AFM images from a MCOOH functionalized gold surface, incubated in the solution of MCOOH thiol for 24 (A) and 65 (B) hours where the SAM shows a higher coverage of the surface. The average roughness of the two imaged surfaces are 0.7 nm and 0.33 nm. In Panel C and D the profiles along the white lines in images A and B respectively.

Although still not perfectly complete, the 65 hours incubation MCOOH SAM (showed in panel B, Figure 4.7) has reached a coverage of 89.9% of the surface compared with the 56.1% coverage of the 24 hour incubation SAM (showed in panel A) and has been deemed sufficiently complete and smooth to allow successive analyses and use with ribosomes and polysomes along with the MOH, MNH$_2$ and M-11CH$_3$ functionalized gold surfaces.

take-off $\theta = 90°$					
Sample	O 1s %	C 1s %	Au 4f %	N 1s %	S 2p %
bare gold	*9.4*	*26.8*	*63.8*	-	-
MCOOH	12.4	28.4	22.3	-	9.8
MNH$_2$	15.2	45.2	30.0	4.0	5.6
MOH	5.8	34.3	56.6	-	3.3
M-11CH$_3$	6.6	32.6	56.3	-	4.4

take-off $\theta = 30°$					
Sample	O 1s %	C 1s %	Au 4f %	N 1s %	S 2p %
bare gold	*6.2*	*36.6*	*57.2*	-	-
MCOOH	14.8	65.9	7.4	-	11.9
MNH$_2$	23.5	56.2	10.7	4.2	5.4
MOH	8.9	41.4	44.5	-	5.1
M-11CH$_3$	5.1	54.4	34.5	-	6

Table 4.2: Chemical composition of bare gold and functionalized gold determined by XPS. Template stripped gold and MCOOH, MNH$_2$, MOH and M-11CH$_3$ functionalized gold samples have been analyzed for oxygen (O 1s), carbon (C 1s), gold (Au 4f), nitrogen (N 1s) and sulfur (S 2p) and their relative percentage determined by integrating the respective curves.

4.2.2.2 Surface chemistry of functionalized gold: XPS characterization

Immediately after functionalization, the gold samples have been analyzed by XPS to asses the chemical composition of the modified surfaces. In Table 4.2 the elemental composition expressed in relative percentages is shown.

XPS analyses confirm the presence of a layer of thiols on the samples surfaces. The proportion of elements come close to the expected ratios between elements composing the molecules of alkanethiols used to functionalize the samples. In particular in the case of the MNH$_2$ functionalized sample, the data taken at an angle θ of 90° show an amount of C almost exactly 11 times higher than the quantities of N and sulfur (they are in proportion 11.3 to 1 to 1.4 respectively) reflecting the composition of the molecule (11 atoms of carbon for every atom of sulfur and nitrogen). This sample showed also a very high quantity of oxygen, 3.8 times greater than nitrogen.

The other samples show in general a slightly higher quantity of oxygen and sulfur than the amount expected from the molecules.

Of particular interest are the core lines of C 1s taken at θ=30°, showed in Figure 4.8 and Figure 4.9

All sample C 1s core line show the peak relative to the CC/CH bond, set at 285 eV. C 1s core line for MCOOH (panel B in Figure 4.8) shows the presence of two more peaks at 286.7 eV and 289 eV, representing respectively the CO ($\sim$286.5) and O-C=O ($\sim$289 eV) bonds[Chuang and Lin, 2007, Lee et al., 2010]. The ($\sim$286.5)
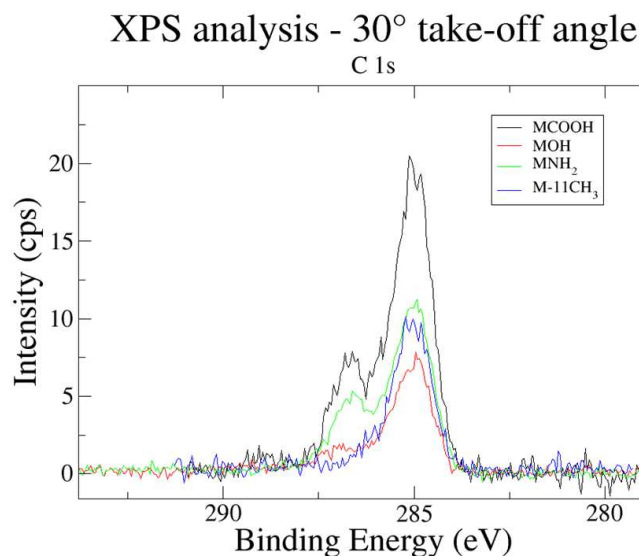
Figure 4.8: XPS core line C 1s for the four functionalized gold surfaces (MCOOH in black, MOH in red, MNH$_2$ in green and M-11CH$_3$ in blue).

peak (attributed to the presence of CO/CN bonds) is also observed in the core lines of MOH and MNH$_2$ functionalized gold (panels C and D, Figure 4.8). A small contribution at this binding energy is observed in the M-11CH$_3$ core line, although only as a shoulder of the main CH peak. This peak intensity is higher than expected, in particular in the MCOOH and MNH$_2$ functionalized samples. In the first case, this peak should be not present, and thus, be similar to the M-11CH$_3$ core line in this region; in the second case the contribution due to the CN bond, is expected to be similar in intensity to that observed on the MOH sample (due to the CO bond in this case). The MNH$_2$ sample shows in its S 2p curve (shown in Figure 4.10 with the MOH S 2p curve for comparison) the noticeable presence of oxidized sulfur species (B.E. $\geq$166 eV [Castner et al., 1996]), along with the double peak at $\sim$ 163.5 eV and 161.8 eV representing respectively the unbound thiol and Au-bound thiol [Dadafarin et al., 2013, Chuang and Lin, 2007, Castner et al., 1996].

4.2.2.3   Surface chemistry of functionalized gold: Tof-SIMS analysis

A mass spectrometry analysis performed on the four functionalized surfaces works as a further confirmation of the presence of thiols linked to the gold surfaces. In Figure 4.11 the negative ions region for MCOOH (panel A), MOH (panel C) and M-11CH$_3$ (panel D), and positive ions region for MNH$_2$ is shown. Peaks marked with [M-H]$^-$ and [M-H]$^+$ indicate the molecular ions for each thiol:
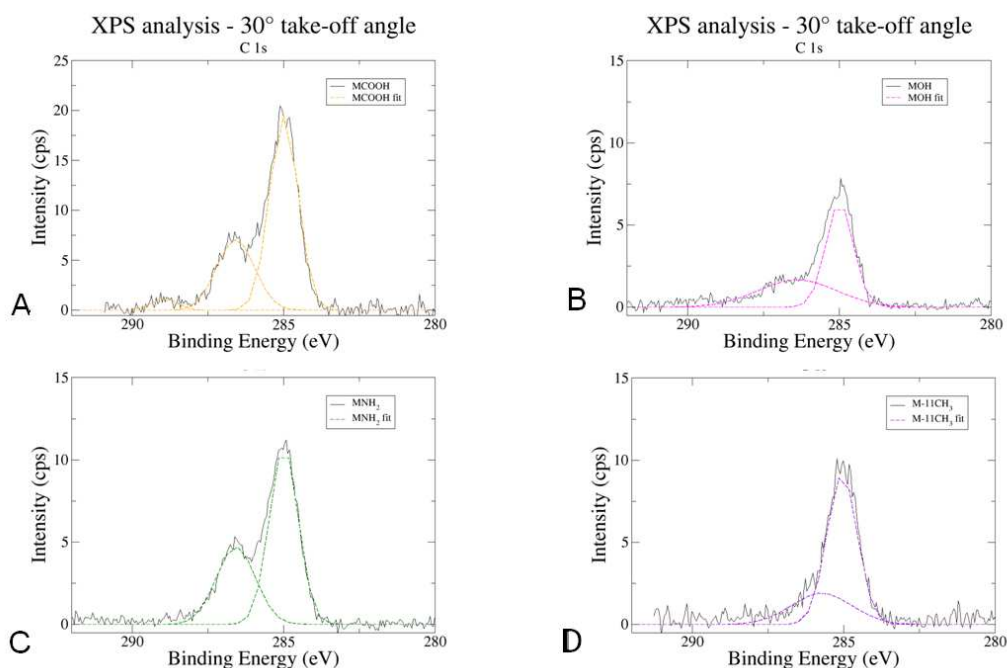
Figure 4.9: MCOOH (A), MOH (B), MNH$_2$(C) and M-11CH (D) C 1s core line fitted with gaussian curves.
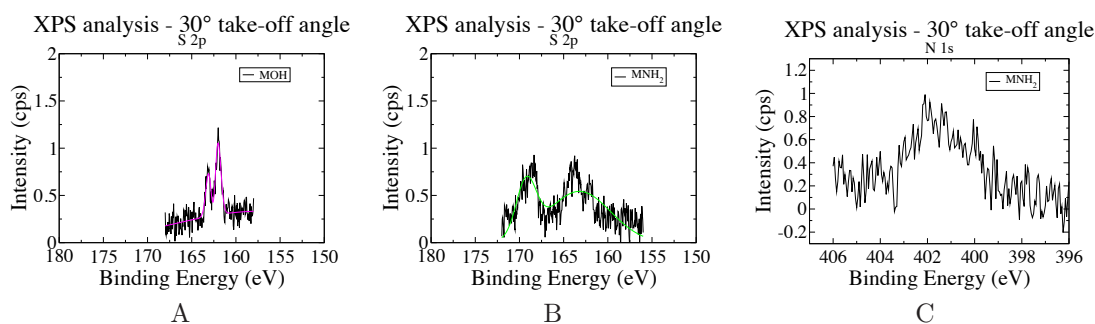
Figure 4.10: Panels A and B: XPS core line S 2p for MOH (A) and MNH$_2$ (B) functionalized gold. MOH gold shows the double peak centered around $\sim$ 163.5 eV and 161.8 eV corresponding to unbound and Au-bound sulfur groups typical in SAM of alkanethiols on gold, while MNH$_2$ presents an additional peak centered at 169.2 representing oxidized sulfur species. Panel C shows the core line N 1s for MNH$_2$.

$$M = \begin{cases} HS-(CH_2)_{10}-COOH \\ HS-(CH_2)_{11}-NH_2 \\ HS-(CH_2)_{11}-OH \\ HS-(CH_2)_{10}-CH_3 \end{cases} \quad for \quad \begin{matrix} MCOOH \\ MNH_2 \\ MOH \\ M-11CH_3 \end{matrix} \quad surfaces$$

and

$$M^* = \begin{cases} {}^-O_3S-(CH_2)_{11}-OH \\ {}^-O_3S-(CH_2)_{11}-CH_3 \end{cases} \quad for \quad \begin{matrix} MOH \\ M-11CH_3 \end{matrix} \quad surfaces.$$

along with numerous combinations of thiol-Au^+ and thiol-Au^- ions expected in the presence of SAMs of thiols on gold.

COOH(CH$_2$)$_{10}$SH − SAM on Au − Negative Ions
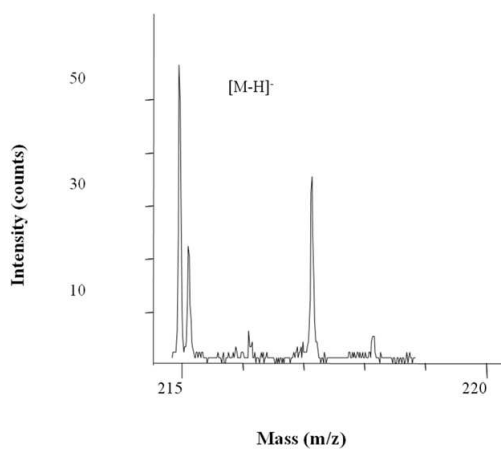
A

NH$_2$(CH$_2$)$_{11}$SH − SAM on Au − Positive Ions

B
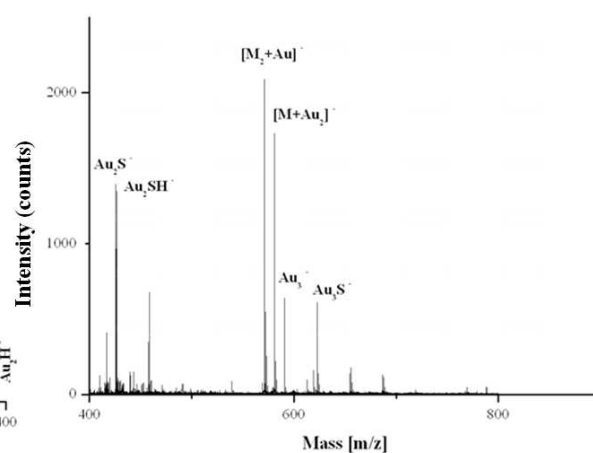
Figure 4.11: Tof-SIMS analysis of gold functionalized with MCOOH (A), MNH$_2$ (B), MOH (C) and M-11CH$_3$ (D). The images shows the ranges where ions composed by the alkanethiols residuals are present.

fraction	H$_1$(nm)	H$_2$(nm)	F$_1$	F$_2$
60S	5.3	10.7	0.748	0.252
80S	5.2	11.8	0.402	0.598

Table 4.3: Position (H$_i$) and fractional area (F$_i$=A_i/A_1+A_2 , where A$_i$ is the area of the ith gaussian) of the two gaussian used to fit the height data shown in Figure 4.12

4.2.3 Ribosome adhesion to gold and functionalized gold surfaces

The four modified surfaces characterized so far expose to the environment different chemical properties. In order to asses the varying capability of the four functionalizations to effectively extract polysomes from a liquid sample and trap them, the four modified surfaces have been tested with aliquots of ribosomes and polysomes previously purified with traditional methods (see section 3.2.3.2 for preparation details).

At first ribosomes extracted by MCF-7 breast cancer cells have been deposited following the procedure described in Section 3.2.3.2 on gold and the functionalized gold samples described in the previous section and their adhesion on such surfaces assessed by AFM analyses, evaluating both the number density and morphological parameters of the adherent objects.

These have been compared with a reference, in order to asses the conservation or degree of eventual degradation ribosomes incur in contact with the different functionalized surfaces. As reference, the ribosome fraction (80S) and the previous one (corresponding to 60S particles) have been deposited on a surface used in literature for AFM polysome imaging (mica treated with Ni^{2+}, [Mikamo et al., 2005]) and the morphological properties (height, minimum and maximum lateral size and aspect ratio - the ratio between maximum and minimum lateral sizes) of the deposited objects have been used as standard to evaluate the integrity of the ribosomes deposited on bare and functionalized stripped gold. Both the 60S and the 80S fractions present a bimodal distribution of the height (see Figure 4.12), with one peak at around 5 nm height and the second one around 11 nm , but their relative abundance differs in the two samples. In the 60S fraction the most abundant component correspond to the 5 nm height peak, while the opposite is true for the 80S fraction, as shown in Table 4.3. Actually, being the two fractions not completely separated in the sucrose gradient (see 3.3), the presence of both 60S and 80S particles is expected in the two samples. We attributed then the 5 nm height peak to 60S particles and the 11 nm height peak to 80S particles. These values are in very good agreement with AFM published data on eucaryotic ribosomes [Fritzsche and Henderson, 1998], but show a decrease respect to their crystallographic values (see data reported in Table 4.4), an effect that is expected due the drying process.

To obtain a reference 80S ribosomal particle, as visualized with AFM in air, we then applied a cutoff filter of 8.2 nm to the AFM images of the 80S fraction deposited on mica treated with Ni^{2+} to account only for the 80S particles and
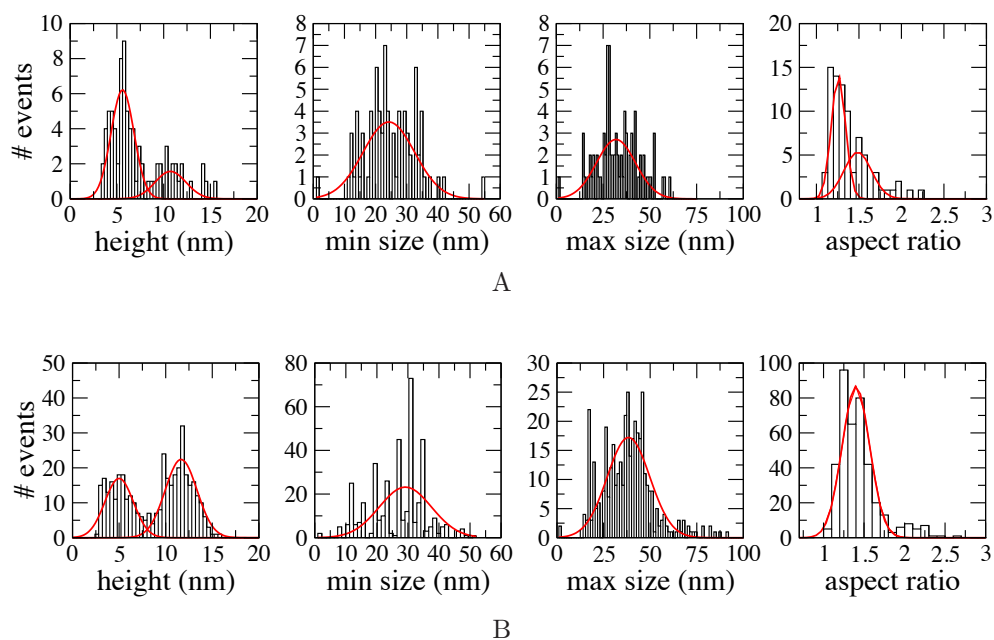
Figure 4.12: Results of grain analysis (performed with Gwyddion software) on pre-polysomal fractions deposited on Mica/Ni^{2+} surface. Panel A: 60S fraction, Panel B: 80S fraction.

particle	A (nm)	B (nm)	C (nm)
60S	26.8	21.4	17.6
80S	29.6	23.1	23.0

Table 4.4: Size of the inertia ellipsoids, computed on the 80S ribosome and on the 60S subunit, using the PDB data of Anger et al. of human ribosome[Anger et al., 2013].

A   B
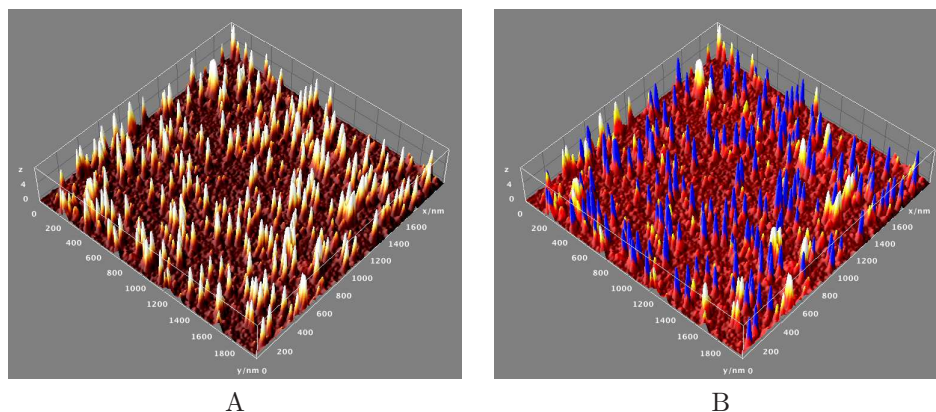
Figure 4.13: In panel A is reported a typical AFM image of fraction 80S deposited on mica treated with Ni^{2+}. In panel B the particles higher than 8.2 nm (80S reference particles) are highlighted in blue. Clusters of two or three particles have been removed manually from the pool on which the grain analysis has been performed.

performed on these masked data a grain analysis, whose results are shown in the histograms in Figure 4.14 and summarized in the Table 4.5. In Figure 4.13 is reported a typical AFM image of these samples before and after filtering for 80S particles.

Discrepancies between the dimensions of the objects observed at the AFM and the crystallographic data are to be expected, partly due to drying of the sample, that causes a shrinking of the actual dimension of the ribosomes, and partly due to flattening of the observed vertical dimensions in case of imaging of soft samples and broadening of the observed lateral distances, due to the AFM tip geometry. Using the relation between actual and measured dimensions (equation 3.3 in section 3.2.5.1) and assuming a tip-radius equal to 8 nm (the nominal radius of the AFM probes used for this sample) it is possible to obtain an estimated value for the
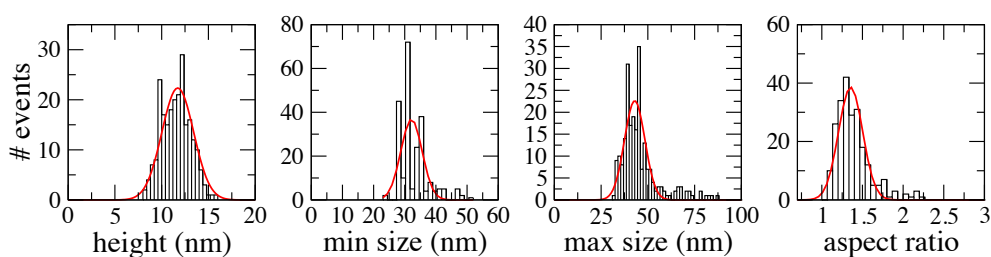
Figure 4.14: Results of the grain analysis performed on the 80S fraction deposited on mica treated with Ni^{2+}, after filtering for the particles with height greater than 8.2 nm. The distributions have been fitted with gaussian curves and their mean and standard deviation values extracted (see Table 4.5).

Height (nm)	Min Size (nm)	Max Size (nm)
11.7±1.7	32.2±3.4	43.0±5.5

Table 4.5: Height and size in nm of the 80S particles, as measured on mica treated with Ni^{2+} after drying and filtering.

actual ribosome lateral size (min and max size in Figure 4.14) of $\sim$ 18.5 nm and $\sim$ 33 nm .

After deposition of ribosomes on gold and functionalized gold, the samples have been thoroughly washed to eliminate ribosomes not adherent to the surfaces and let dry to be observed with the AFM in air environment and AC mode as described in section 3.2.5.1. The aliquots of ribosomes have been diluted ten times (see Section 3.2.3.2 for details) before the deposition, rather than used at the concentration they presented after the sucrose gradient purification, to allow a more clear visualization of the single ribosomes.

In Figure 4.15 an example of AFM image (area a 2×2 μm^2) of ribosomes adhering to gold stripped from mica sample on is shown.
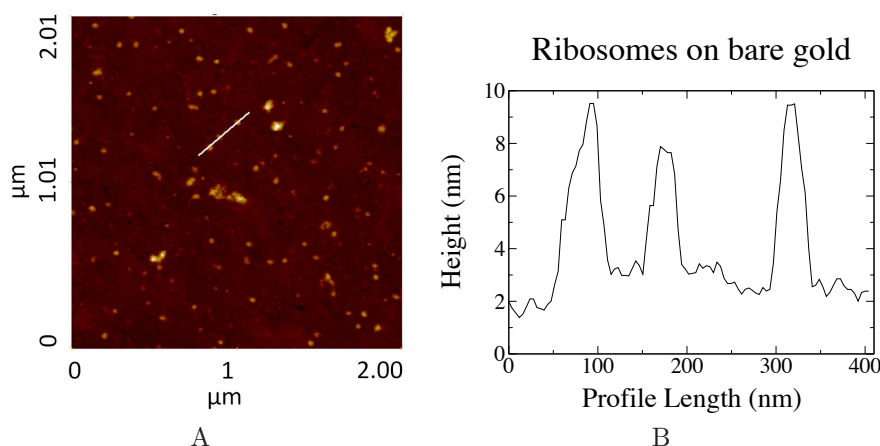
Figure 4.15: Panel A: 2×2 μm^2 area AFM image of ribosomes deposited on gold stripped from mica, taken in air environment, in tapping mode with AC200TS cantilevers. Panel B: a cross-section along the white line, showing three ribosomes.

The gold surface shows a uniform distribution of spherical objects with similar sizes, mostly isolated though a few cluster of 2-4 objects can be observed as well as some smaller deposited material. A grain-analysis was performed with Gwyddion software on several images, to extract the geometrical characteristics. The distributions shown in Figure 4.16 have been fitted with Gaussian curves and used
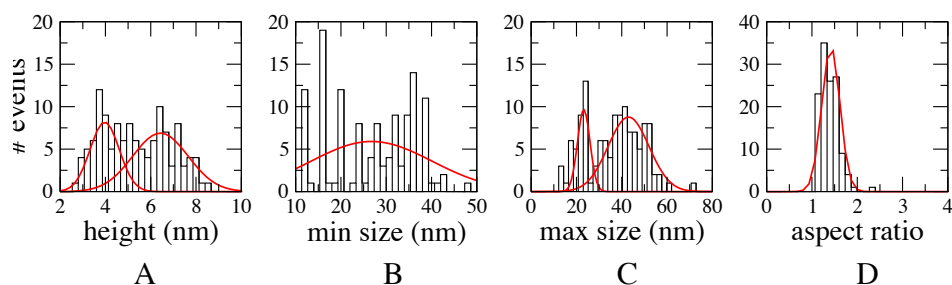
Figure 4.16: Grain-analysis of ribosomes deposited on gold stripped from mica. Panel A to C: height, minimum and maximum size distributions are shown; panel D: the ratio between the the maximum and minimum size.

to obtain mean (μ) and standard deviation (σ) of the distribution. The values obtained for height, minimum and maximum size are respectively (5.1$\pm$ 2.2) nm, (29.3$\pm$ 10.6) nm and (34.3$\pm$18.0) nm. All three parameters are smaller than those identified with the 80S fraction deposited on mica (reported in Table 4.5), in fact, they show a greater resemblance with the 60S fraction both in height (60S on mica height $\sim$ 5.3 nm, see Table 4.3) and in lateral size, that for 60S on mica was $\sim$ 24 nm and $\sim$ 32 nm. This proves a certain degree of degradation occurring on ribosomes deposited on bare gold.

Using equation 3.3 in section 3.2.5.1 to correct the tip-broadening effect, assuming a tip-radius equal to 7 nm , the lateral size values can be converted in $\sim$15.8 nm and $\sim$21 nm.

The same ribosomal fraction is deposited on MCOOH, MOH, MNH$_2$and M-11CH$_3$ functionalized gold, in the same condition applied to the deposition on bare gold, and observed at the AFM in air environment and semi-contact mode. An example image for every sample is shown in Figure 4.17 along with the physical characteristic distribution resulting from grain-analysis. The mean and standard deviation values are summarized in Table 4.6. The ribosome sample deposited on the surface M-11CH$_3$ aggregates in large bodies (see Figure 4.17, panel G), where ribosomes could not be observed. For this surface then no quantitative analyses were possible.

Ribosomes deposited on MCOOH and MOH functionalized gold show a double distribution. On MCOOH the two populations show values similar to he 80S fraction used as reference although the height of the second population H$_2$ is (8.8$\pm$1.1) nm, slightly lower than the $\sim$11 nm observed in the 80S reference fraction deposited on mica (see reference data in Table 4.5 and 4.3). Furthermore the proportion between the two populations can be expressed as the fractional area of the two gaussians relative to the height distribution, that is 0.318 for the population 1, and 0.682 for population 2. These values are very similar to the ones obtained with the 80S fraction deposited on mica used as reference. This indicates that not only MCOOH surface is able to retain ribosomes but does not introduce any
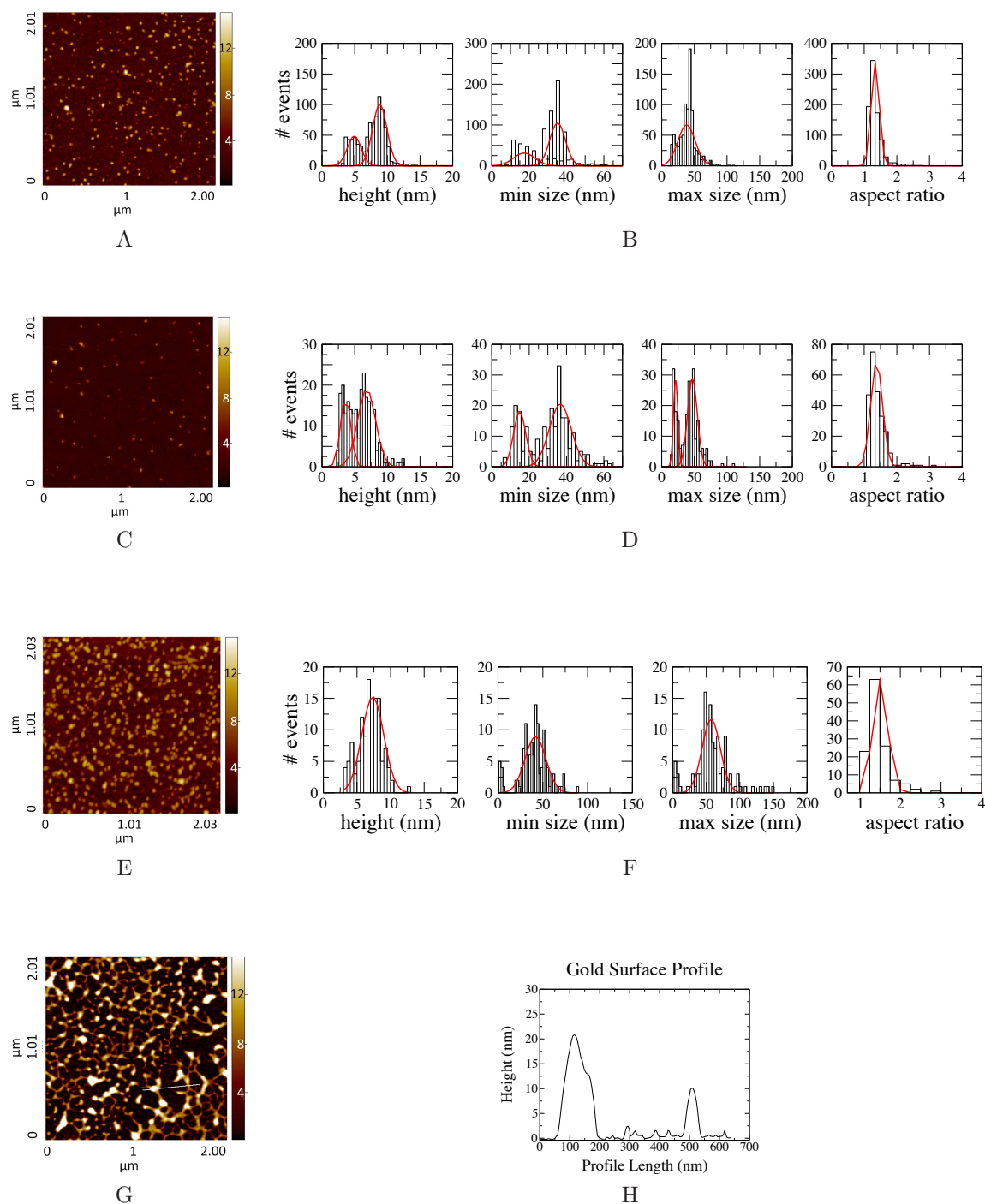
Figure 4.17: $2{\times}2\ \mu m^2$ AFM image of ribosomes deposited on MCOOH (A) and MOH (C) taken with the Cypher instrument in air environment, semi-contact mode with a AC 240 TS, and AC 200 TS. $2{\times}2\mu m^2$ images of MNH_2(E) functionalized gold taken with the MDT Solver, with a NSC35 cantilever and $1{\times}1\ \mu m^2$ image on M-11CH$_3$ (G) functionalized gold taken with the Cypher instrument with a AC 200 TS cantilever. On the right: height, minimum and maximum lateral size and aspect ratio distributions obtained by grain-analysis of ribosomes deposited on MCOOH (B), MOH (D), MNH_2(F) functionalized gold. Panel G: ribosomes deposited on M-11CH$_3$ functionalized gold. The height profile traced along the white line is reported in panel H.

Sample	H_1 $\mu \pm \sigma$ (nm)	H_2 $\mu \pm \sigma$ (nm)	Min Size $_1$ $\mu \pm \sigma$ (nm)	Min Size $_2$ $\mu \pm \sigma$ (nm)	Max Size$_1$ $\mu \pm \sigma$ (nm)	Max Size$_2$ $\mu \pm \sigma$ (nm)
Gold	5.1± 2.2		29.3± 10.6		34.3± 18.0	
MCOOH	4.9±1.0	8.8±1.1	17.3±5.8	35.2±4.2	-	43.1±6.8
MOH	3.6±0.8	6.8±1.4	14.9±3.3	36.6±5.9	21.4±3.4	47.0±7.5
MNH$_2$	7.3± 1.6		41.8± 11.6		57.3± 13.6	

Table 4.6: Height and lateral size values of the gaussian used to fit the morphological value distributions of the ribosomes deposited on gold and functionalized gold shown in Figure 4.17.

degradation in their shape.

On the MOH functionalized gold surfaces the two population are in the same proportion. Furthermore, both population show a lower height than the reference: (3.6±0.8) and (6.8±1.4) nm compared to the 5 and 11 nm of the 60S and 80S references. Both characteristics indicate a small degree of degradation incurred by ribosomes deposited on this surface. Ribosomes deposited on MNH$_2$ show a single population, with height lower than the reference (7.3± 1.6 nm) and larger lateral sizes (41.8±11.6 and 57.3±13.6) and with bigger variations than the distributions observed on MCOOH and MOH. This is probably due to the fact that MNH$_2$ samples have been observed with a different instrument and different tips (with a nominal radius of 8 nm, instead of 7 nm). Applying again the formula to correct the tip-broadening effect (equation 3.3 in section 3.2.5.1) the MNH$_2$ corrected lateral sizes ($\sim$27.3 nm and $\sim$ 51.3 nm) result still too big compared not only to the reference but even to the MCOOH ribosomes ($\sim$22.1 nm and $\sim$33.2).

Finally ribosomes deposited on M-11CH$_3$form an high degree of agglomerates, several nm high, formed probably from such degraded ribosomal material that are not even recognizable as single ribosomes.

As a numerical estimator of the affinity of ribosomes for the different functionalized surfaces, the density of ribosomes adherent on the different surfaces has been evaluated and shown in Table 4.7 depositing the same aliquot of ribosomal fraction and following the same procedure used so far (section 3.2.3.2 for details) but diluting the sample only five times, instead of 10, a compromise adopted in order to have data statistically more robust but still avoid as much as possible ribosome clusterization.

Among the functionalized surfaces, ribosomes show a marked tendency to adhere to the MNH$_2$ and bare gold samples. The MNH$_2$ surface shows a positive charge distribution at physiological pH due to the positive charge of the amino groups exposed on such a surface. A major degree of adherence occur on the bare gold surface, although as suggested in the previous section small degree of shape degradations may occour on these kinds of surface.

Slightly less effective are the MCOOH and MOH surfaces, while on the hydrophobic surface, as already reported, it has not been possible to observe recognizable ribosomes.

Sample	ribosome density (n·10^8/cm^2)
bare gold	117±13
MCOOH	84±4
MNH$_2$	132±11
MOH	52±12
M-11CH$_3$	n.d.

Table 4.7: Ribosome density on functionalized gold.

Sample	H$_1$ $\mu \pm \sigma$ (nm)	H$_2$ $\mu \pm \sigma$ (nm)	H$_3$ $\mu \pm \sigma$ (nm)	Width $_1$ $\mu \pm \sigma$ (nm)	Width $_2$ $\mu \pm \sigma$ (nm)	Lenght$_1$ $\mu \pm \sigma$ (nm)	Length$_2$ $\mu \pm \sigma$ (nm)
Gold	6.1± 2.2	13.1±1.7		26.7± 7.7	90.0±18.0	39.8± 15.9	128.5±20.7
MCOOH		8.6±2.2		34.2±3.5	79.2±14.0	39.5±6.7	112.5±24.0
MNH$_2$	4.2± 0.7	7.6±2.3	14.5±1.5	21.3± 9.4	78.8±28.4	30.3± 5.1	87.8±60.3

Table 4.8: Height and lateral size (width and length) values of the gaussian used to fit the morphological value distributions of the polysomes deposited on gold and functionalized gold shown in Figure 4.18.

4.2.4 Polysome adhesion to gold and functionalized gold surfaces

A fraction of heavier polysomes has then been deposited on gold and functionalized gold surfaces following the procedure described in section 3.2.3.2. The aliquot chosen for this deposition is a medium-heavy weighted fraction, (fraction 12 in Figure 3.3, section 3.2.3.2), that comprises polysomes formed by 6-12 ribosomes each. The aliquot has been diluted 4 times, to deposit approximately the same quantity of material used in the ribosome deposition experiment described in the previous paragraph. In Figure 4.18 AFM images of the deposited polysomes taken on 2×2 μm areas are shown along with the physical characteristic distribution resulting from grain-analysis. The mean and standard deviation values are summarized in Table 4.6.

Once again polysomes have been compared to a reference: Viero and coworkers [Viero et al.,] have performed similar depositions of polysomes using differently weighted fraction of MCF-7 polysomes on mica sheet treated with nickel ions. The distributions found after grain-analysis are reported in Figure 4.19. The two distributions reported refers to fractions slightly lighter (medium molecular weight) and heavier (high molecular weight) than the one used for deposition on gold.

Polysomes deposited on gold (panel A) are imaged as globular or rod-shaped isolated clusters of ribosomes (about ten ribosomes per cluster, in yellow) occasionally linked by strand-like features (in purple). This duality in shape is reflected by the size distributions, divided in two population: a first composed by smaller objects with an height of (6.2±2.2) nm, minimum size (width) of (26.7±7.7) nm and
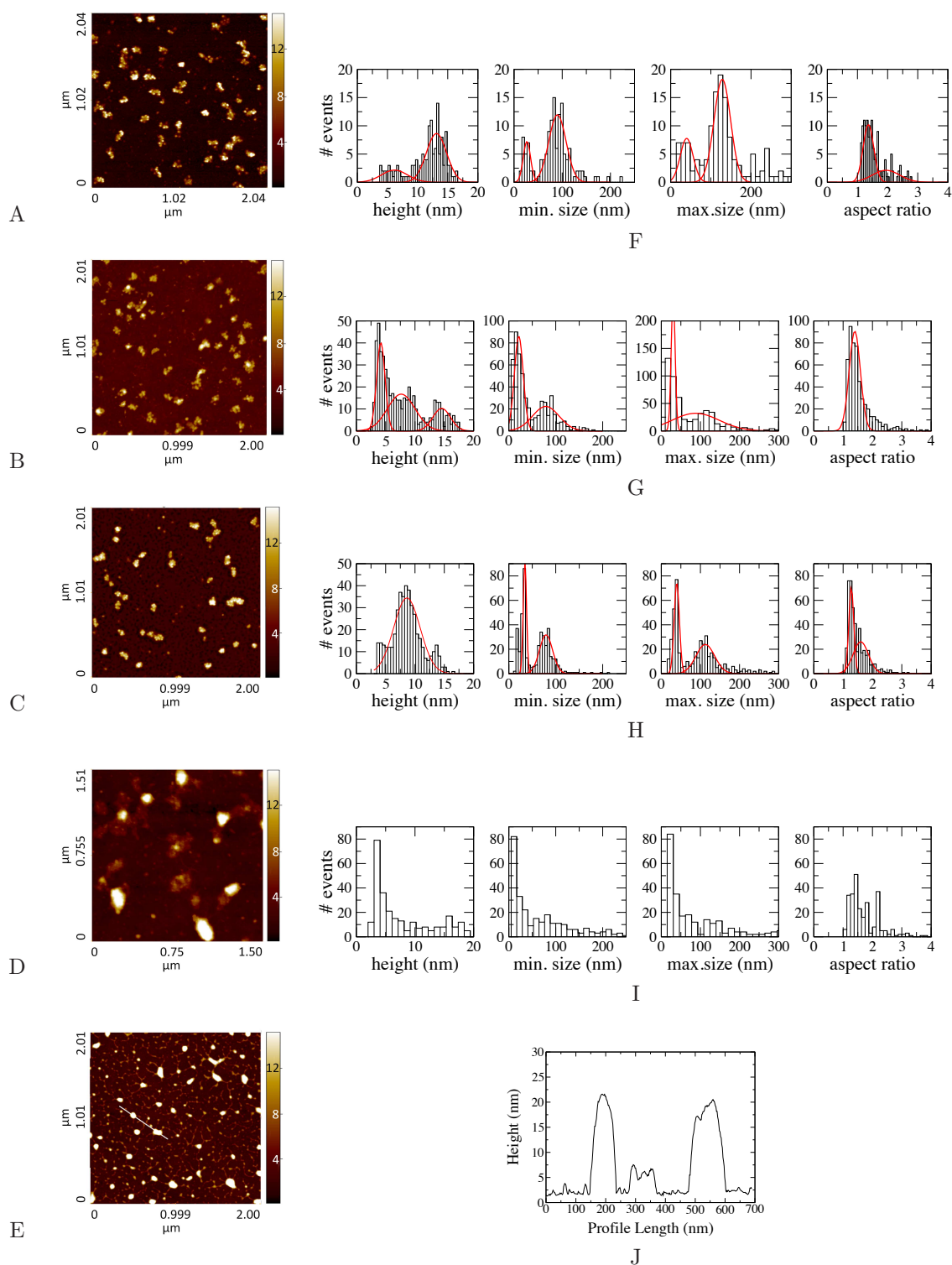
Figure 4.18: $2{\times}2\ \mu m^2$ AFM image of medium-heavy weighted polysome fraction deposited on gold (A) and MNH$_2$(B), MCOOH (C), MOH (D) and M-11CH$_3$(E) functionalized gold. The z-range color-scale is 15 nm. On the right: height, minimum lateral size), maximum lateral size and aspect ratio distributions obtained by grain-analysis of polysomes deposited on gold (F) and MNH$_2$(G), MCOOH (H), MOH (I) functionalized gold. Panel J: cross-section along the white line of material deposited on M-11CH$_3$ functionalized gold.
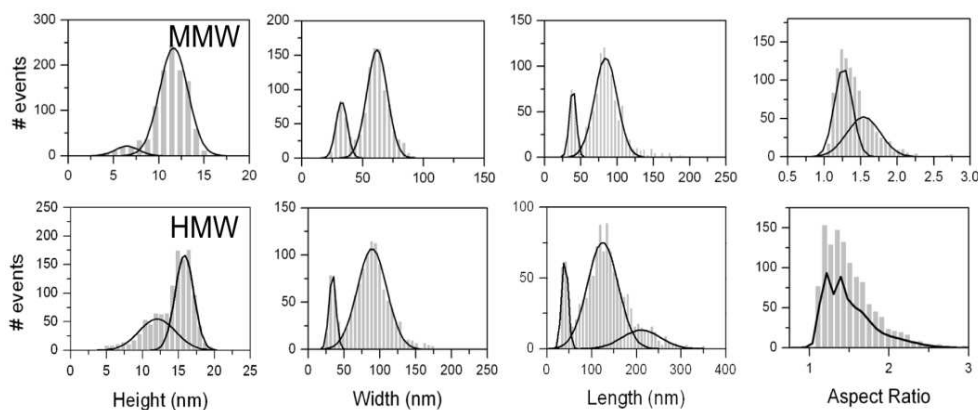
Figure 4.19: Results of grain analysis (performed with Gwyddion software) on a medium weighted (MMW) and high weighted (HMW) polysomal fractions deposited on Mica/Ni^{2+} surface [Viero et al.,].

maximum size (length) of (39.8±15.9) nm, and a second composed of larger objects with an height of (13.1±1.7) nm, minimum size of (90.0±18.0) nm and maximum size of (128.5±20.7) nm showing a good conservation of shape and distributions compared with the reference (height $\sim$ 6 and 12 nm for the MMW fraction and $\sim$ 12 and 16 nm for the HMW fraction

Polysomes on MNH$_2$ and MCOOH functionalized gold retain similar size values for the population of bigger objects (height of (14.5±1.5) nm, width of (78.8±28.4) nm and length of (87.8±60.3) nm for the MNH$_2$ and (8.6±2.4) nm, (79.2±14.0) nm and (112.5±24.0) nm for MCOOH. On MNH$_2$ the presence of small strand-like material is also observed (in purple in Figure 4.18 panel B and

On MCOOH this presence is not observed, but it is possible than its presence is masked by the SAM that, as mentioned in section 4.2.2.1, is not completely formed.

Polysomes deposited on the neutrally charged surfaces MOH and M-11CH$_3$ functionalized gold show a higher degree of degradation, especially on the latter, where the results obtained after deposition of ribosomes are repeated.

In Table 4.9 the density of polysomes adherent on the different surfaces is shown expressed as number of objects on a cm^2.

As in the case of ribosomes the functionalization that most effectively entrap polysomes on its surface is the positively charged MNH$_2$ surface, but, judging from AFM images this kind of surface is also prone to retain other material present in the polysomal fractions. Indeed surfaces endowed with amino functionalities are known to favour adhesion of DNA ([Pasquardini et al., 2011] and Sections 4.3 and 4.5.2 of this work) and RNA (Section 4.5.2).

Following the MNH$_2$ surface in its capability to retain an high number of polysomes per cm^2, and although only slightly better than gold and MOH in this aspect, does not cause the degree of degradation present especially in polysomes

Sample	polysome density $(n \cdot 10^8/cm^2)$
bare gold	15±4
MCOOH	19±5
MNH$_2$	30±6
MOH	14±7
M-11CH$_3$	n.d.

Table 4.9: Number of polysomes adherent on gold and functionalized gold surfaces after deposition (1 hour at 4°C in Hepes buffer 10 mM, pH 7,5) and extensive washing in buffer Hepes and DEPC water.

deposited on the latter surface.

4.3 DNA adhesion to functionalized gold

In a purification device aimed at the isolation of polysomes form cell lysate, nucleic acids different from the RNA associated to polysomes (namely, mRNA under translation, rRNA or even translation regulatory miRNA) are unwanted components. At the same time, surfaces used to bind polysomes, ideally should not retain their associated mRNA, once freed from the polysome.

The nature of DNAs and RNAs interaction with functional surfaces will be explored more in detail in this section and in section 4.5.2 of this work.

In order to test the propensity of this functionalizations to entrap general nucleic acids a series of experiment of nucleic acid deposition on functionalized gold have been performed.

E. coli Bacteriophage λDNA has been chosen as a probe nucleic acid molecule for this kind of experiment: it is a ∼17 μm long [Caro, 1965] double stranded molecule and less fragile than RNA; this characteristics simplify not only the handling of the samples, but also make it easier the observation with the AFM. λDNA was deposited on gold and functionalized gold following the procedure reported in section 3.2.4 and observed after washing and drying of the samples in air environment, in semi-contact mode. In Figure 4.20 2D images and 3D renderings of λDNA deposited on gold and functionalized gold are shown.

The highest quantity of DNA can be observed on MNH$_2$ where several strands can be clearly observed. This is expected, and reported in literature [Nakagawa et al., 2005, Pasquardini et al., 2011]: both the deposition and observation have been performed at pH 7.5; in this condition the amine exposed on the MNH$_2$ functionalized surfaces are in their protonated form, while the DNA is negatively charged (due to the deprotonated state of the phosphate groups along the DNA carbon backbone) favoring an electrostatic attraction between the two molecules. On MOH and especially M-11CH$_3$, as in the case of ribosomes and polysomes, cluster of non-clearly identifiable objects are present. On the MOH surface these clusters are often linked by strands, perhaps due to the aggregation of DNA molecules.
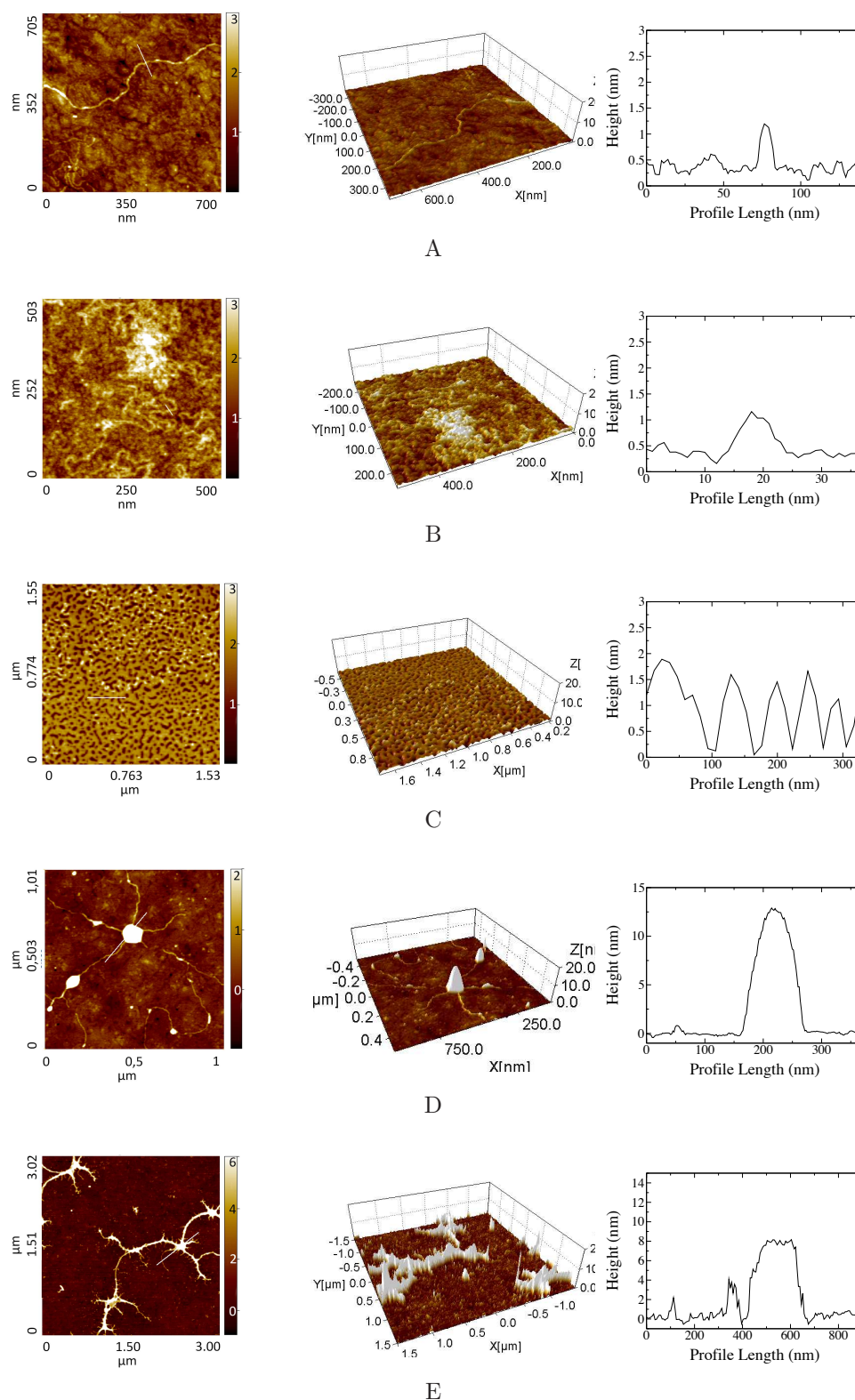
Figure 4.20: λDNA deposited on gold (A), MNH₂(B), MCOOH (C), MOH (D) and M-11CH₃(E) functionalized gold are shown. The images have been recorded with the AFM Cypher instrument, in semi-contact mode in air environment. The lateral dimension and Z-range of the color scale are reported for every 2D image. The 3D renderings were obtained with SPIP software.
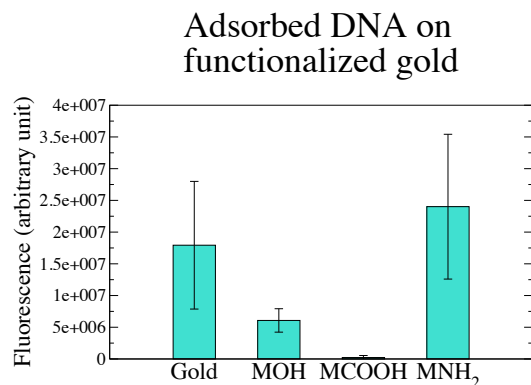
Figure 4.21: Average value of fluorescence intensity of DNA adsorbed on gold and functionalized gold, stained with PG

On bare gold some molecules have been observed, although in amounts far smaller than on MNH_2, while on MCOOH surface none has been observed.

To have a further confirmation of these results, as well a quantitative comparison of the quantities of DNA adsorbed on these surfaces, further experiments have been carried out. Genomic DNA has been deposited on gold, MOH, MCOOH and MNH_2 functionalized gold and observed after staining with a fluorescent dye (PG) specific for double stranded DNA with a fluorescence microscope (see section 3.2.4 for deposition procedure, and section 3.2.1.2 for observation specifics). In Figure 4.21 the mean fluorescence intensity calculated on several images and expressed in arbitrary units is reported.

Differently from the AFM observations, the quantities of DNA adsorbed on gold and MNH_2 functionalized gold result more similar., The quantity of DNA adsorbed on MOH samples is lower, around a third respect to gold.

The most interesting result is however that the scarce propensity of DNA of adsorbing on MCOOH surfaces observed with the AFM is confirmed.

4.4   Gold substrates: conclusions

The interaction between polysomes and different kinds of functionalized gold surfaces was investigated.

The functionalized surfaces have proven to be able to entrap ribosomes and polysomes with varying degree of efficiency and shape conservation. In particular gold functionalized with carboxyl acid (MCOOH) and amino (MNH_2) terminated thiols have both the capability of retain polysomes without introducing observable shape degradations, that was observed instead on MOH and M-11CH$_3$ functionalized gold surfaces, and in small degree in ribosomal fraction deposited on bare gold.

Differently from the MCOOH treated surfaces, MNH_2 functionalized gold has

also shown a great propensity to entrap nucleic acids, namely DNA.

Therefore, while slightly less efficient in its capability to attract high quantities of polysomes, a carboxyl acid functionalization seems to be the most promising for polysome purification, while a functionalization with amino groups is most apt for nucleic acid entrapment on surfaces.

4.5 Silicon oxide substrates

In the following sections the results obtained on the thiol-gold model will be transferred on different substrates: silicon-oxide, Pyrex and PDMS are materials widely employed in the realization of microsystems. These kind of materials all belong to a class of hydroxylated substrates that can be functionalized exploiting SAM formed by molecules containing a silane group -Si-O-.

In order to obtain a surface endowed with the same chemical properties than the MCOOH functionalization obtained on gold the formation of SAM composed by two organic silanes containing carboxyl acids will be attempted on flat silicon oxide samples. These substrates will be used to replicate the results obtained with the deposition of polysomes on MCOOH gold, before proceeding with a proof-of-principle demonstration of the effective use of a silicon oxide/Pyrex microdevice thus functionalized for extraction of RNA from polysomes.

As previously stated, the interaction between and amino functionalized surface and nucleic acid will be explored more in detail using the force-distance mode of an AFM system.

4.5.1 Functionalized silicon oxide

Flat surfaces of thermally grown silicon oxide (TG-SO) were silanized with two organic silanes, CST and triCAS, containing respectively 1 and 3 carboxyl functional groups. The silanization has been performed using four different procedures illustrated in section 3.2.2.3: in Silanization 1P plasma-treated TG-SO samples will be functionalized with triCAS by an incubation in water; in Silanization 2P the same molecule has been used in a mixture of organic solvents (ethanol and toluene); in Silanization 3P plasma treated TG-SO has been functionalized with CST in a mixture of organic solvents at pH 5 and in Silanization 4W the same molecule and procedure has been used on TG-SO after a treatment aimed to enrich the surface of many hydroxyl groups as possible, to favour the SAM formation reaction [Hau et al., 2003].In the following section the morphological and chemical characteristics of silanized samples will be analyzed with AFM and XPS before proceeding with polysome deposition.

4.5.1.1 Surface characterization

TG-SO surfaces are extremely smooth, with an average roughness S_a of (0.18±0.01) nm, comparable with gold stripped from mica (0.15±0.01) nm, showed in section 3.2.5.1. Plasma treated TG-SO functionalized with CST and triCAS in solvents do not show any significant increase in the average roughness.

In order to confirm the presence of the silane layer adsorbed on the surface the functionalized and bare TG-SO surfaces have been analyzed by XPS. In Table 4.10 the elemental composition of the plasma treated, wet treated and four silanized samples are reported, expressed as relative percentages, derived from analyses performed at 30° take-off angle, corresponding to an analysis depth of $\sim$ 3-4 nm. All
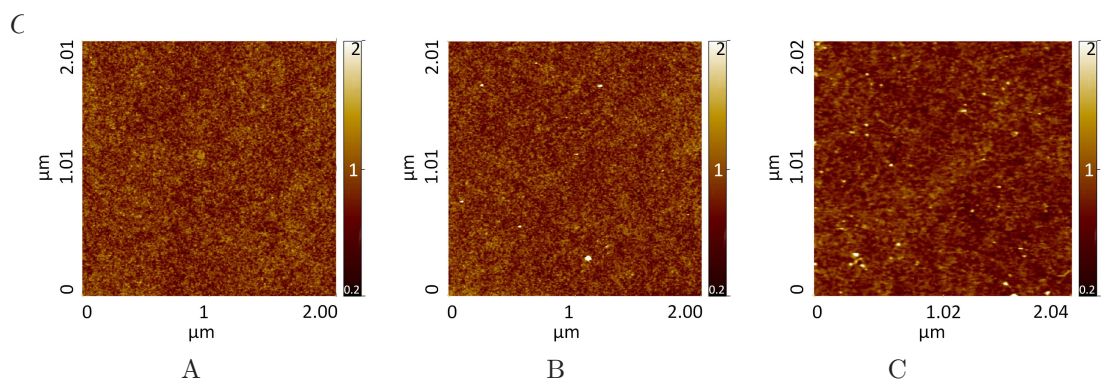
Figure 4.22: $2 \times 2 \ \mu m^2$ AFM images of plasma treated TG-SO before (A) and after functionalization with CST (B) in organic solvents (Silanization 3) and triCAS (C) in organic solvents (Silanization 2).

take-off $\theta = 30°$				
Sample	O 1s %	C 1s %	N 1s%	Si 2p%
Plasma treated TG-SO	68.0	6.2	-	25.8
TG-SO Silanization 1P	58.5	15.9	0.7	24.9
TG-SO Silanization 2P	55.9	16.1	0.5	27.5
TG-SO Silanization 3P	57.8	16.0	-	26.3
Wet treated TG-SO	65.2	6.2	-	28.6
TG-SO Silanization 4W	59.7	12.4	-	27.8

Table 4.10: Chemical composition of TG-SO samples treated as described in section3.2.2.3: oxygen (O 1s), carbon (C 1s), nitrogen (N 1s) and silicon (Si 2p) relative percentage.

th silanizated samples show an increased amount of the carbon contents of about 2 to 3 times respect to the bare TG-SO.

A further confirmation of the presence of triCAS on the samples silanized with procedures 1P and 2P, is the small quantity of nitrogen that is detected on such samples. .

All samples (in Figure 4.23 and Figure 4.24 the core lines detected with a take-off angle of 30° are shown) show in the C 1s core line the peak relative to the CC/CH bond, set at 285 eV. The silanized surfaces all show the presence of 2 more peaks corresponding to oxidized carbons, namely the C=O (~289 eV) and CO (~286.5 eV) components, typical of molecules containing carboxy groups.

4.5.1.2 Polysome deposition

The same fraction of medium-high heavy polysomes used to evaluate their adhesion on functionalized gold samples has been deposited on plasma treated TG-SO and
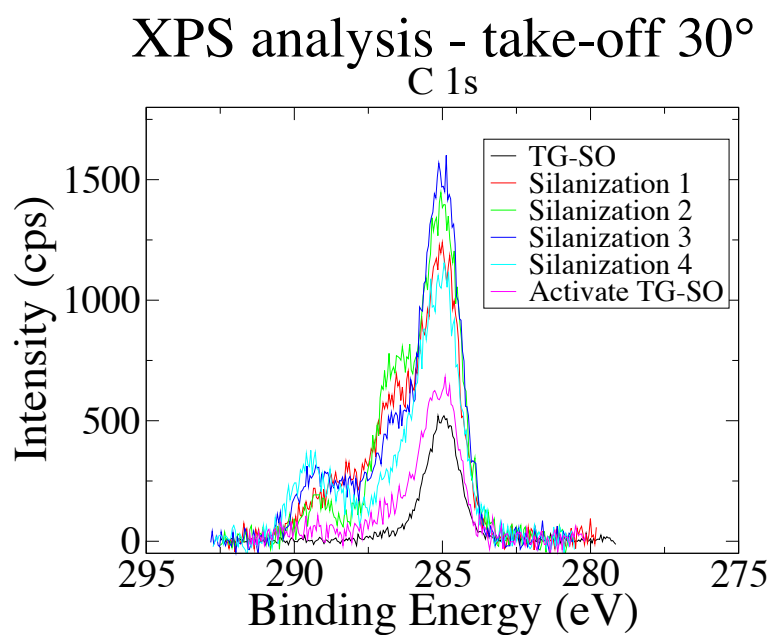
Figure 4.23: XPS C 1s core lines of plasma treated TG-SO (black), "wet treated" TG-SO (magenta) and TG-SO treated following Silanization 1 (red), Silanization 2 (green), Silanization 3 (blue) and Silanization 4 (cyan) procedures. An increase of the carbon content is clearly visible in the silanized samples respect to the plasma treated and the wet treated samples (where carbon constitutes a residual contamination). The analyses have been performed with a KRATOS instrument.
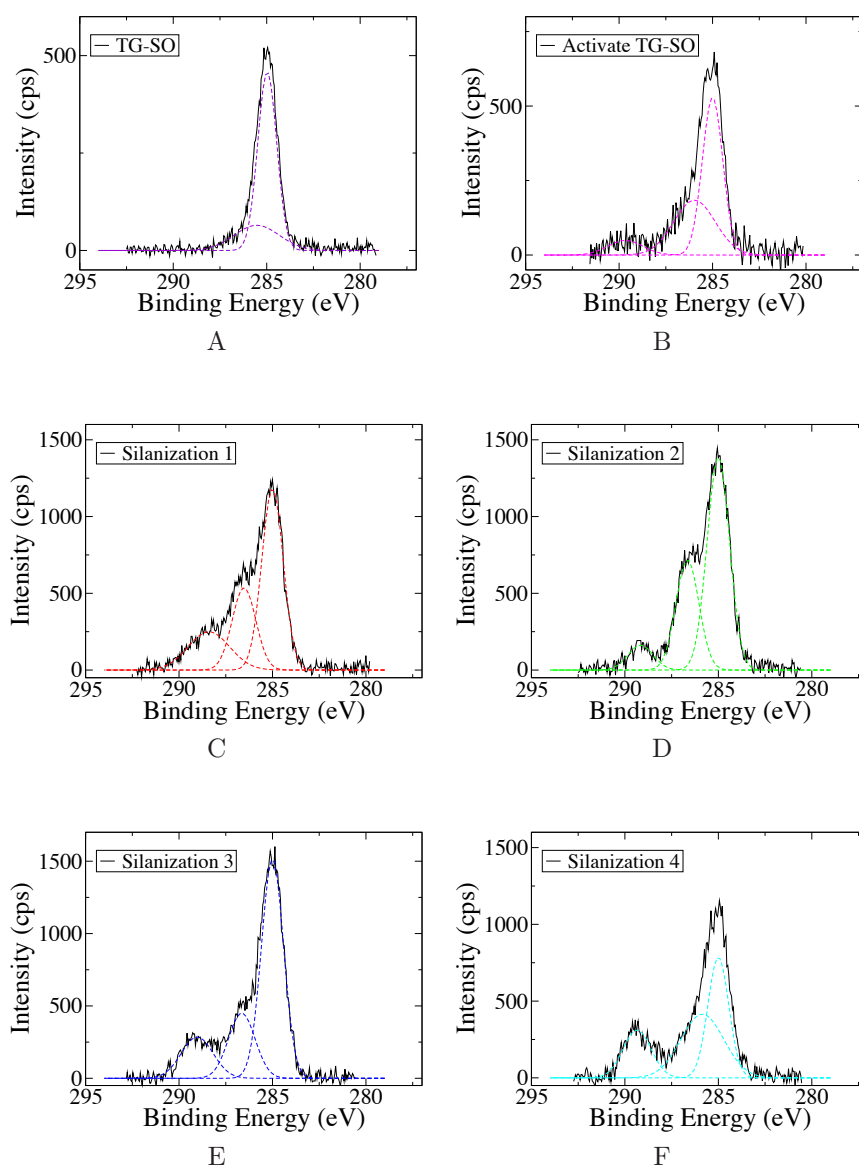
Figure 4.24: The C 1s core lines of plasma activated TGSO (Panel A), wet activated TGSO (Panel B), and silanized TGSO (Panel C to F) are shown alongside their fit with gaussian curves. All four silanized surfaces show the presence of 2 peaks corresponding to the C=O ($\sim$289 eV) and CO ($\sim$286.5 eV) typical of carboxyl acids absent in the plasma activated TGSO (Panel A) and present in small amount in the wet activated sample (Panel B) where they can be due to the presence of carbon contaminats.The analyses have been performed with a KRATOS instrument.

on to four functionalized TG-SO samples with the procedure described in section 3.2.3.2. The samples were extensively washed, dried and observed at the AFM in air environment. Images of polysomes adherent to the TG-SO and functionalized surfaces are shown in Figure 4.25, , treated with triCAS (panels B and C) and CST (panel D). From the images the number density of polysomes adherent to the different surfaces has been evaluated and the results are reported in Table 4.12. The morphological characteristics of the deposited polysomes have been extracted performing a grain-analysis on several images, whose results are reported in Figure 4.25 and Table 4.11.

Sample	H_1 $\mu \pm \sigma$ (nm)	H_2 $\mu \pm \sigma$ (nm)	Width $_1$ $\mu \pm \sigma$ (nm)	Width $_2$ $\mu \pm \sigma$ (nm)	Lenght$_1$ $\mu \pm \sigma$ (nm)	Length$_2$ $\mu \pm \sigma$ (nm)
TG-SO		13.8± 5.0	28.7± 10.2	66.4±4.9	37.7± 2.9	89.0±15.4
Silanization 1	4.5±0.6	11.0±2.2	18.6±3.7	68.8±24.4	37.9±1.1	104.8±17.9
Silanization 2		12.1±3.6	32.5± 7.8	68.9±8.6	39.3± 6.9	90.2±15.0
Silanization 3		5.7±2.2	23.6± 9.0	58.3±19.9	36.3±13.4	96.3±25.7
MCOOH gold		*8.6±2.2*	*34.2±3.5*	*79.2±14.0*	*39.5±6.7*	*112.5±24.0*

Table 4.11: Height and lateral size (width and length) values of the gaussian used to fit the morphological value distributions of the polysomes deposited on silanized TG-SO. Data relative to polysomes deposited on MCOOH functionalized gold described in section 4.2.4 are reported for comparison.

Polysomes deposited on plasma treated TG-SO and on the surfaces treated with triCAS (Silanization 1 and 2) present similar situations: a fair number of polysomes adheres on functionalized surfaces without showing any marked shape degradation. The lateral sizes distributions present once again a the presence of more populations although this characteristic results less marked than in case of polysomes deposited on gold. Polysomes deposited on plasma treated TG-SO functionalized with CST (Silanization 3) instead show a certain degree of degradation: the polysomal height, observed both on the reference sample deposited on mica/Ni^{2+} (see Figure 4.19,

Sample	polysome density (n·10^8/cm^2)
TG-SO	7±2
Silanization 1	15±3
Silanization 2	14±1
Silanization 3	12±3
MCOOH gold	*19±5*

Table 4.12: Number of polysomes adherent on plasma treated TG-SO and functionalized plasma treated TG-SO surfaces after deposition and extensive washing. Results for gold surfaces functionalized with MCOOH are also reported for comparison.
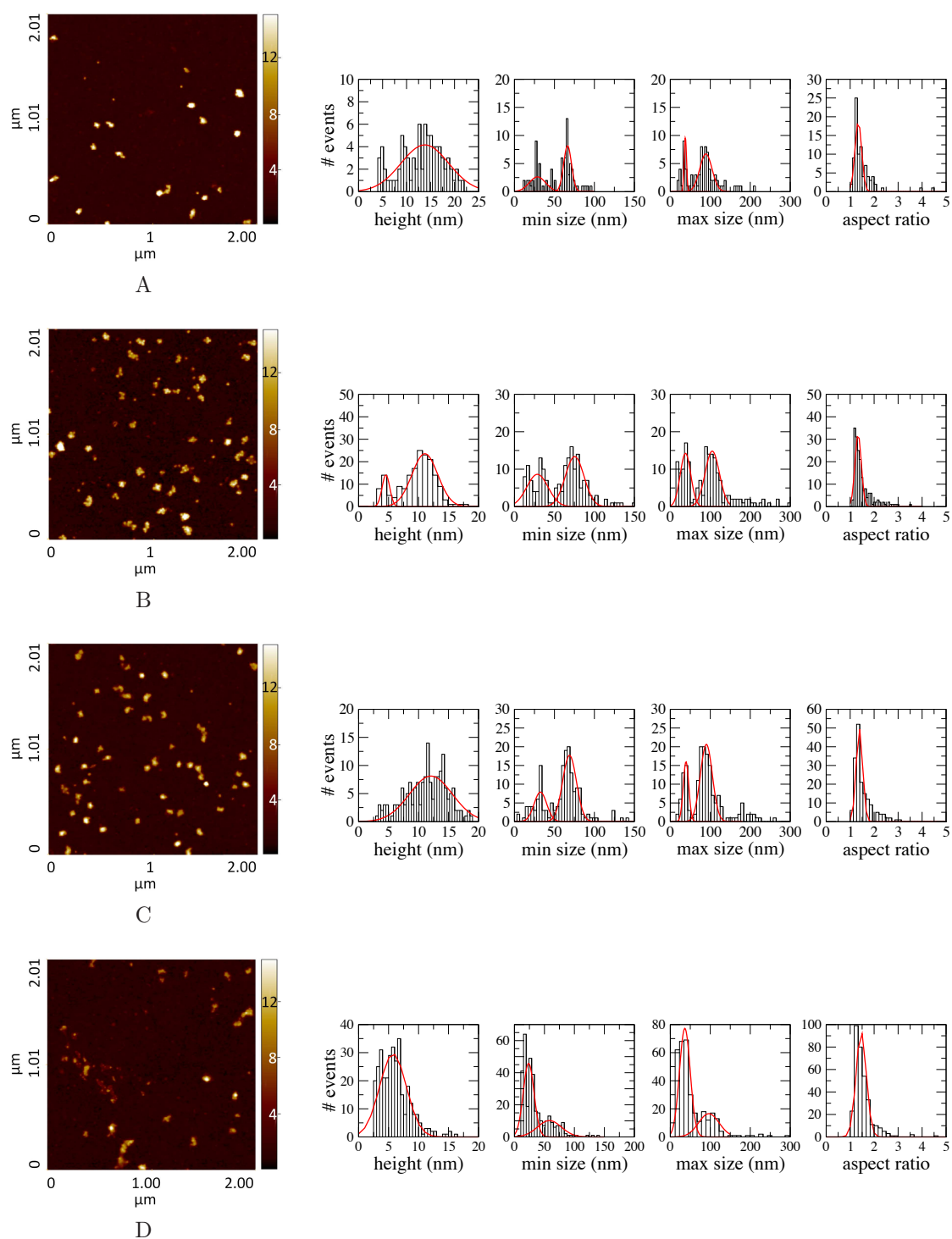
Figure 4.25: 2×2μm AFM images of polysomes deposited on bare plasma treated TG-SO (Panel A) and functionalized with triCAS in water (silanization 1, Panel B), triCAS in ethanol/toluene (silanization 2, Panel C); plasma treated TG-SO functionalized with CST (silanization 3, Panel D).

pag. 56) and on the other three TG-SO samples is comprised between 10 and 15 nm while in this case the average height is lower, ~ 6nm. Furthermore, differently than the other TG-SO samples, about two thirds of the visualized objects contribute a population of smaller bodies, characterized by lower width and length values (see Figure 4.25). In Table 4.11 the mean and standard deviation values obtained in section 4.2.4 on MCOOH functionalized gold are reported for comparison. The distribution mean and deviation values obtained using triCAS (Silanization 1 and 2) are those that more closely resemble the results obtained on MCOOH gold, although, on samples treated using the first procedure (Silanization 1) some isolated smaller objects can be observed that cause the presence of a second peak in the height distribution ($H_1 = 4.5\pm0.6$ nm), not observed in the other cases, and lower values in the first population in the width distribution (18.6 ± 3.7 nm compared with the ~30 nm observed on both Silanization 2 treated TG-SO and MCOOH functionalized gold). Comparing the number density of objects adherent on the surface (data reported in Table 4.12) TG-SO silanizated with triCAS results to be the most capable to retain objects, yielding results comparable with those obtained on MCOOH functionalized gold. TG-SO functionalized with CST yield similar numerical results, but an high fraction of these objects are constituted by degraded polysomes.

4.5.2 DNA and RNA interaction with functionalized surfaces: force distance measurement

A more detailed study on the interaction between nucleic acids and amino functionalized substrates is presented in the following pages with the aim to develop surfaces able to selectively capture and release nucleic acids.

Force distance experiments (see section 3.2.5.4) have been exploited to measure the interaction between short nucleic acids molecules and a functionalizated surface. A mica substrate has been chosen as standard ultra-flat surface, and functionalized with a SAM of amino terminated silane (APTMS): the amino-functionalization being the one that better interacts with DNA (as observed in section 4.3 on functionalized gold surfaces). Short molecules of double strand DNA and single strand RNA, modified with a cyclic dithiol group (DTPA) were immobilized on gold coated AFM tips (see section 3.2.5.4 for details on sample and AFM tip preparation, as well as the experiment specifics).

As already mentioned, DNA and RNA molecules are negatively charged under physiological conditions, due to the presence of charged phosphate groups along the backbone of the nucleic acid. Under the same condition the majority of the amino groups are in their protonated forms, so the APTMS SAM expose a positive surface, prone to attract negative molecules. Instead, at basic pH the amino groups are mostly in their unprotonated form, thus the APTMS SAM surface becomes neutral. This offer the possibility to control the charge distribution of the substrate surface simply changing the pH of the solution in which the experiment is carried out.

To verify the effective electrostatic behavior of the nucleic acid/APTMS surface interaction we performed experiments in buffers with the same ionic strength, to
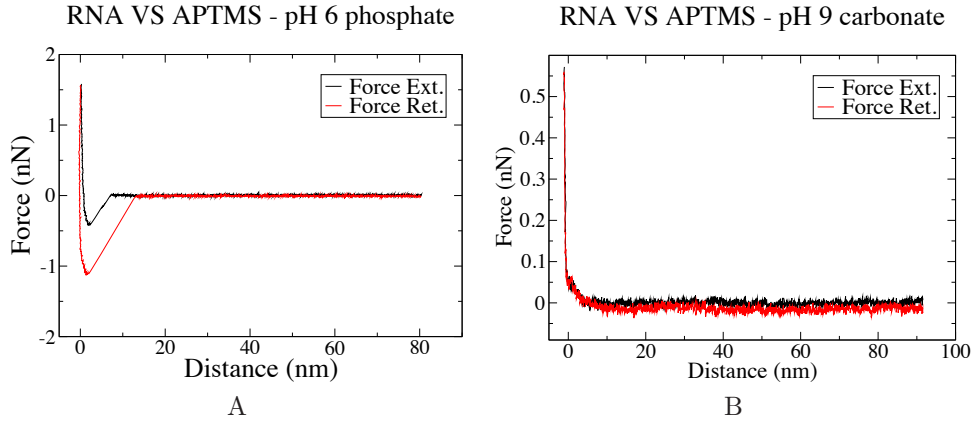
Figure 4.26: Force versus distance curve in case of an (A) attractive interaction and (B) non attractive/repulsive interaction between AFM tip and sample surface.

minimize the interference of eventual counter-ions, or cationic bridges. The pH varied from acid pH (the lower pH was 4.5 for DNA tips and 5 for RNA tips) to a basic pH (10.5 in both cases). The experiments have been performed recording on several hundreds of points, cantilever deflection data vs. z piezo position, converted to force versus distance curves as detailed in section 3.2.5.4.

Two distinctive kinds of curves were obtained: one set characterizing the typical attractive interaction between the tip and the sample surface (panel A in Figure 4.26) the second one being typical instead of repulsive interaction (see panel B in Figure 4.26).

From every curve the intensity of interaction has been obtained (see section 3.2.5.4 for details) and these data were collected in a distribution histogram for every measured pH value. In Figure 4.27 are reported the distributions (plotted as box-plot in which the boxes represents the inter-quartile range and the whiskers the 10th and 90th percentile) of adhesion intensity recorded at every pH.

Both RNA and DNA tips show a marked dependance of the adhesion intensity on the pH. This dependence occurs very slightly also for the control bare gold tip. As expected, for both DNA and RNA tips the intensity of the interactions with the amino coated surface increases lowering the pH, where the charge density of the exposed amino groups becomes positive. Assuming a dependance of the interaction F on the average surface charge only, as in the following formula:

$$F(pK, A, B) = A \left(1 - \frac{10^{-pK} \cdot 10^{pH}}{1 + 10^{-pK} \cdot 10^{pH}} \right) + B \qquad (4.1)$$

where A and B are normalization parameters, one can fit the average interaction of DNA and RNA functionalized tips vs pH obtaining the dashed curves that are reported in Figure 4.27, panel A and B. The same fit give a pK value for the APTMS surface of 7.2 and 5.9 for the DNA and RNA cases respectively, with a decrease of several pH units respect to the value typical of free organic primary

amines ($\sim 10 - 11$ [Allinger et al., 1980]). The fitted value however, agrees very well with the value of 7 that is reported in [van der Vegte and Hadziioannou, 1997], where such shift of the pK value is attributed to ion solvation effects and an excess electrostatic free energy of the surface.

Comparing RNA tip (panel B of Figure 4.27) with DNA tip (panel A of Figure 4.27) one can note that a clear onset of a interaction well above the values of those typical of gold tips happens only at pH=6 for RNA tip, while for DNA tip the experimental data indicate a more gradual change of the interaction vs pH.

Moreover, one should note that the average force vs pH data reported in panels A and B of Figure 4.27 are actually obtained by considering only the attractive type curves (see panel A in Figure 4.26). On the other hand, at every pH value, repulsive curves can be present in different amount respect to the total number of acquired data. In Figure 4.27, panel C is reported the percentage of repulsive curves that is present at every pH, both for DNA tip (red circles) and RNA tip (blue stars). For both tips the fraction of repulsive type curves increases with the pH of the solution, tough some repulsive events are presents for low pH (~ 4.5) in the RNA case. When DNA tip is involved, the fraction of repulsive events increases gradually from zero (pH<= 6.5) up to 100% at pH >10. This result can be explained as an electrostatic effect related to the degree of ionization of the amino surface, which is reported to decrease monotonically for such a surface vs pH, reaching zero at pH=10 [van der Vegte and Hadziioannou, 1997]. In the RNA tip case, instead, the onset of repulsive curves lags by ~ 1 pH units and a substantial presence of attractive events is detected at every pH. This different behavior agrees very well with data on adhesion and elution of miRNA [Santini et al., 2013] in comparison with DNA adhesion and elution from surfaces [Pasquardini et al., 2011]. Also it is worth noting that DNA tips concern double stranded nucleic acid, which is supposed to be in B form in the used solutions, while RNA tips are covered with single strand RNAs, which is expected to assume a more random, unstructured, conformation. In this latter case some interactions can happen between bases and the amino surface, leading to the presence of attractive interactions at high pH.
.

4.6 Silicon/Pyrex microdevice

In the following pages, the results observed on functionalizations of silicon oxide plane samples will be applied to a microdevice built in silicon/Pyrex. A first model of utilization protocol will be outlined and a verification of the feasibility of the whole process of polysome isolation and RNA extraction will be reported.

4.6.1 RNA Extraction verification

The microdevice that will be presented in the following section is thought as a proof-of-priciple for an integrated system capable to perform both polysomes capture starting e.g. from a cell lysate, and the subsequent mRNA extraction from the immobilized polysomes in a few, semi-automated steps. The two main steps
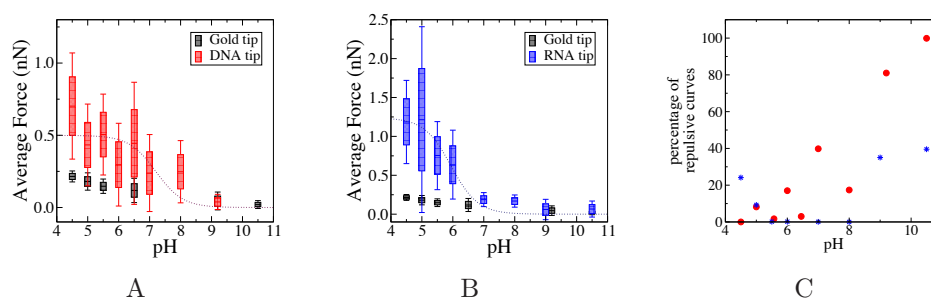
Figure 4.27: The pH dependence of the intensity of adhesion recorded with bare gold tips (black), "DNA tips" (red, panel A) and "RNA tips" (blue, panel B). The box-plots convention used is: mark - mean of the distribution, box - inter-quartile range (50% data), whiskers - 10th and 90th percentile (80%) data. Data in panel A has been fitted with the formula 4.1, while in panel B the fit of the same data is reported for comparison. In panel C the percentage of "non interaction/repulsive" curves registered for every pH point, for DNA tips (red full circles) and RNA tips (blue stars).

performed in such a device are a) the immobilization of polysomes on the functionalized microchannel surfaces, b) after a washing step to remove the unbound sample the polysomes trapped on the surfaces of the microdevices will be treated with an opportune method aimed to release their mRNA molecules. Ideally, this treatment should be able to disassemble the ribosomal subunits without disrupting them: the released mRNA is then free in the solution and should not interact with the functionalized surfaces, while the ribosomal subunits are still trapped to them, allowing us to collect a "eluted fraction" of RNA greatly enriched in polysomal mRNA. To perform this "elution" step, different strategies can be chosen: performing thermal incubation steps with temperatures not greater than 60°C, altering the saline equilibrium of the solution or varying the pH are among the simplest strategies, although the last one could vary the charge distribution of the functionalized surface which is at the base of the entrapment of polysomes and ribosomes on the surface, thus releasing a high amount of interfering material (rRNA) and nullify the mRNA purification purpose of this microdevice.

In the following pages a proof of utilization will be described to verify the efficiency of recovery and the quality of the RNA extracted from a functionalized silicon/Pyrex microdevice.

The microdevice, described in section 3.2.6.1, has a 100 μm deep, 500 μm and 50 cm long microchannel, etched in the silicon base and covered by Pyrex glass. The microchannel, whose surfaces will be functionalized to performed the extraction of polysomes from the sample injected in it, is designed as a serpentine; this geometry was chosen to prevent the formation of micro-vortexes during sample injection, as to avoid the premature disruption of the polysomes that may be caused by rough handling of the sample. This design also offers an high surface to volume ratio: a volume of 25 μl is in contact with a functionalized surface of 11 cm^2.
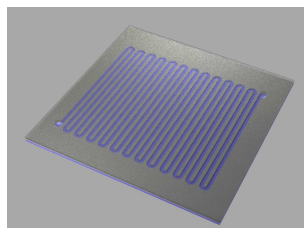
Figure 4.28: A 3D rendering of the silicon/Pyrex microdevice used in the course of this work. The microdevice area is 3×3 cm. Dimensions of the microchannel are: 100 μm depth, 500 μm width and 50 cm long. Volume contained: 25 μl.

As a first evaluation experiment four microdevices have been functionalized with the triCAS and CST silanes, with four different protocols, similar to those used to silanize plane silicon oxide samples, as described in section 3.2.6.1, while a fifth was used without functionalization, as a control experiment.

The microdevices were used to extract polysomes from an undiluted aliquot of the same polysomal fraction purified by sucrose gradient (fraction 12) used to evaluate the polysome adhesion on functionalized plane gold and silicon oxide samples described in the precedent sections of this chapter. The extraction protocol is described in detail in section 3.2.6.2.

The polysomal fraction was injected in the five devices and incubated 1 hour at 4°C to allow adhesion of polysomes in condition similar to the ones used for plane samples. At the end of the incubation the sample containing unbound material (unbound fraction) has been collected.

As an elution treatment both a thermal approach and a saline concentration alteration has been performed: after collecting the unbound fraction, TE buffer containing 1 mM of EDTA has been injected microdevice, that was then heated for 10 minutes at 50°C. EDTA is known to sequester Mg^{2+}, required to preserve the unity of the ribosomal subunits.

The sample extracted after the elution treatment was stained with a fluorescent dye RG (along with the unbound fraction) and analyzed with the spectrofluorimeter (see section 3.2.1.2 for details of the analysis procedure) to quantify the RNA content; the results are reported in Figure 4.29.

The RNA contained in the samples extracted from all microdevices after the elution treatment is considerably higher than the RNA contained in the unbound fraction: with small differences all the microdevices were able to extract RNA from a polysome fraction with an high efficiency.

A thermal treatment has been performed on the unbound fractions and to the initial stock fraction 12 to free the RNA from the polysomes there contained and allow the comparison of the fluorescence results. However the fact that the signal of the stock is lower than the eluted samples suggests that a single thermal step may not be sufficient to allow the RG dye to access to the RNA, thus the thermal treatment has been repeated (data not shown). The efficiency of RNA recovery has been later worked out, as the difference between the eluted fraction signal and the
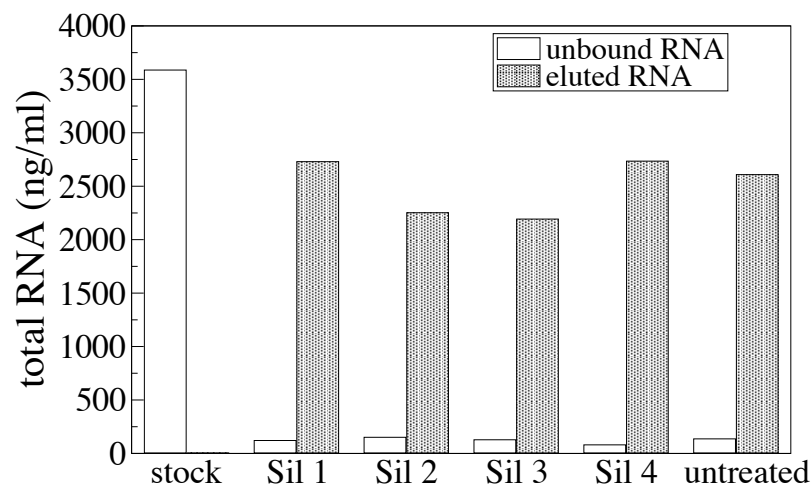
Figure 4.29: RNA recovery from functionalized silicon/Pyrex microdevices. The RNA content of unbound fraction (white bars) and eluted fraction (gray bars) extracted before and after the elution treatment from microdevices functionalized with: 1. triCAS in water (Silanization 1), 2. triCAS in ethanol/toluene solution (Silanization 2), 3. CST in ethanol/water at pH 5 (Silanization 3), 4. wet activation followed by silanization with CST in ethanol/water at pH 5 (Silanization 4) and 5. untreated were stained with RG fluorescent dye (RG) and quantified recording by spectrofluorimetry. The RNA contained in the samples extracted from all microdevices after the elution treatment is considerably higher than the RNA contained in the unbound fraction, meaning that the majority of the RNA (i.e. the polysomes) has been efficiently trapped into the microdevice. The first bar (stock) refers to the initial fraction 12, injected in the microdevice. Both this sample and the unbound fraction have undergone an incubation at 50°C for 10 minutes to denature the polysomes and make RNA accessible to the RG dye.

sum of the stock signal and the unbound fraction for every microdevice, resulting in a efficiency of $\sim 76\%$ with respect to the incubated sample.

The quality and integrity of the RNA extracted from the microdevices has been assessed by an Agilent Bioanalyzer. In Figure 4.30 the electropherograms relative to the eluted fractions from the five microdevices.

The signal associated with polysomal components (RNA) is showed in Panel A, for comparison. All the eluted samples show signals relative to components smaller/lighter than the polysomal associated RNA, with variable composition, intensity and degree of degradation. The eluted RNA from the microdevice silanized with triCAS in water solution (protocol Silanization 1, panel B) is the one with the least sign of degradation , and at the same time it shows two intense peaks attributed to the 18S and 28S rRNA. The microdevice treated with the same molecule but the ethanol/toluene protocol (Silanization 2, panel C) on the contrary is the one with the least and most spread peaks, suggesting a minor efficiency (observed also in the fluorescence signal in Figure 4.29, el. 2), and a poorer quality of recovered RNA. The performance of this microdevice is very similar to the one of the untreated device, suggesting an ineffectiveness of the functionalization process to enhance polysome adhesion on the micr-device surfaces.

The remaining microdevices signals are almost identical and their performances seems to be halfway between that of the Silanization 1 device, and Silanization 2/untreated device.

These first evaluation, coupled with the results in section 4.5.1.2 highlighting how, among the four functionalized TG-SO plane samples, those functionalized with the protocol Silanization 1P, (triCAS in water solution) were capable of immobilize the highest number of polysomes per cm^2 without visible signs of degradations.

Therefore, this kind of functionalization has been chosen as the most promising for further analysis:

a further evaluation of the performance of this kind of microdevice functionalization has been carried out.

A further cleaning step has been added before functionalization and polysome purification, by autoclave treatment for 20 minutes at 120° and extensive rinsing in RNase -free water of the microdevices, in order to decrease possible degradation of the mRNA due to RNases free on their surfaces.

All polysomal fraction indicated as fraction 10 to 14 in Figure 3.3 in section 3.2.3.1 have been reunited and used for the purification and extraction procedure as described previously, from at least three microdevices functionalized with Silanization M1 and untreated. The extracted mRNA has been quantified after staining with RG fluorescent dye and their quality checked with by Bioanalyzer, the result reported in 4.31. In panel A the quantification of unbound and eluted RNA from functionalized (red) and untreated (blue) microdevice are reported on the left, and the efficiencies of absorption (obtained as the difference between the stock and unbound RNA quantities) and elution expressed in percentage respect the initial quantity of RNA (stock). These can be considered as separate estimators of the performance of the microdevices in regards of the two steps of polysome immobilization and RNA extraction, respectively. In both cases the silanized
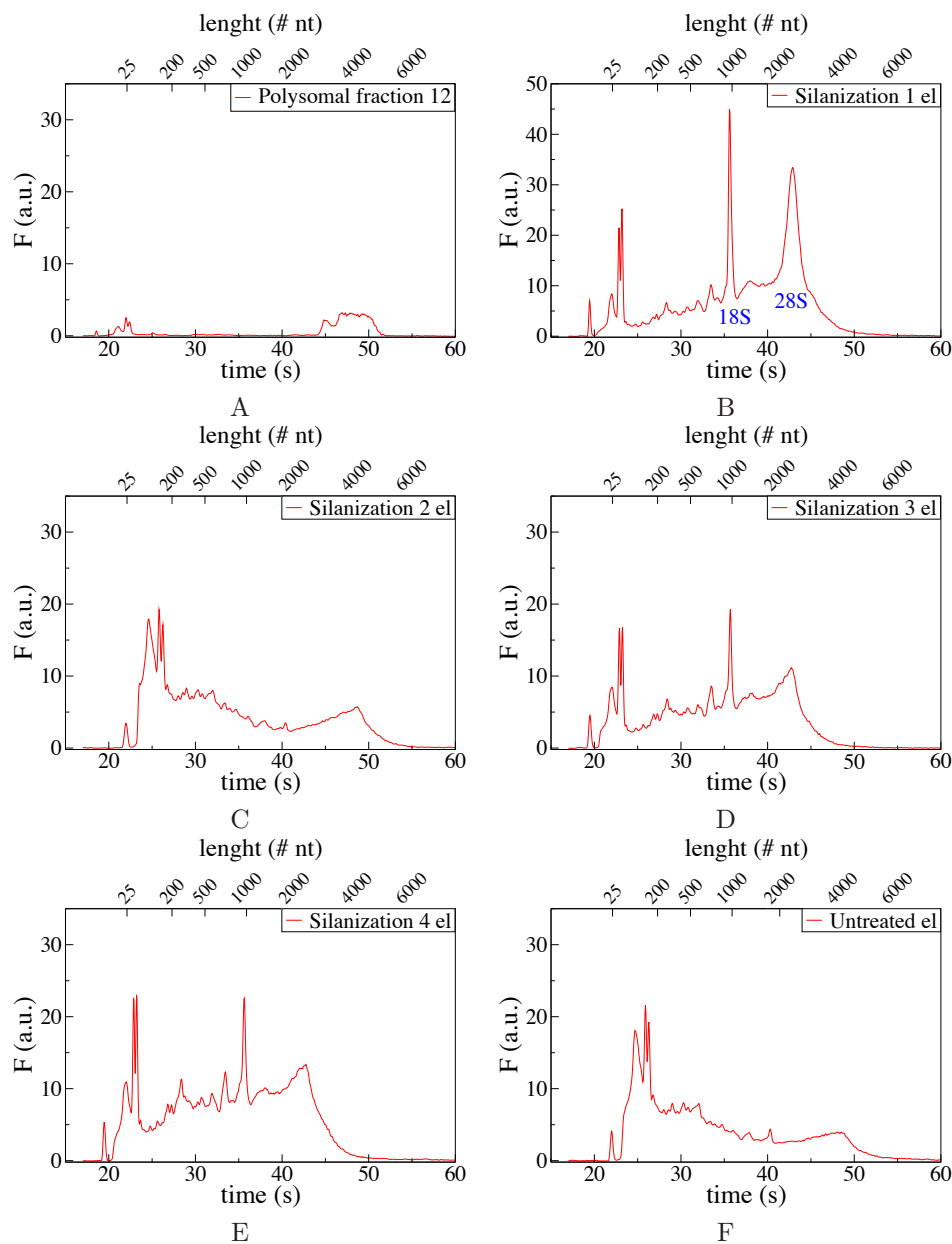
Figure 4.30: Panel A. Bioanalyzer electropherogram of the original polysomal fraction. Eluted RNA from microdevices functionalized with: B. triCAS in water (Silanization 1), C. triCAS in ethanol/toluene solution (Silanization 2), D. CST in ethanol/water at pH 5 (Silanization 3), E. wet activation followed by silanization with CST in ethanol/water at pH 5 (Silanization 4) and F. untreated. In panel B, the peaks relative to the rRNA 18S and 28S are marked.

microdevice show an higher efficiency: the RNA adsorbed via immobilization of polysomes constitutes the 88.0% in the silanized microdevice and the 69.7% in the untreated device, while the RNA extracted after the elution process is 73.3% of the initial quantity for the silanized microdevice and 55.7% for the untreated device.

As can be seen from the Bioanalyzer results shown in Panel B, Figure 4.31, the quality of RNA extracted from silanized microdevices (eluted fraction in black) is shifted towards the peaks on the left (identified with ribosomal and polysomal intact mRNA, see Figure 4.30, panel A for comparison) while it results mainly composed by shorter fragments in the case of the untreated microdevice (eluted fraction in green), showing a greater degree of degradation.

4.7 Silicon substrate: conclusions

Silicon oxide substrates have been silanized with two molecules containing carboxyl functional groups following four different protocols for silanization (either in water or organic solvents for triCAS molecule and either on plasma treated or wet activated silicon oxide samples for CST molecule). The interaction polysomes and these four samples was investigated.

Samples functionalized with triCAS both in water or solvents showed a slightly better capability to entrap polysomes with a good degree of shape conservation, resulting in surfaces whose performance replicated closely those of gold surfaces modified with a similar functionalization (MCOOH gold).

A functionalization similar to the MNH_2treated gold, that showed a good propensity to entrap nucleic acids, has been reproduced on mica using an aminosilane. Taking advantage of the possibility to control the charge distribution of this surface, its interaction with DNA and RNA has been characterized by force-distance AFM experiments, confirming the electrostatic attraction and repulsion as the driving force of this kind of adhesion approach.

Finally, a proof-of-principle verification of a purification microsystem based on carboxyl functionalized silicon/Pyrex surfaces for isolation of polysome-bound RNA has been carried out, finding the best results in terms of efficiency (73%) and quality of the extracted RNA for microdevices silanized with triCAS molecules in water.

A
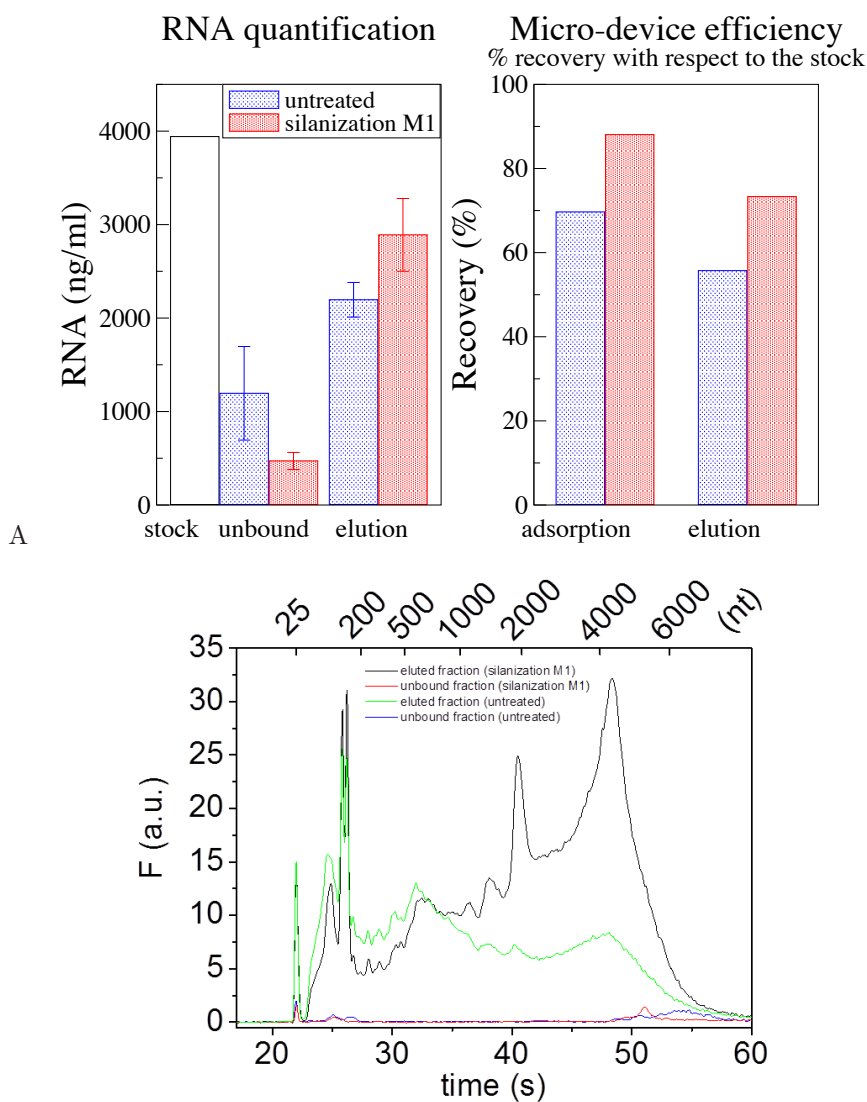
B

Figure 4.31: Panel A: RNA recovery from silicon/Pyrex microdevices treated with Silanization 1 (red bars) and untreated (blue bars). On the left the average RNA content of unbound and eluted fractions extracted before and after the elution treatment from microdevices are reported. On the right the percentage of absorption and elution for the two kinds of microdevice are reported. To avoid the problem due to insufficient accessibility of the RNA in the stock to the RG dye, mentioned in Figure 4.29, this aliquote has undergone a further thermal step, and then been diluted 25 times to avoid signal saturation. Panel B: Bioanalyzer electropherogram from the mRNA extracted before and after thermal elution treatment from a microdevice functionalized with Silanization 1 (unbound fraction in red and eluted fraction in black, respectively) and untreated microdevice (unbound fraction in blue and eluted fraction in green).

Chapter 5

Conclusions

Actively translated mRNA isolation is commonly achieved in research laboratories by a time-consuming and laborious procedure. In this work an alternative strategy has been considered: a miniaturized Lab-on-a-Chip device that integrates isolation of polysomes and extraction of their associated mRNA from small amout of sample. In this work microdevices with a volume of 25 μl have been used, but our results can easily transferred to systems designed to work with volumes scaled to the range required by the application. This approach offers several advantages to the traditional method, as high speed and simplicity of the procedure, and the possibility, previously not feasible, to work with quantities of sample smaller than tens of ml. In particular the complete operation of polysome isolation and mRNA extraction will be performed with few simple steps lasting about a couple of hours in total, while the traditional method (centrifugation in sucrose gradient and mRNA extraction in phenol/chloroform) may take up two days of work and requires a skilled operator.

The working strategy of the microdevice is based on the immobilization of unmodified polysomes on the opportunely treated surfaces of the device microchannels walls.

As a strategy to enhance polysome adhesion to the microdevice surfaces, chemical functionalization by formation of Self-Assembled Monolayers (SAM) composed by molecules sporting opportune functional groups has been chosen. This approach constitutes a method to tailor the surface chemical properties of a substrate by easy and low-cost procedures, requiring small quantities of reagents and achievable without expensive instrumentation.

SAM formed by alkanethiols on gold have been adopted as a model to evaluate polysome adhesion to different surface chemistry. Since both ribosomes and nucleic acids present charged groups exposed to the environment, molecules capable to endow surfaces with different charge distribution have been used to form SAM on gold (MCOOH and MNH$_2$) or to obtain hydrophilic and hydrophobic surfaces (MOH and M-11CH$_3$). After morphological and chemical characterization of the SAMs formed by these four molecules, carried out mostly by AFM and XPS, polysome adhesion has been evaluated with the AFM by observing riboso-

mal and polysomal fractions (previously purified by traditional sucrose gradient centrifugation) deposited on the four functionalized surfaces and on bare gold. The functionalized surfaces have been proven to be able to entrap ribosomes and polysomes with varying degree of efficiency and shape conservation. In particular gold functionalized with carboxyl acid (MCOOH) and amino (MNH$_2$) terminated alkanethiols both showed the capability of retain polysomes without introducing observable shape degradations, a phenomenon observed instead on MOH and M-11CH$_3$ functionalized gold surfaces, and in small degree also observed in ribosomal fractions deposited on bare gold. The functionalized surfaces have been then evaluated regarding their ability to immobilize nucleic acids, in particular DNA. Among the fucntionalized surfaces, MNH$_2$ on gold has shown a great propensity to retain DNA molecules on its surface, while again MOH and M-11SH introduced a certain degree of aggregation in the deposited material.

Therefore the carboxyl acid functionalization (MCOOH) presented itself as the most promising for polysome purification purposes, showing the ability to immobilize a satisfactory amount of good quality polysomes, while retaining in a very few degree nucleic acids. MNH$_2$ surfaces presented a similar capability to immobilize polysomes but also a great propensity to entrap DNA. This make this kind of functionalization unsuitable for actively translated mRNA isolation, being this surface able to immobilize both polysome-bound and total RNA without distinction; but make it more apt for nucleic acid purification. Indeed, amino-functionalized surfaces have been successfully applied to DNA purification microdevices [Nakagawa et al., 2005, Pasquardini et al., 2011, Potrich et al., 2012].

Carboxyl functionalization have been then replicated on a material more common in micro-fabrication, namely silicon oxide.

Thermally grown silicon oxide (TG-SO) plane samples have been functionalizated with two silanes, exposing one or three carboxyl groups (CST and triCAS respectively), and their capability to immobilize polysomes has been evaluated with the same methods and criteria used for functionalized gold samples.

The functional samples, showed similar results, closely comparable with those found on MCOOH gold, with triCAS functionalized samples showing a slightly better capability to immobilize shape-conserved polysomes, while signs of degradation were observed on CST surfaces.

Amino-silanes were used to functionalize mica surfaces and, taking advantage of the possibility to control the charge distribution of this surface changing the bulk pH, its interaction with DNA and RNA has been characterized by force-distance AFM experiments, confirming the electrostatic contribution to the nucleic acid adhesion phenomenon.

Finally, a silicon/Pyrex microdevice (volume 25 μl) has been functionalized with both triCAS and CST and used to perform a proof-of-principle evaluation of the polysome isolation and RNA extraction, using previously purified polysomal fractions. Extraction of mRNA from the polysomes immobilized on the microchannel surface has been achieved with a thermal treatment to denature the ribosomes and free the associated mRNA. The sample extracted from the microdevices after the thermal treatment where quantified with a fluorescent dye and their quality checked with capillary electrophoresis .

The microdevice functionalized with triCAS was the best performer, extracting RNA with an efficiency $> 70\%$ after an hour of incubation of the polysomal fraction.

Ideally the elution process should be able to disassemble the ribosomal subunits, without releasing their constituent rRNA. The results here presented are quite promising, showing the elution of the different classes of RNA, which could be further separated adding a module able to select and retain the mRNA e.g. taking advantage of their polyA tails..

Chapter 6

Aknowledgements

I would like to thank all the colleagues and friends that supported me throughout this Ph.D. experience:

First of all, a huge thank to Lorenzo, that with endless patience helped me, thought me and spurred me onward till this moment.

A lot of my gratitude goes also to Cristina and Laura, for all their support and all the things they thought me, with their biologist/physicists hybrid approach. And of course to Cecilia for welcoming and giving me the opportunity to work in her group for the last years.

Thank to my "twin-sister" Marta with whom I spent time, jokes, seminars and lessons aplenty, and to all the people with whom I shared the lab and the everyday life here in FBK: Francesco, Gaia, Valentina, Matteo, Manuela, Laura, Alberto (Framba), Veronica and Roberto, Alberto (Franzoi), Valeria, Paola, Gabriella, Sonja, Aurora, Josè, Liaisan, Gabriella, Mauro, Carlo and Daniele.

Finally thanks to my friends and family for their presence. To my parents for enduring this "long period of anxiety" for me, to my sister for being there with a word and a kick onward whenever I needed (or she felt in the mood), to Fabrizio for sustaining me especially in these last months, to Emmanuel, who tried is best to distract me one moment, and make me write my thesis the next, and to all my friends from Trento, Riva and Arco for all the moments spent together.

Bibliography

[Albayrak and Danışman, 2013] Albayrak, E. and Danışman, M. F. (2013). Helium diffraction study of low coverage phases of mercaptoundecanol and octadecanethiol self-assembled monolayers on au(111) prepared by supersonic molecular beam deposition. *The Journal of Physical Chemistry C*, 117(19):9801–9811.

[Alberts et al., 2008] Alberts, B., Johnson, A., Lewis, J., Raff, M., Roberts, K., and Walter, P. (2008). *The Molecular Biology of the cell, 5th Edition*. © Garland Science.

[Algire et al., 2002] Algire, M. A., Maag, D., Savio, P., Acker, M. G., Tarun, Jr, S. Z., Sachs, A. B., Asano, K., Nielsen, K. H., Olsen, D. S., Phan, L., Hinnebusch, A. G., and Lorsch, J. R. (2002). Development and characterization of a reconstituted yeast translation initiation system. *RNA*, 8(3):382–397.

[Allinger et al., 1980] Allinger, N. L., Cava, M. P., de Jongh, D. C., Johnson, C. P., Lebel, N. A., and Stevens, C. L. (1980). *Organic Chemistry*. Worth Publishers Inc.: New York.

[Anger et al., 2013] Anger, A. M., Armache, J.-P., Berninghausen, O., Habeck, M., Subklewe, M., Wilson, D. N., and Beckmann, R. (2013). Structures of the human and drosophila 80s ribosome. *Nature*, 497(7447):80–85.

[Bhattacharyya and Klapperich, 2008] Bhattacharyya, A. and Klapperich, C. M. (2008). Microfluidics-based extraction of viral rna from infected mammalian cells for disposable molecular diagnostics. *Sensors and Actuators, B: Chemical*, 129:693–698.

[Butt et al., 2005] Butt, H.-J., Cappella, B., and Kappl, M. (2005). Force measurements with the atomic force microscope: Technique, interpretation and applications. *Surface Science Reports*, 59:1–152.

[Caro, 1965] Caro, L. G. (1965). The molecular weight of lambda dna. *Virology*, 25:226–236.

[Castner et al., 1996] Castner, D. g., Hinds, K., and W., G. D. (1996). X-ray photoelectron spectroscopy sulfur 2p study of organic thiol and disulfide binding interaction with gold surfaces. *Langmuir*, 12:5083–5086.

[Chen et al., 2007] Chen, L., Manz, A., and Day, P. J. R. (2007). Total nucleic acid analysis integrated on microfluidic devices. *Lab Chip*, 7(11):1413–1423.

[Cho et al., 2007] Cho, Y.-K., Lee, J.-G., Park, J.-M., Lee, B.-S., Lee, Y., and Ko, C. (2007). One-step pathogen specific dna extraction from whole blood on a centrifugal microfluidic device. *Lab Chip*, 7(5):565–573.

[Chuang and Lin, 2007] Chuang, W.-H. and Lin, J.-C. (2007). Surface characterization and platelet adhesion studies for the mixed self-assembled monolayers with amino and carboxylic acid tterminated functionalities. *J Biomed Mater Res A*, 82(4):820–830.

[Crevillén et al., 2007] Crevillén, A. G., Hervás, M., López, M. A., González, M. C., and Escarpa, A. (2007). Real sample analysis on microfluidic devices. *Talanta*, 74:342–357.

[Dadafarin et al., 2013] Dadafarin, H., konkov, E., and Omanovic, S. (2013). Electrochemical functionalization of a 316l stainless steel surface with a 11-mercaptoundecanoic acid monolayer: Stability studies. *Int. J. Electrochem. Sci*, 8:369–389.

[Del Prete et al., 2007] Del Prete, M. J., Vernal, R., Dolznig, H., Müllner, E. W., and Garcia-Sanz, J. A. (2007). Isolation of polysome-bound mrna from solid tissues amenable for rt-pcr and profiling experiments. *RNA*, 13(3):414–421.

[Dorywalska et al., 2005] Dorywalska, M., Blanchard, S. C., Gonzalez, R. L., Kim, H. D., Chu, S., and Puglisi, J. D. (2005). Site-specific labeling of the ribosome for single-molecule spectroscopy. *Nucleic Acids Res*, 33(1):182–189.

[Fritzsche and Henderson, 1998] Fritzsche and Henderson (1998). Ribosome substructure investigated by scanning force microscopy and image processing. *Journal of Microscopy*, 189(1):50–56.

[Halbeisen and Gerber, 2009] Halbeisen, R. E. and Gerber, A. P. (2009). Stress-dependent coordination of transcriptome and translatome in yeast. *PLoS Biol*, 7(5):1–15.

[Halbeisen et al., 2009] Halbeisen, R. E., Scherrer, T., and Gerber, A. P. (2009). Affinity purification of ribosomes to access the translatome. *Methods*, 48:306–310.

[Hau et al., 2003] Hau, W. L. W., Trau, D. W., Sucher, N. J., Wong, M., and Zohar, Y. (2003). Surface-chemistry technology for microfluidics. *Journal of Micromechanics and Microengineering*, 13(2):272.

[Hegner et al., 1993a] Hegner, M., Wagner, P., and Semenza, G. (1993a). Immobilizing dna on gold via thiol modification for atomic force microscopy imaging in buffer solutions. *FEBS Lett*, 336(3):452–456.

[Hegner et al., 1993b] Hegner, M., Wagner, P., and Semenza, G. (1993b). Ultralarge atomically flat template-stripped au surfaces for scanning probe microscopy. *Surface Science*, 291:39–46.

[Hoffman and Ilan, 1974] Hoffman, W. L. and Ilan, J. (1974). Purification on hydroxyapatite of liver ribosomes and polysomes from unfasted mice. *Biochim Biophys Acta*, 366(2):199–214.

[Hong et al., 2004] Hong, J. W., Studer, V., Hang, G., Anderson, W. F., and Quake, S. R. (2004). A nanoliter-scale nucleic acid processor with parallel architecture. *Nat Biotechnol*, 22(4):435–439.

[Hooper et al., 1999] Hooper, A., Fisher, G. L., Konstandinidis, K., Jung, D., Nguyen, H., Opila, R., Collins, R. W., Winograd, N., and Allara, D. L. (1999). Chemical effedct of methyl and methyl ester groups on the nucleation and growth of vapor-deposited aluminium films. *J. Am. Chem. Soc.*, 121(35):8052–8064.

[Hui et al., 2007] Hui, W. C., Yobas, L., Samper, V. D., Heng, C.-K., Saxon Liw, S., Ji, H., Chen, Y., Cong, L., Li, J., and Lim, T. M. (2007). Microfluidic systems for extracting nucleic acids for dna and rna analysis. *Sensors and Actuators, A: Physical*, 133:335–339.

[Hutter and Bechhoefer, 1993] Hutter, J. L. and Bechhoefer, J. (1993). Calibration of atomic-force microscope tips. *Review of Scientific Instruments*, 64:1868–1873.

[Inada et al., 2002] Inada, T., Winstall, E., Tarun, Jr, S. Z., Yates, 3rd, J. R., Schieltz, D., and Sachs, A. B. (2002). One-step affinity purification of the yeast ribosome and its associated proteins and mrnas. *RNA*, 8(7):948–958.

[Jelenc, 1980] Jelenc, P. C. (1980). Rapid purification of highly active ribosomes from escherichia coli. *Analytical Biochemistry*, 105(1):369 – 374.

[Kirillov et al., 1978] Kirillov, S. V., Makhno, V. I., Peshin, N. N., and Semenkov, Y. P. (1978). Separation of ribosomal subunits of escherichia coli by sepharose chromatography using reverse salt gradient. *Nucleic Acids Res*, 5(11):4305–4315.

[Kricka, 1998] Kricka, L. J. (1998). Miniaturization of analytical systems. *Clinical Chemistry*, 44(9):2008–2014.

[Kudo et al., 2010] Kudo, K., Xi, Y., Wang, Y., Song, B., Chu, E., Ju, J., Russo, J. J., and Ju, J. (2010). Translational control analysis by translationally active rna capture/microarray analysis (trip-chip). *Nucleic Acids Res*, 38(9):e104.

[Lee et al., 2010] Lee, S.-H., Lin, W.-C., Kuo, C.-H., Karakachian, M., Lin, Y.-C., Yu, B.-Y., and Shyue, J.-J. (2010). Photooxidation of amine-terminated self-assembled monolayers on gold. *The Journal of Physical Chemistry C*, 114(23):10512–10519.

[Lien et al., 2007] Lien, K.-Y., Lee, W.-C., Lei, H.-Y., and Lee, G.-B. (2007). Integrated reverse transcription polymerase chain reaction systems for virus detection. *Biosensors and Bioelectronics*, 22:1739–1749.

[Love et al., 2005] Love, J. C., Estroff, L. A., Kriebel, J. K., Nuzzo, R. G., and Whitesides, G. M. (2005). Self-assembled monolayers of thiolates on metals as a form of nanotechnology. *Chem Rev*, 105(4):1103–1169.

[Maguire et al., 2008] Maguire, B. A., Wondrack, L. M., Contillo, L. G., and Xu, Z. (2008). A novel chromatography system to isolate active ribosomes from pathogenic bacteria. *RNA*, 14(1):188–195.

[Mathews et al., 2000] Mathews, M. B., Sonenberg, N., and Hershey, J. W. (2000). *Translational Control of Gene Expression*, chapter Origins and Principles of Translational Control, pages 1–32. Cold Spring Harbor Laboratory Press, Cold Spring Harbor, NY.

[Mikamo et al., 2005] Mikamo, E., Tanaka, C., Kanno, T., Akiyama, H., Jung, G., Tanaka, H., and Kawai, T. (2005). Native polysomes of saccharomyces cerevisiae in liquid solution observed by atomic force microscopy. *J Struct Biol*, 151(1):106–110.

[Nakagawa et al., 2005] Nakagawa, T., Tanaka, T., Niwa, D., Osaka, T., Takeyama, H., and Matsunaga, T. (2005). Fabrication of amino silane-coated microchip for dna extraction from whole blood. *J Biotechnol*, 116(2):105–111.

[Pasquardini et al., 2011] Pasquardini, L., Lunelli, L., Potrich, C., Marocchi, L., Fiorilli, S., Vozzi, D., Vanzetti, L., Gasparini, P., Anderle, M., and Pederzolli, C. (2011). Organo-silane coated substrates for dna purification. *Applied Surface Science*, 257:10821–10827.

[Potrich et al., 2012] Potrich, C., Lunelli, L., Pasquardini, L., Sonn, D., Vozzi, D., Dallapiccola, R., Marocchi, L., Ferrante, I., Rossotto, O., and Pederzolli, C. (2012). One-shot genetic analysis in monolithic silicon/pyrex microdevices. *Biomedical Microdevices*, 14:1103–1113.

[Pradet-Balade et al., 2001] Pradet-Balade, B., Boulmé, F., Beug, H., Ernst, W. M., and Garcia-Sanz, J. A. (2001). Translation control: bridging the gap between genomics and proteomics? *Trends in Biochemical Sciences*, 26(4):225 – 229.

[Price et al., 2009] Price, C. W., Leslie, D. C., and Landers, J. P. (2009). Nucleic acid extraction techniques and application to the microchip. *Lab on a Chip*, 9:2484–2494.

[Santini et al., 2013] Santini, G. C., Potrich, C., Lunelli, L., Pasquardini, L., Vaghi, V., and Pederzolli, C. (2013). Innovative microrna purification based on surface properties modulation. *Colloids and Surfaces B: Biointerfaces*, pages in press, doi 10.1016/j.colsurfb.2013.12.033.

[Sanz et al., 2009] Sanz, E., Yang, L., Su, T., Morris, D. R., McKnight, G. S., and Amieux, P. S. (2009). Cell-type-specific isolation of ribosome-associated mrna from complex tissues. *Proc Natl Acad Sci U S A*, 106(33):13939–13944.

[Singer et al., 1997] Singer, V. L., Jones, L. J., Yue, S. T., and Haugland, R. P. (1997). Characterization of picogreen reagent and development of a fluorescence-based solution assay for double-stranded dna quantitation. *Anal Biochem*, 249(2):228–238.

[Stroeve, 2004] Stroeve, P. (2004). *Dekker Encyclopedia of Nanoscience and Nanotechnology - 6 Volume Set*, chapter Self-Assembled Monolayers: Adsorption and Desorption from Alkanethiols on Gold, pages 3738–3746. Taylor & Francis.

[Suni et al., 2002] Suni, T., Henttinen, K., Suni, I., and Mäkinen, J. (2002). Effects of plasma activation on hydrophilic bonding of Si and SiO_2. *Journal of The Electrochemical Society*, 149(6):G348–G351.

[Uemura et al., 2008] Uemura, S., Iizuka, R., Ueno, T., Shimizu, Y., Taguchi, H., Ueda, T., Puglisi, J. D., and Funatsu, T. (2008). Single-molecule imaging of full protein synthesis by immobilized ribosomes. *Nucleic Acids Res*, 36(12):e70.

[Ulman, 1996] Ulman, A. (1996). Formation and structure of self-assembled monolayers. *Chem Rev*, 96(4):1533–1554.

[van der Vegte and Hadziioannou, 1997] van der Vegte, E. W. and Hadziioannou, G. (1997). Acid-base properties and the chemical imaging of surface-bound functional groups studied with scanning force microscopy. *The Journal of Physical Chemistry B*, 101:9563–9569.

[Vericat et al., 2010] Vericat, C., Vela, M. E., Benitez, G., Carro, P., and Salvarezza, R. C. (2010). Self-assembled monolayers of thiols and dithiols on gold: new challenges for a well-known system. *Chem Soc Rev*, 39(5):1805–1834.

[Viero et al.,] Viero, G., Lunelli, L., Passerini, A., Bianchini, P., Gilbert, R. J. C., Bernabò, P., Tebaldi, T., Diaspro, A., Pederzolli, C., and Quattrone, A. Three distinct types of ribosome assemblies modulated by translation are the building blocks of polysomes. (In preparation).

[Zanetti et al., 2005] Zanetti, M. E., Chang, I.-F., Gong, F., Galbraith, D. W., and Bailey-Serres, J. (2005). Immunopurification of polyribosomal complexes of arabidopsis for global analysis of gene expression. *Plant Physiol*, 138(2):624–635.